NASA Contractor Report 174640

Direct Simulations of Chemically Reacting Turbulent Mixing Layers

James J. Riley and Ralph W. Metcalfe

Flow Research Company

Kent, Washington

March 1984

Prepared for

NATIONAL AERONAUTICS AND SPACE ADMINISTRATION
Lewis Research Center
Under Contract NAS 3-23531

TABLE OF CONTENTS

1. SUMMARY

The objectives of this work are (i) to extend the technique of direct numerical simulations to turbulent, chemically reacting flows, (ii) to test the validity of the method by comparing computational results with laboratory data, and (iii) to use the simulations to gain a better understanding of the effects of turbulence on chemical reactions. In particular, we address the effects of both the large-scale structure and the smaller-scale turbulence on the overall reaction rates, examine the relationship between infinite reaction rate and finite reaction rate chemistry, and compare some of the results of our calculations with existing theories and laboratory data.

The scope of work to do this involved the following. First, existing computer codes were modified to treat the present problem. Next, extensive numerical testing of the computer codes was performed. Finally, in order to examine the effects of the mixing layer turbulence, both the large-scale structure and the smaller-scale turbulence, on the overall reaction rates, a sequence of three problems was computed: (i) reactions on a unidirectional (one-dimensional) mixing layer, (ii) reactions on a mixing layer experiencing large-scale, two-dimensional vortex rollup, and (iii) reactions on a three-dimensional turbulent mixing layer. The simulations of the two-dimensional mixing layer with vortex rollup are intended to model the large-scale structure in the mixing layer, whereas the three-dimensional simulations contain both the large-scale structure and the smaller-scale turbulence.

The numerical testing involved the comparison of computed results with exact solutions for a number of different cases. Both rigid body rotation and vortex rollup flow fields were used. The work greatly extended the results of earlier work on the advection of a passive scalar on a rigidly rotating flow field (the color problem) to include also diffusion, chemical reaction, and more complex flows. We have found that high accuracy of the spectral methods observed in the advection case is also obtained when these further complications are present. Our results indicate that spectral numerical methods may prove to be useful in the future both for solving the model equations for combustor processes as well as for future studies of chemically reacting turbulent flows employing direct numerical simulations.

The approach of direct numerical simulations allowed extensive examination and interpretation of the reaction process. From the one-dimensional simulations, we found that we could easily compute finite reaction rates near the fast reaction limit, that the results were fairly insensitive to the initial conditions (for the class of initial conditions computed), and that the results were in reasonable agreement with theoretical predictions.

For the two-dimensional simulations, we found that in all of the cases computed, the vorticity field and the product field approximately coincided. From the computation of volume averages, we observed the enhancement of the overall reaction rate due to the vortex rollup. It also appeared that the merging of vortex cores was a more significant mechanism in increasing the overall reaction rate than the straining of the reaction interface. Significant species segregation was apparent, so that, for example, the product of the average concentrations was approximately equal to and opposite the correlation between the fluctuating concentrations. Some of the higher order correlations were also examined.

In the three-dimensional simulations, the contour plots indicated that the vortex rollup takes longer to develop, and the vortices and braids are not as distinct as in the two-dimensional case. Also, the vortices that develop are not strongly correlated laterally. Both the contour plots and the statistical results indicated that the spatial segregation was also not as strong as in the two-dimensional case, probably due to the weaker vortex rollup as well as the effects of smaller-scale, three-dimensional turbulence.

Comparisons were made between the simulation results and results using similarity theory. Approximately linear growth rates of various computed length scales, including the mean velocity half-width, the mean vorticity thickness, and the mean product thickness, were obtained and were in agreement with the theory. Similarity scaling was found to collapse quite well the results for the average reactant concentrations, the rms fluctuating reactant concentrations, the concentration correlations, the average product concentrations, and the rms fluctuating product concentrations.

Some limited comparisons were made with laboratory data. Computed profiles that were qualitatively similar to corresponding laboratory profiles were obtained for the average reactant concentrations, the rms fluctuating reactant concentrations, the average product concentrations, the rms fluctuating product concentrations, and the concentration correlations.

We have made some comparisons with existing theories. One such theory has suggested, in addition to using the equations for the average concentrations, including the equations for the concentration fluctuations and correlation. These equations can be closed by neglecting certain triple moments when compared to certain lower order terms. However, our results indicate that the triple moment terms are as important as other terms in the equations, so an assumption of this type will probably lead to poor predictions. Another proposition is to model the mean reaction term, assuming that it will be proportional to the average concentration of the lean species divided by a turbulent time scale. We have found that such an assumption will only be moderately successful if applied to our case. Finally, it has been suggested that the concentration correlation of the reacting species can be estimated in terms of that for the nonreacting case, which is much easier to model. Although this was proposed mainly for statistically homogeneous flows, we find that it is a reasonable approximation for our reacting flow simulations.

2. INTRODUCTION

The need for improved combustor efficiency, reduction in pollutant emissions, the use of alternative fuels, improved component durability, and better combustor outflow characteristics demands an improved understanding of and predictive capabilities for the various combustor processes. In a jet engine combustor, the geometry, flow rates, locations of fuel injectors, and other similar features govern the performance of the combustor. The ability to model the effects of these features on combustor performance can greatly aid in the design of combustors, reducing development time and leading to more optimum designs. Modeling can also minimize the extent of testing and aid in the definition of a test program and the interpretation of resulting data.

Modeling the combustor processes is a very complicated task, involving numerical models for the combined chemical, thermodynamic, and aerodynamic processes. One of the critical features of the aerodynamics, especially with regard to its effects on the chemical reactions, is the highly unsteady turbulent motion in the combustors. When the time scales of the chemical reactions are of the same order as, or much less than, the turbulent mixing time, which is often the case in combustors, then the reaction rates are controlled by the ability of the turbulence to bring the chemical species together. Hence, the overall reaction rates depend more on the turbulent mixing time and less on the specific reaction rates (Toor, 1962).

It is clear that proper treatment of the effects of turbulence is usually an essential part of a good combustor model. However, at the present time the ability to model the turbulence and its effects on combustors is very limited (see, e.g., Mellor and Ferguson, 1980). This is especially true for cases where the reaction times are not either very fast or very slow compared to the turbulent mixing times (see, e.g., O'Brien, 1981; Libby and Williams, 1981).

In order to treat the complex, unsteady behavior of turbulence, statistical methods are generally introduced, and one of two main approaches is usually followed: the moment equation method or the probability density function method. In the first, the moment equation approach, averages (usually time averages) of the relevant physical variables are introduced, and the governing chemical/aerodynamic equations are averaged. This leads to a closure problem, wherein there are more unknown quantities than equations. This problem is resolved by introducing ad hoc assumptions relating various

unknown quantities and thus closing the system of equations. (See, e.g., Libby and Williams, 1981, or Donaldson and Varma, 1976, for discussions of this approach.) The main difficulty with this approach is in proposing reasonable closure models. This is especially true for the reaction rate terms in the equations for the chemical species concentrations. For example, the instantaneous reaction rate r for a binary reaction with an Arrhenius rate is

$$r = -R\rho C_1 C_2 \exp(-T_a/T_e)$$

where C_i is the molar concentration of the species i, T_e is the temperature and T_a the activation temperature, R is the rate constant, and ρ the mixture density. If the exponential is expanded in terms of (T_a/T_e), then we see that the average of r depends on an infinite series of averages of the product of C_1C_2 with inverse powers of T_e. It is very difficult to truncate the series and propose reasonable models relating these averages to lower order averages needed to close the equations (see, e.g., Borghi, 1974). Furthermore, the problem becomes even more intractable for more complex reactions. An alternative is to derive equations for the reaction rate term (Donaldson and Varma, 1976) and to close the equations at a higher order. However, this leads to many more unknowns and equations, and more obscure closure assumptions are also necessary.

The second approach, the probability density function (pdf) approach, relies on the equation for the (joint) pdf for the relevant physical variables. (See O'Brien, 1981, for a review of this approach.) The closure problem for the reaction rate term does not arise. However, closure problems for other terms, in particular for the mixing term, do appear, and ad hoc closure assumptions are again necessary. A considerable amount of theoretical work has addressed these closure problems (e.g., Curl, 1963; Dopazo, 1976; Pope, 1979; Janicka and Kollman, 1979), and an appreciable amount of progress has been made. The numerical solution of the resulting equations can become very difficult. This is because the number of independent variables in this approach, which is equal to the sum of the usual independent variables plus the dependent variables in the original problem, can be very large. In order to avoid this difficulty, Monte-Carlo methods have been introduced (Pratt, 1976; Pope, 1979). (See Appendix B for a brief discussion of the relationship between the present approach and Monte-Carlo methods.)

Hybrid methods have also been used. For example, the pdf approach of Janicka and Kollman (1979) has employed moment equations for the turbulence kinetic energy and dissipation rates in addition to the equation for the pdf. In another approach, assumptions have been made for the form of the probability density function, which can be used to derive closure assumptions for the moment equations (see, e.g., Jones and Whitelaw, 1982).

The pdf approach can be very useful in the limit of an infinite reaction rate, since the conserved scalar approach can often be employed. In this limit the statistics of the reacting species concentrations and of the thermodynamic variables can for some cases be found in terms of the pdf of a conserved scalar (see, e.g., O'Brien, 1971; Bilger, 1980).

In order to more adequately model the turbulence and its effects on combustor performance using either the moment equation approach or the pdf approach, there is a need for better information concerning the turbulence/chemistry interaction. This will allow the formulation of better models and more adequate testing of the proposed models. There is also a need for improved numerical methods in order to more accurately compute solutions to the model equations. To address these needs is the main thrust of the present work.

In the past 5 to 10 years an alternative computational methodology has become available for studying transitioning and turbulent flows. Termed direct numerical simulations, this approach involves the numerical solution of the detailed evolution of the complex turbulent velocity field. Using very efficient numerical methods (e.g., pseudospectral methods), we can accurately solve the fully nonlinear (possibly low-pass filtered) equations of motion, so that closure assumptions are only necessary (if at all) for the smaller-scale motions, which have been filtered out. Statistical data are obtained by performing spatial, temporal, and/or ensemble averages over the computed flow field.

This procedure is analogous to performing experiments in the laboratory. However, it has the advantages that (i) much more statistical information of interest can be obtained (since the entire flow field is known at every time step), (ii) parameters can be varied easily, (iii) experimental conditions are more controllable, and (iv) the effects of large-scale structures can be directly addressed. The technique also offers the advantage of circumventing

the closure problem. The main disadvantage is the limited spatial and temporal resolution available, which limits the range of space and time scales (and hence the maximum Reynolds number) that can be included in the simulations. At the present time, the approach is usable only as a research tool.

Direct numerical simulations have been successfully applied to the testing of turbulence theories, from analytic theories (e.g., Orszag and Patterson, 1973; Herring et al., 1973) to second-order closure modeling assumptions (e.g., Herring, 1974; Schumann and Patterson, 1978). These simulations have been used to address questions of basic physics of the atmospheric boundary layer (Deardorff, 1974), of turbulent diffusion (Riley and Patterson, 1974), of mixing layer control through forcing (Riley and Metcalfe, 1980a), and of sound generation (Metcalfe and Orszag, 1974). Furthermore, successful validation studies have been carried out for homogeneous decay (Mansour et al., 1979), turbulent wakes (Riley and Metcalfe, 1980b), mixing layers (Riley and Metcalfe, 1980a), and turbulent boundary layers (Moin and Kim, 1982; Patera and Orszag, 1981). The approach clearly has potential for use in turbulent reaction flows.

The objectives of the work discussed herein are (i) to extend the technique of direct numerical simulations to turbulent, chemically reacting flows, (ii) to test the validity of the method by comparing computational results with laboratory data, and (iii) to use the simulations to gain a better understanding of the effects of turbulence on chemical reactions. In particular, we address the effects of both the large-scale structures and the smaller-scale turbulence on the overall reaction rates, examine the relationship between infinite reaction rate and finite reaction rate chemistry, and compare some of the results of our calculations with existing theories and laboratory data.

In extending this method to chemically reacting flows, it is important to take a step-by-step approach, beginning with simpler problems and then proceeding on to more complex ones. We choose as a first step to address the problem of an idealized turbulent mixing layer undergoing an irreversible binary reaction with no heat release.

In addressing the objectives of this study, this work will have an impact on the main thrusts of the NASA-Lewis Combustion Fundamentals Program as enunciated by Mularz (1983), i.e., combustion modeling, model validation,

fundamental experiments, and numerical methods. With regard to combustion modeling, direct numerical simulations is an approach which first, although in the near term will only be applied to simplified problems, may in the longer term be useful as a combustion model. Second, results of the simulations, in analogy to laboratory experiments, can be used for model validation. Third, fundamental experiments can be performed with the simulations to elucidate basic physical processes. And fourth, as part of the methodology development, we have introduced spectral numerical methods into reacting flow problems. These numerical methods may prove to be very useful in the future in solving the appropriate model equations.

The scope of work to do this involved the following. First, existing computer codes were modified to treat the present problem. Next, extensive numerical testing of the computer codes was performed. Finally, in order to examine the effects of the mixing layer turbulence, both the large-scale structures and the smaller-scale turbulence, on the overall reaction rates, a sequence of three problems was computed: (i) reactions on a unidirectional (one-dimensional) mixing layer, (ii) reactions on a mixing layer experiencing large-scale, two-dimensional vortex rollup, and (iii) reactions on a three-dimensional turbulent mixing layer. The simulations of the two-dimensional mixing layer with vortex rollup are intended to model the large-scale structures in the mixing layer, whereas the three-dimensional simulations contain both the large-scale structures and the smaller-scale turbulence.

In the next section we discuss related work that is especially pertinent to the present study. In the third section we explain the methodology of applying direct numerical simulations to chemically reacting flows. In the fourth section we present our results for the tests of the numerical schemes and for the sequence of reaction calculations. Finally, in the last section we summarize our results, discussing their implications and also possible future directions.

3. BACKGROUND

Several studies of turbulence using numerical simulations have been carried out that are closely related to the present study. Riley and Metcalfe have addressed the development of free turbulent shear flows (without chemical reactions) using direct numerical simulations, in particular computing axisymmetric turbulent wakes (Riley and Metcalfe, 1980b) and turbulent mixing layers (Riley and Metcalfe, 1980a; Metcalfe and Riley, 1981). Since the present study is an extension of this work, it will be briefly reviewed. Also Nielsen and Hill (1977; see also Hill, 1979), Ghoniem et al. (1982), and Ashurst and Barr (1981) have performed numerical simulations of two-dimensional turbulent-like flows with chemical reactions. This work will also be briefly discussed.

Riley and Metcalfe (1980b) applied direct numerical simulations to the downstream development of the turbulent wake of an axisymmetric body. The purpose of the calculations was to determine whether the simulations could accurately portray the physics of this free turbulent shear flow. The approach was to use laboratory data to initialize the flow, to compute the downstream development of the flow, and to compare the results with data at the appropriate downstream distances. The calculations were fully three-dimensional and time-dependent. No modeling was used, so there were no parameters to adjust. The results showed good agreement between the simulations and laboratory data (to within about 5% for the mean velocity and 10% for the turbulence intensities) and good agreement with similarity theory. In addition, several new features, such as intermittency at the wake edge, which were not in the initial conditions, developed in the simulations.

A similar approach was used to study a turbulent mixing layer (Riley and Metcalfe, 1980a), again for the purpose of validation of the methodology. The mixing layer calculation was initialized using the laboratory data of Wygnanski and Fiedler (1970). The temporally growing layer, rather than the spatially growing layer (as in the laboratory experiments), was computed. This was done because the numerical methods are much simpler for the temporally growing layer, while the physical processes are much the same. Figure 1, taken from Riley and Metcalfe (1980a), is a typical sequence of plots of constant contours of lateral vorticity, which display the rollup of the layer. This compares qualitatively with photographs from laboratory data (see, e.g., Chandrsuda et al., 1978).

Some idea of the quantitative behavior of the mixing layer simulations can be seen by examining the statistical properties of the mean velocity profile. Laboratory data and similarity theory show that the temporal growth of the mixing layer, as measured by its mean velocity profile half-width z_M, should be linear. Figure 2 (Metcalfe and Riley, 1981) shows the growth of z_M for calculations on two different computational meshes (using two different computer codes). In both cases the linear growth is exhibited, although at slightly different rates. Brown and Roshko (1974) have estimated the spatial growth rate of z_M from laboratory experiments. If we assume that space and time are related by the transformation

$$x = \frac{1}{2}(U_1 + U_2)t$$

then these data give

$$\frac{1}{U}\frac{d}{dt} z_M = 0.0275$$

which is close to the values obtained from the simulations. Here U_1 is the free-stream speed of the high-speed layer, U_2 is the free-stream speed of the low-speed layer, and $U = U_1 - U_2$ is the velocity difference across the mixing layer.

The spatial development of the mixing layer can be further studied by examining the development of the mean velocity, nondimensionalized by U, as a function of transverse distance, nondimensionalized by z_M. Similarity theory and laboratory experiments show that this scaling should collapse the data. Figure 3 (Metcalfe and Riley, 1981) shows that both simulations exhibit this behavior. The results for the 64^3 case show that the data collapse is maintained over a time period in which the layer increases by a factor of over 5.

In addition to addressing the question of validation of the methodology, Riley and Metcalfe (1980a) also used the simulations to resolve questions of anomalous countergradient momentum fluxes observed in the mixing layer experiments of Wygnanski et al. (1980) and Ho and Huang (1982). Using the three-dimensional simulations discussed above, and also two-dimensional calculations of multiple vortex rollup, Riley and Metcalfe concluded that the anomalous results were due to the suppression of subharmonic modes by the

harmonic forcing used in the experiments. The experiments by Ho and Huang (1982) have supported this conclusion.

Some work has also been carried out addressing chemical reactions occurring on two-dimensional, turbulent-like flows. Nielsen and Hill (1977) computed the mass conservation equations for chemical species undergoing convection, diffusion, and irreversible chemical reaction on two-dimensional, homogeneous turbulent velocity fields. Reasonable agreement was obtained between simulation results and O'Brien's (1969) independence hypothesis for single species reactions. Toor (1962) hypothesized that the decay of the covariance of the concentrations for a two-species reaction is insensitive to the rate of reaction if the reactants have equal diffusivities and are present in stoichiometric proportions. This hypothesis was also successfully tested in this study.

Ghoniem et al. (1982) studied the turbulent combustion in a lean propane-air mixture in the mixing layer behind a backward-facing step. They used Chorin's (1973) random vortex method to compute the time development of the two-dimensional, large-scale structures in the flow field. The flame was treated as a constant-pressure deflagration acting at the interface between two media and propagating locally at a prescribed normal burning velocity. Their results were compared to visualizations from a corresponding laboratory experiment using high-speed schlieren photography to observe the flame fronts. The comparisons indicated good qualitative agreement between the experimental and simulated results.

Some related simulations were carried out by Ashurst and Barr (1981). They also used vortex methods to compute the two-dimensional aspects of a mixing layer, but used the flux-corrected transport scheme (Zalesak, 1979) and the conserved scalar technique (assuming infinite reaction rates) to treat the reaction. Their results demonstrated, in particular, the dramatic effect of the large-scale structure in the mixing layer on the diffusion flame propagation.

Some mainly theoretical studies carried out by Marble (1982) and his coworkers (see also Karagozian, 1982, and Norton, 1983) are also relevant to our work. Using asymptotic analyses for very fast reactions and hence very narrow flame fronts, they studied the effects of an isolated vortex on a laminar flame front. The isolated vortex can be considered to be a simple

model for the large-scale structure in a turbulent mixing layer. They found that the augmentation of the fuel consumption due to the vortex is proportional to $\Gamma^{2/3}D^{1/3}$, and the radius of the core of combustion products is proportional to $\Gamma^{1/3}D^{1/6}t^{1/2}$. Here, Γ is the circulation of the vortex, and D the reactant diffusivity.

4. METHODOLOGY

In order to extend the method of direct numerical simulations of turbulence to chemically reacting flows, we start by addressing a turbulent mixing layer with the following characteristics.

i. Binary, single-step, irreversible chemical reaction ($A + nB \rightarrow$ product) with negligible heat release. This implies (a) no temperature effects on the reaction rates and (b) no effects of the reactions on the flow field.

ii. Very small Mach number flow so that, together with (i.b), the flow is incompressible.

iii. The statistical properties of the flow are invariant with respect to translations in the lateral (y) and flow (x) directions. (See Figure 4 for the problem geometry in the calculations.) That is, the statistical properties of the flow depend only on the transverse coordinate (z) and time. This enables us to compute temporally developing mixing layers instead of spatially developing ones usually studied in the laboratory.

iv. The initial conditions for the reacting species are that the reactants are not premixed, with species A in the bottom half and species B in the top half of the flow (see Figure 4).

The first characteristic allows us to study the effects of turbulence on the overall chemical reation rates without the complication of the reaction influencing the turbulence. Although the latter element is critical in treating combustion problems, it is important in beginning the application of direct numerical simulations to chemically reacting flows that a step-by-step approach be taken and not too many complications be introduced at one time. This is also the reason for the second characteristic. Several laboratory experiments carried out in recent years have been subject to the same restrictions (i.e., i and ii) and have provided data with which to compare the results of our simulations (e.g., Konrad, 1977; Breidenthal, 1978; Mungal, 1983; and Choudbury et al., 1983).

The temporally growing layer (characteristic iii) rather than the spatially growing layer is treated because the numerical methods are much simpler for the temporally growing layer, while the physical processes are

much the same. For example, in order to treat the spatially growing layer numerically, inflow and outflow boundary conditions are needed, which are very difficult to correctly implement for this problem. In the temporally growing case, periodic boundary conditions can be used, which are very simple to implement, especially using spectral numerical methods. For coflowing mixing layers as $\lambda = (U_1 - U_2)/(U_1 + U_2)$ becomes small, where U_1 and U_2 are the free-stream velocities on the high- and low-speed sides of the layer, the differences between the two approaches should also become small. Finally, by addressing the temporally growing case, the problem can be defined as statistically homogeneous in two directions (x and y), so that averages can be taken in these two directions, increasing the statistical confidence in the results.

The above assumptions imply that the (molar) concentrations of the reactants, say C_A and C_B, satisfy the following diffusion-reaction equations:

$$\frac{\partial}{\partial t} C_A + \underset{\sim}{u}\cdot\nabla C_A = -RC_AC_B + D_A\nabla^2 C_A \tag{1}$$

$$\frac{\partial}{\partial t} C_B + \underset{\sim}{u}\cdot\nabla C_B = -nRC_AC_B + D_B\nabla^2 C_B \tag{2}$$

Here the stoichiometric coefficient n, the reaction rate coefficient R, and the diffusivities D_A and D_B are all constants. The velocity field $\underset{\sim}{u}$ satisfies the incompressible Navier-Stokes equations:

$$\frac{\partial}{\partial t} \underset{\sim}{u} + \underset{\sim}{u}\cdot\nabla\underset{\sim}{u} = -\frac{1}{\rho}\nabla p + \nu\nabla^2\underset{\sim}{u} \tag{3}$$

$$\nabla\cdot\underset{\sim}{u} = 0 \tag{4}$$

where p is the pressure, ρ is the constant density, and ν is the constant kinematic viscosity.

For the reaction defined above, the molar concentration of the product field, C_P, satisfies

$$\frac{\partial}{\partial t} C_P + \underset{\sim}{u}\cdot\nabla C_P = RC_AC_B + D_P\nabla^2 C_P \tag{5}$$

where D_P is the molecular diffusivity.

For lateral boundary conditions, we define the flow field and reactants to be periodic in the flow (x) and lateral (y) directions with periods L_x and L_y, respectively. This is consistent with statistical homogeneity in these directions. It has been found (see, e.g., Riley and Metcalfe, 1980b) that if the length of periodicity is large with respect to integral spatial scales, then the influence of the periodicity assumption is minimal. In the transverse (z) direction, we define free-slip boundary conditions. In particular, these imply that

$$\frac{\partial}{\partial z} u(x,y,z)\Big|_{z = 0, L_z} = 0 \tag{6}$$

$$\frac{\partial}{\partial z} v(x,y,z)\Big|_{z = 0, L_z} = 0 \tag{7}$$

$$w(x,y,0) = w(x,y,L_z) = 0 \tag{8}$$

Here L_z is the length of the computational domain in the z-direction. Free-slip conditions have less influence on the flow field than no-slip conditions, since the lateral velocities are not required to be zero at the boundaries, and are easy to implement numerically.

In order to solve the governing equations of motion subject to the prescribed boundary conditions, we use pseudospectral numerical methods. We choose these methods because in related problems they have been shown to be at least twice as accurate in each spatial dimension compared to finite difference schemes with the same resolution (Peyret and Taylor, 1983; Haidvogel, et al., 1980), and they are competitive in computational efficiency. Furthermore, they are very accurate in treating phase information (Orszag, 1971), which is of particular importance in computing chemical reactions. One of the benefits of this study is the first application of spectral numerical methods to chemically reacting flows.

Pseudospectral numerical methods as applied to this problem involve expanding the dependent variables in Fourier-sine/cosine series, i.e.,

$$\left\{u,v,C_A,C_B\right\} = \sum_{|k_1|<K_1} \sum_{|k_2|<K_2} \sum_{0\le k_3<K_3} \left\{\hat{u},\hat{v},\hat{C}_A,\hat{C}_B\right\} \exp\left[2\pi i\left(\frac{k_1 x}{L_x} + \frac{k_2 y}{L_y}\right)\right] \cos\left(\pi\frac{k_3 z}{L_z}\right) \tag{9}$$

$$w = \sum_{|k_1|<K_1} \sum_{|k_2|<K_2} \sum_{0\le k_3<K_3} \hat{w} \exp\left[2\pi i \left(\frac{k_1 x}{L_x} + \frac{k_2 y}{L_y}\right)\right] \sin\left(\pi \frac{k_3 z}{L_z}\right) \qquad (10)$$

(See Orszag and Pao, 1974, for a detailed discussion of a similar application of pseudospectral methods.) Here $\underset{\sim}{k}$ is the wave number vector, $\underset{\sim}{K}$ is the truncation wave number vector, and $\hat{g}$ denotes the transform of g. Note that these expansions satisfy the boundary conditions exactly. Solving Equations (1) through (5) by pseudospectral methods involves evaluating the spatial derivatives in Fourier space but computing the nonlinear terms in physical space. Our numerical algorithm uses fast Fourier transforms to evaluate the transforms and inverse transforms, and either Adams-Bashforth or leap-frog time differencing on the nonlinear terms and Crank-Nicolson (implicit) time differencing on the diffusion terms.

In our series of numerical tests, to be described in the next section, which was conducted prior to the numerical simulations, we found that small negative concentrations sometimes developed, due to numerical errors. This was especially true when steep gradients in concentration were present. These negative regions occasionally caused spurious effects when computing the reaction rate terms and sometimes led to numerical instabilities. (See McRae et al., 1982, for a discussion of this problem and various methods to alleviate it.) In order to avoid this problem, at regular intervals during the calculations we imposed the following restriction on the reactant concentrations:

$$C(\underset{\sim}{x},t) = \begin{cases} \tilde{C}(\underset{\sim}{x},t) & \tilde{C} \ge 0 \\ 0 & \tilde{C} < 0 \end{cases} \qquad (11)$$

Here $\tilde{C}$ is the value of the concentration prior to applying the restriction. Other, more sophisticated filtering schemes were considered (e.g., the nonlinear filter suggested by Forester, 1977), but this scheme was found adequate to maintain numerical stability and accuracy and was easy to implement. (See Appendix A for a discussion of the types of numerical difficulties that arise in computing reactions and our approach to dealing with them.)

Two computer codes were developed, a two-spatial-dimension plus time code (the 2D code) and a three-spatial-dimension plus time code (the 3D code),

which employed almost identical numerical schemes. The 2D code was used extensively in the numerical testing portion of our study, for the one- and two-dimensional simulations, and for debugging the 3D code. The 2D code employs either 64x64 or 128x128 point computational grids, with execution times of approximately 0.35 and 1.4 sec/time step, respectively. These times are not representative of an optimized code since additional scalar fields were computed, as were detailed conservation statistics at every time step. The 3D code employs either 32x32x32 or 64x64x64 point computational grids, with execution times of approximately 0.7 and 7.0 sec/time step, respectively. The 3D code, developed in cooperation with Steven A. Orszag, has somewhat better execution times for a given number of grid points since it has been fully vectorized and optimized to run on the NASA-Lewis Cray 1S computer.

We have treated both finite-rate and infinite-rate reactions. To compute the finite-rate case, we directly solve Equations (1) through (5), subject to the boundary conditions discussed. The reaction rate constant R must be kept small enough that we can adequately resolve the reactant fields, which can develop steep gradients when R is large. To solve the infinite reaction rate case, we use the conserved scalar approach (see, e.g., Toor, 1962; O'Brien, 1971; Ashurst and Barr, 1981). Consider the scalar defined by

$$\theta = C_A - C_B \tag{12}$$

[θ is sometimes referred to as a conserved scalar of the Schvab-Zeldovitch type (Williams, 1965).] If we assume that the diffusivities of C_A and C_B are equal, then subtracting Equation (2) from Equation (1) shows that θ is a conserved scalar quantity satisfying

$$\frac{\partial}{\partial t}\theta + \underset{\sim}{u}\cdot\nabla\theta = D\nabla^2\theta \tag{13}$$

where $D = D_A = D_B$. If the reaction rate is infinite, then the two reactants cannot coexist at the same physical point, i.e., the species are segregated. In this case, the reactants are directly related to the conserved scalar θ by

$$C_A = \begin{cases} \theta & \theta \geq 0 \\ 0 & \theta < 0 \end{cases} \tag{14}$$

$$C_B = \begin{cases} 0 & \theta \geq 0 \\ -\theta & \theta < 0 \end{cases} \tag{15}$$

Therefore, in the fast reaction limit, by computing the time history of the conserved scalar θ, we can obtain the entire time history of the reactants.

We can also obtain the product field in the infinite rate case by considering the conserved scalar defined by

$$\phi = C_P + C_A \tag{16}$$

Assuming that the diffusivity of the product is the same as for both of the reactants, then by adding Equations (1) and (5) we find that ϕ also satisfies Equation (13), i.e., it is a conserved scalar. (Note, however, that the initial conditions for ϕ are different than those for θ.) Once C_A has been obtained using θ, then C_P can be obtained from ϕ.

For initial conditions for the reactant concentrations, we use the following functional forms:

$$C_A(\underset{\sim}{x},0) = 1 - \frac{1}{z_o\sqrt{\pi}} \int_{-\infty}^{z} \exp\ -\zeta^2/z_o^2\ d\zeta \tag{17}$$

$$C_B(\underset{\sim}{x},0) = \frac{1}{z_o\sqrt{\pi}} \int_{-\infty}^{z} \exp\ -\zeta^2/z_o^2\ d\zeta \tag{18}$$

Note that there are no initial concentration fluctuations. The initial product concentration, $C_P(\underset{\sim}{x},0)$, is taken to be identically zero. We choose these functional forms because they give profiles not unlike those measured in the laboratory (see, e.g., Konrad, 1977), they are smooth and easily resolvable using sine/cosine expansions, and analytic solutions can be obtained for special cases using these initial conditions.

In order to separate the effects of the large-scale, quasi-two-dimensional structure and the smaller-scale three-dimensional turbulence in a mixing layer on the overall reaction rates, we have considered a series of three simulations. The simulations all have the same initial conditions for concentration, but differ in the initial conditions on the velocity fields. The three components in the series are (i) laminar, unidirectional flow, (ii) two-dimensional vortex rollup, and (iii) three-dimensional flow with vortex rollup and smaller-scale turbulence. The two-dimensional simulations model the large-scale structures in the mixing layer, and the three-dimensional

simulations contain both the large-scale structures as well as the smaller-scale turbulence. The initial conditions for these three flows are defined as follows.

For the laminar, unidirectional flow, the initial velocity is taken to be

$$\underset{\sim}{u}(\underset{\sim}{x},0) = \left[U(z),0,0 \right] \tag{19}$$

$$U(z) = \frac{U}{2} \tanh \left(0.55 \frac{z}{z_M} \right) \tag{20}$$

Here U is the velocity difference across the layer, and z_M is the distance from the plane of symmetry to the transverse plane where the mean velocity rises to one-half its free-stream value. This profile is a good approximation to the mean velocity profiles measured in the laboratory in a mixing layer downstream of a splitter plate. The time development of this field is very simple, since the nonlinear terms in the momentum equation [Equation (3)] are identically zero. The profile broadens with time as the velocity diffuses in the transverse direction. With the kinematic viscosity set to zero, the velocity field remains stationary in time. The chemistry problem is also greatly simplified for this case, since the convection terms in the species conservation equations are also identically zero. Therefore, mathematically the problem reduces to the one-dimensional problem of the diffusion of one species into another, which has been studied extensively and for which exact solutions are available (e.g., Burke and Schumann, 1928).

For the two-dimensional vortex rollup case, we define the initial conditions for the velocity field as

$$\underset{\sim}{u}(\underset{\sim}{x},0) = \left[U(z) - \frac{\partial}{\partial z} \psi(\underset{\sim}{x}), \frac{\partial}{\partial x} \psi(\underset{\sim}{x}), 0 \right] \tag{21}$$

The mean velocity is the same as in the previous case. However, a perturbation has been added to it in terms of a stream function ψ defined by

$$\psi(\underset{\sim}{x}) = \psi_H(\underset{\sim}{x}) + \psi_{SH}(\underset{\sim}{x}) \tag{22}$$

Here ψ_H is the stream function for the most unstable mode of the mean velocity profile, and ψ_{SH} is the stream function of the subharmonic of the most unstable mode. (See Michalke, 1964, for a discussion of the properties of these modes and Riley and Metcalfe, 1980a, for results of calculations using these initial conditions.) The presence of only the fundamental mode in the mixing layer produces a single vortex rollup. When the subharmonic is added in, but

out-of-phase* with the fundamental, then a second rollup occurs (see the figures discussed in Section 6.2 of this report and Peyret and Taylor, 1983, p. 4, for contour plots of the vorticity field during rollup). The calculations reported here have used various initial conditions consisting of the fundamental mode alone, the subharmonic mode alone, and the fundamental and subharmonic modes added together out-of-phase.

The methodology for initial conditions for the three-dimensional case is similar to that used by Riley and Metcalfe (1980a) in their three-dimensional simulations. (See also Riley and Metcalfe, 1978, and Orszag and Pao, 1974, for a discussion of this initialization procedure.) The initial velocity field is written as

$$\underset{\sim}{u}(\underset{\sim}{x},0) = \left[U(z) + u'(\underset{\sim}{x}),\ v'(\underset{\sim}{x}),\ w'(\underset{\sim}{x})\right] \tag{23}$$

where again the mean velocity is taken to be the same as in the two previously discussed cases. The fluctuating velocity field $\underset{\sim}{u}'$ is defined by

$$\underset{\sim}{u}'(\underset{\sim}{x}) = P\left\{I(z)\ \underset{\sim}{A}(\underset{\sim}{x})\right\} \tag{24}$$

where the form function I(z) is used to define the transverse profile of the root-mean-square (rms) velocity, and the operator P is a projection operator (in Fourier space) used to insure that the initial velocity field is incompressible. The vector $\underset{\sim}{A}$ is written in terms of its Fourier-sine/cosine transform [See Equations (9) and (10)], and its spectral amplitudes are chosen so that the velocity field $\underset{\sim}{u}'$ has the longitudinal (x) energy spectrum

$$E_1(k_1) = \frac{2}{\pi}\,\tilde{u}^2\,\frac{\Lambda}{1 + k_1^2\,\Lambda^2} \tag{25}$$

where Λ is the longitudinal integral scale and $\tilde{u}$ the turbulence intensity. The laboratory data of Wygnanski and Fiedler (1970) were used to initialize the

*The term "out-of-phase" means that the cores of the fundamental mode vortices do not coincide with the cores of the subharmonic vortex.

flow. The initial rms profile, which defines the function I(z), was taken to be

$$\frac{\tilde{u}(x)}{U} = 0.18 \exp\left(-0.147 \frac{z^2}{z_M^2}\right) \tag{26}$$

where z_M is as defined above. (Note that the exponential coefficient is given incorrectly in Riley and Metcalfe, 1980a, and in Peyret and Taylor, 1983, p. 257). The longitudinal integral scale Λ, which defines the energy spectrum [Equation (25)], was taken to be

$$\frac{\Lambda}{z_M} = 2.0 \tag{27}$$

In the three-dimensional simulations, in order to obtain a single vortex rollup, the size of the computational domain in the streamwise direction, L_x, was taken to be equal to the wavelength of the fundamental mode. To obtain a double rollup, L_x was extended to be the wavelength of the subharmonic.

In a particular realization of the flow field, the vector $\underset{\sim}{A}$ is generated numerically, consistent with the energy spectrum defined by Equation (25), using a pseudorandom-number generator. The resulting velocity field is a very complex, three-dimensional field which, when averaged, has approximately the desired mean velocity, turbulence intensity, and longitudinal energy spectrum. As previously mentioned, the temporally growing mixing layer is consistent with statistical homogeneity in the x-y plane (or along the x-axis in the two-dimensional case). Therefore, to obtain statistical quantities from our simulations, averages were taken in x-y planes at a given z, i.e.,

$$\overline{f(\underset{\sim}{x})} = \frac{1}{N_x N_y} \sum_{i,j=1}^{N_x,N_y} f(i\Delta x, j\Delta y, z) \tag{28}$$

Here N_x and N_y are the number of grid points in the x- and y-directions, respectively, and $(\Delta x, \Delta y, \Delta z)$ define the computational grid spacing. These averages correspond to averages computed from data obtained from probes fixed in space in a laboratory experiment in which the flow moved past the probes.

In the results presented, velocities are nondimensionalized by U, the mean velocity difference across the layer. Time is nondimensionalized by the

inverse of the maximum initial mean vorticity, $T = (dU/dz)^{-1}$, and distances are nondimensionalized by the length, $L = UT$. Species concentrations are normalized by $C_\infty = C_{A\infty}$, the free-stream value of C_A. Important nondimensional numbers for our problem are the Reynolds number, $R_L = UL/\nu$, the Schmidt number, $Sc = \nu/D$, and the first and second Damkohler numbers, $D_I = LRC_\infty/U$ and $D_{II} = L^2RC_\infty/D$. The latter describe the ratio of the convection time scale to the reaction time scale and the ratio of the diffusion time scale to the reaction time scale. Table 1 contains a list of these parameters for the calculations discussed in this report.

Note that, for the cases reported herein, we have, without loss of generality, taken the stoichiometric coefficient to be 1. We have only considered the restricted case where the diffusivities of both of the reactants and the product are the same and have only treated reacting species whose free-stream concentrations are in stoichiometric proportion, i.e., $C_{A\infty} = C_{B\infty}$. Realizing that the numerical resolution requirements for the velocity field and species concentration fields are very similar, we have also selected the Schmidt number to be O(1). Note that this is approximately the case in most gaseous mixtures. The entire range of reaction rates is considered, from no reaction, through moderate speed reactions, to the infinite reaction rate limit.

The Reynolds number was kept low enough to adequately resolve the fluid motion on the computational grid. The maximum turbulent Reynolds number, where the turbulent Reynolds number is defined by

$$R_\lambda = \frac{\tilde{u}\lambda}{\nu} \tag{29}$$

with λ the Taylor microscale, was about 50. This is considerably lower than turbulent Reynolds numbers for related laboratory experiments. For example, in the experiments of Breidenthal (1978), who worked with chemical reactions in water, the turbulent Reynolds number was typically the order of several hundred. This difference in Reynolds numbers does not appear to be too important for quantities that depend principally on the large-scale structure of the turbulent flow, e.g., the mean velocity and turbulence intensities (see Riley and Metcalfe, 1980a, and Metcalfe and Riley, 1981). However, for reactions occurring on turbulent flows, which depend critically on the small-scale turbulence stretching out the reaction zone to enhance the overall reaction rate, this difference in Reynolds numbers could be significant.

For nonreacting flows, high Reynolds number cases have been considered by introducing subgrid-scale modeling (see, e.g., Deardorff, 1970; Moin and Kim, 1982). This involves spatially filtering the primitive dynamic equations so that only resolvable scales of motion are left. (The technique is then often referred to as large eddy simulations.) The effects of the filtered, or subgrid-scale, motions are modeled in a manner similar to usual turbulence closure models. The hope is that, since (i) there is little energy in the subgrid scales and (ii) small-scale turbulent motions tend to be universal, this approach offers a significant advantage over the Reynolds averaging approach. For the studies reported herein, we have resolved all the significant scales of motion by lowering the Reynolds numbers and reaction rates, thus avoiding any subgrid-scale modeling assumptions. Questions of subgrid-scale modeling for reacting flows can be addressed at a later time.

5. NUMERICAL TESTS

In order to determine the effectiveness of applying pseudospectral numerical methods to reacting flow problems and also to validate the computer codes, we defined a series of test problems of increasing complexity. The first several were based upon the color problem, i.e., the advection of a passive scalar field by a velocity field consisting of rigid body rotation. Exact, analytical, time-dependent solutions for the concentration fields were obtained in specific cases. Other tests were carried out for more complex flow fields by examining the conserved scalar, i.e., the difference between the two computed concentrations of reacting species [see Equation (12)]. The velocity field computations were checked by comparing computed solutions with solutions obtained from other validated computer codes. Among the critical factors affecting the numerical accuracy in computing reacting flows are the tendency to develop steep concentration gradients for large reaction rates and the spurious effects caused by the presence of negative concentration values, which occur near regions containing steep gradients. As mentioned in the previous section, a simple filtering scheme [see Equation (11)] was used to avoid this latter problem.

The first case computed was the color problem (see, e.g., Orszag, 1971; McRae et al., 1982). In this problem, initially conically distributed concentration fields are rigidly advected in a circular motion around an axis of rotation. There is no diffusion or chemical reaction. The exact solution at time t is just the initial field rotated through the angle Ωt, where Ω is the angular velocity of advection. This is a nontrivial test of the numerical scheme, since the equations are solved in a fixed frame of reference so that the concentration field is rotated through the computational grid. Figure 5 is a plot of the initial concentration field for these tests, showing a localized, conical distribution. All of the tests using the rigidly rotating flow field were performed on a square 64x64 point computational grid with each side of length π, the rotation rate Ω was 2π, and the time stepping was selected to give 2000 time steps per revolution so that time-stepping errors were negligible. In these first color problem tests, the filtering scheme was not used. Figure 6 shows the concentration field after one revolution. Since the exact solution after one revolution should just be equal to the initial field, a comparison of Figures 5 and 6 shows the distortion of the solution due to

numerical errors. Clearly the sharp peak and other features of the cone are accurately maintained. The maximum deviation from the exact solution (L_∞-error) is 2.36%. These results are similar to those of Orszag (1971) and should be compared with the results of McRae et al. (1982), which were obtained using other numerical methods and are of significantly poorer quality.

To determine the accuracy of computing the reaction rate terms in Equations (1) and (2), we computed the rigid rotation color problem just described, but with the reaction rate terms active. We chose the initial concentration fields to be identical. The exact solution for the concentration of either species can be easily found to be

$$C(\underset{\sim}{x}',t) = \frac{C(\underset{\sim}{x}',0)}{1 + R\, C(\underset{\sim}{x}',0)\, t} \tag{30}$$

where $C(\underset{\sim}{x},0)$ is the initial concentration field, and $\underset{\sim}{x}'$ is the position $\underset{\sim}{x}$ measured in the rotating coordinate system. The peak value of the initial concentration was 1.0. Figure 7 is a plot of the computed concentration field after one-half revolution with no reaction, while Figure 8 gives the concentration of either of the reactants at the same time for a case with the reaction rate coefficient R equal to 1.0. Due to the reaction process, the shape has changed somewhat, and the peak value has dropped to 0.66. Again small oscillations are observed throughout the field, with the L_∞-error equal to 2.76% of the initial peak value. Figure 9 shows the results of a similar calculation at one-half revolution with R equal to 4.0. The peak has dropped to a value of 0.334, and the L_∞-error is 2.64% of the initial maximum.

The accuracy of the calculation of the diffusion terms (without reaction) in Equations (1) and (2) can be determined by computing the evolution on the rigidly rotating flow field of the scalar field with the initial condition

$$C(x,z,0) = \exp\left(-\frac{x^2}{x_o^2} - \frac{z^2}{z_o^2}\right) \tag{31}$$

In the rotating reference frame ($\underset{\sim}{x}'$), the analytical solution is

$$C(x',z',t) = \frac{1}{\sqrt{\left(1 + \frac{4Dt}{x_o^2}\right)\left(1 + \frac{4Dt}{z_o^2}\right)}} \exp\left[-\frac{x'^2/x_o^2}{\left(1 + \frac{4Dt}{x_o^2}\right)} - \frac{z'^2/z_o^2}{\left(1 + \frac{4Dt}{z_o^2}\right)}\right] \tag{32}$$

Figure 10 is a contour plot and Figure 11 is a perspective plot of the initial concentration field, and Figures 12 and 13 show the resulting computed concentration field after one revolution. The comparison with the exact solution shows that the errors are within 1% of the peak value.

To test the numerical accuracy with both the diffusion and reaction terms present, we chose to address the evolution of two species diffusing and reacting across a mixing layer and use solutions which could be obtained for the conserved scalar [see Equation (12)]. In these and the following simulations with chemical reactions, the filtering scheme [Equation (11)] was applied every N time steps. In an accurate calculation, the solution should not depend strongly on N, and we found that choosing N between 5 and 15 worked well. For the initial concentration profiles given by Equations (17) and (18), and for the laminar, unidirectional flow field [Equation (19)], the exact solution for the conserved scalar field θ can be found to be

$$\theta(z,t) = \frac{2}{z_o\sqrt{\pi\left(1 + \frac{4Dt}{z_o^2}\right)}} \int_{-\infty}^{z} \exp\left(\frac{-\zeta^2/z_o^2}{1 + \frac{4Dt}{z_o^2}}\right) d\zeta \qquad (33)$$

Using the 2D code with a 64x64 point computational grid, the one-dimensional mixing layer problem was computed for a range of diffusivities and reaction rate coefficients (see Table 1). The conserved scalar θ was computed from the difference between the two computed concentration fields and was then compared to the exact solution. Errors were less than 1% of the maximum concentrations.

We next applied the same initial concentration profiles, but used the two-dimensional vortex rollup velocity field [see Equations (21) and (22)]. A 64x64 point computational grid was again used. The diffusion reaction equations were solved for C_A and C_B on this flow field, and the conserved scalar computed from these solutions. The conserved scalar was also computed directly by solving the diffusion equation (without reaction). Because of the fast convergence of the spectral series for θ, its numerical solution can be obtained very accurately when it is solved for directly. The solution for θ is independent of the reaction rate R, and so is equally valid when steep gradients in C_A and C_B are present. Thus, a comparison of solutions for θ computed by the two different methods serves as a useful check of the methodology. For run MR04A, Figure 14 gives a contour plot of the conserved

scalar computed indirectly from the difference between the species concentrations, and Figure 15 gives a similar plot for the conserved scalar computed directly, both at the time of 12, at which vortex rollup has occurred. Except in the very smallest details of the +1 and -1 contours, the plots are virtually identical. These results are typical of the cases computed. This approach of using the conserved scalar as a numerical check was used throughout our subsequent calculations, both with the 2D and 3D codes.

We also checked the accuracy of each calculation by computing the species conservation invariant

$$I = \int_V \left(C_A + \frac{1}{n} C_B - 2C_P \right) \, dv \tag{34}$$

In the simulations listed in Table 1, over the course of a calculation this quantity generally deviated from the initial value by less than 0.02%.

The accuracy of the velocity field computation was checked by comparing a calculation of nonlinear vortex pairing in a mixing layer with previous calculations performed using a different numerical code that had been fully debugged and validated (Riley and Metcalfe, 1980a). The results of the calculations using the two codes were essentially identical. This completed the testing and debugging of the 2D code.

The 3D code, which was developed in collaboration with Steven A. Orszag, was validated by using it to compute two-dimensional problems and comparing the results with those from the 2D code simulations. Test runs were made for the two-dimensional reacting mixing layer, both with and without vortex rollup. In addition, in order to test the three-dimensional capabilities of the code, separate calculations were made with the direction of the mean flow parallel to each of the horizontal axes. Finally, the velocity field was checked by performing simulations of fully turbulent mixing layers and comparing the results with previous simulations made with different computer codes (Riley and Metcalfe, 1980a; Metcalfe and Riley, 1981).

6. NUMERICAL RESULTS

6.1 One-Dimensional Mixing Layer

The first in our series of simulations was the calculation of the time development of the concentration of reacting species on a one-dimensional mixing layer. The purposes of these simulations were (i) to examine the dependence of the overall reaction rate on the reaction rate coefficient R, on the diffusivities [see Equations (1) and (2)], and on the initial concentration profiles and (ii) to establish a base against which to compare the effects of vortex rollup and three-dimensional turbulence on the overall reaction rates.

The initial conditions for the concentration of the reacting species are given by Equations (17) and (18), and those for the velocity field are given by Equations (19) and (20). As discussed in Section 4, for this case the convective terms in the species concentration equations [Equations (1) and (2)] and the Navier-Stokes equations [Equation (3)] are identically zero, so that the velocity field does not influence the behavior of the concentration fields. The problem reduces to that of the interdiffusion and reaction of the two species, which has received much attention in the past. Burke and Schumann (1928) obtained the exact solution to this problem for the special case of an infinite reaction rate and initial concentrations defined by

$$C_A(z,0) = C_{A\infty} H(-z) \tag{35}$$

$$C_B(z,0) = C_{B\infty} H(z) \tag{36}$$

where $H(z)$ is the Heaviside step function, and $C_{A\infty}$ and $C_{B\infty}$ are the free-stream values of C_A and C_B, respectively. For the case of the reactant concentrations in stoichiometric proportion away from the reaction zone (i.e., $C_{A\infty} = C_{B\infty}$), their solution for the total (integrated) product becomes

$$\hat{P} = \int_{-\infty}^{\infty} C_P(\zeta,t)\, d\zeta = 2C_{A\infty} \left(\frac{Dt}{\pi}\right)^{1/2} \tag{37}$$

The notation $\hat{f}$ is used to denote the result obtained by integrating f over the entire domain in z.

The one-dimensional calculations were carried out for the range of parameters listed in Table 1. Figure 16 contains plots of the total product versus time taken from simulations for two different values of the reaction rate coefficient R. Also shown is the exact solution [Equation (37)] obtained by Burke and Schumann. The values of R were near the maximum that could be used in the simulations while still maintaining sufficient numerical accuracy. We see that, in the finite reaction rate cases, the product formation has approximately the same time dependence as in the infinite reaction rate case, that the overall reaction rate is somewhat insensitive to the value of the reaction rate coefficient for these examples (an increase in the reaction rate coefficient by a factor of 2 produces only about a 5% increase in the overall reaction rate), and that the total product is closely approaching the infinite reaction rate limit. Our interest is primarily in reactions that are controlled more by diffusion and convection than by the actual local value of the chemical reaction rate. Thus, we have chosen to address these faster reaction rate (and infinite reaction rate) cases in our study.

Figure 17 contains results for the total product versus the diffusivity for a fixed value of time (t = 24). We see that again the values are close to the infinite reaction rate results, the dependence on the diffusivity being approximately to the one-half power. Figure 18 shows results for the total product versus time for a given reaction rate coefficient and diffusivity but for two different initial concentration profiles. The length scale in the definition of the initial profiles [z_o in Equations (17) and (18)] differed by a factor of 4 in the two cases. The effect of this difference in profiles is not very significant, especially for larger times. This is probably due to the fact that the reaction rates initially are very high, due to the initial overlap of the two species, causing the rapid buildup of steep concentration gradients along the reaction interface. These steep gradients depend mainly on the balance established between the diffusion and reaction at the interface and so are somewhat insensitive to the initial profile. The reaction then proceeds at a rate that is approximately diffusion-limited. This insensitivity to the initial concentration profile is also exemplified by our comparisons of computed results with the theory of Burke and Schumann (in Figures 16 and 17). Our initial concentration profiles are not discontinuous, as is assumed by the theory, and yet the computed results are in reasonable agreement with the theory.

6.2 Two-Dimensional Mixing Layer

The second in our series of simulations was the two-dimensional mixing layer. In these simulations, a small perturbation is added to the initial velocity field [see Equations (21) and (22)], which causes the flow field to roll up. This vortex rollup is qualitatively similar to that observed in laboratory visualizations of laminar and turbulent mixing layers and has some quantitative features in common with them as well (Riley and Metcalfe, 1980a). This two-dimensional vortex rollup appears to be the essential large-scale structure in a three-dimensional, turbulent mixing layer (see, e.g., Browand and Ho, 1983). The two-dimensional simulations thus allow us to separate out the effects of the large-scale structure from the smaller-scale turbulence and, at the same time, to take the first step in simulating the turbulent mixing layer. The purposes of this step in our series of simulations are (i) to isolate these large-scale structures in the mixing layer and (ii) to examine their influence on the chemical reactions.

For these simulations, the same initial conditions for the concentration fields are used as for the one-dimensional case [Equations (17) and (18)]. The perturbation added to the initial velocity field was in the form of the most unstable (fundamental) mode and/or the subharmonic of this mode. The mathematical solutions for these modes are obtained by solving the Orr-Sommerfeld equation for the velocity profile, given by Equation (20), and are discussed in detail by Michalke (1964).

Figure 19 gives a sequence of constant contour plots of the vorticity for the case where the initial perturbation consisted of the most unstable mode alone (Case 1). Because vorticity is conserved following a fluid element (except for diffusive effects) for two-dimensional flows, vorticity is useful as a tracer to visualize the flow. Vortex rollup is discernible at a time of 4, the rollup attains its maximum extent at about a time of 12, after which the vortex collapses since there is no subharmonic present for pairing to take place. When the subharmonic alone is present (Case 2, see Figure 20), vortex rollup is underway at a time of 12, the maximum extent of rollup occurs at about a time of 24, and subsequently the layer collapses. The behavior of these two flows is very similar, the characteristic length and time scales being a factor of about 2 greater for the subharmonic case (Acton, 1976). Finally, when the fundamental and subharmonic are added together out-of-phase

(Case 3, see Figure 21), a double rollup occurs, the primary rollup occurring at about a time of 8, and the secondary rollup peaking at about a time of about 24. The growth of the mixing layer, as measured by z_M, the distance from the axis of symmetry to the point at which the average value has attained one-half of its free-stream value, is given for each of these cases in Figure 22. The general qualitative conclusions obtained from the contour plots are evident. (See Riley and Metcalfe, 1980a, for a more detailed discussion of the mechanics of the growth and collapse of the vortex cores.)

The contour plots of the concentrations of the reactant and product fields give considerable insight into the reaction history. Figure 23 contains contour plots of species A and B for Case 1 at the time of 12, when the rollup has been completed and collapse has just begun. We see that large regions of fluid containing species A have been convected from the upper into the lower region and vice versa. The reaction zone is defined by the interface between the two species and has been lengthened significantly by the vortex rollup. The gradients of the two species appear very steep at this interface. Constant contours of the product field are given in Figure 24 for the same time. We see that the product field is located along the reaction zone, that it has very steep gradients along the braids of the vortices, and that it is more diffuse in the vortex core. It is interesting to compare the constant contour plots of the product field and vorticity field (Figure 19d). Both only exist near the reaction zone, gradually diffusing outward, so that their appearances are very similar. A contour plot of the product field at a time of 24 (Figure 25) shows that, after collapse has occurred, mixing and reaction continue in the central layer, causing a somewhat uniform concentration of product there.

Figure 26 contains a sequence of constant contour plots of the concentration of species A for Case 2, the subharmonic rollup case. The severe stretching of the reaction zone and vortex rollup are clearly visible by a time of 24. Again, we see a large region of fluid containing species A protruding into that containing species B. At the time of 36, collapse has occurred, and species A has almost been depleted in the interior of the vortex core. Therefore, although the reaction interface has been significantly lengthened by the vortex rollup, it has also been shortened due to the depletion of species A (and species B) in the vortex interior. This latter effect has been conjectured in several theories (see, e.g., the "flame shortening" mechanism discussed by Marble and Broadwell, 1977). Figure 27 is

a constant contour plot of the product at the time of 24. The product again appears somewhat diffuse in the vortex core but localized along a thin region in the braids. Comparing Figure 27 with the contour plot for the vorticity at the same time (Figure 20b), the similarity in the profiles for these quantities is again noted.

Figure 28 contains a sequence of constant contour plots of the concentration of species A for Case 3, the double rollup case. The rollup of the fundamental mode and the initial stages of the subharmonic are evident at the time of 12. At a time of 24, the peak in the second rollup has occurred. However, species A has been significantly depleted in the vortex core at this time, another example of flame shortening. By a time of 36, collapse is occurring, and the continued stretching of the reaction interface and flame shortening are clearly evident. The fact that flame shortening has happened somewhat sooner for Case 3 than Case 2 (compare Figures 26b and 28b) indicates that more reactant is being consumed in Case 3, so that the double rollup causes a larger overall reaction rate. Figure 29 shows the product field at a time of 24. The vortex core, in which the product is rather diffuse, is clearly evident, as well as the thin layer of product along the braids. Comparing Figure 29 with the corresponding plot for the vorticity (Figure 21b) again shows the similarity between the two quantities.

As in the one-dimensional case, calculations were performed for different initial concentration profiles and different reaction rate coefficients (see Table 1). For the range of concentration profile length scales [z_o defined in Equations (17) and (18)] studied, the results were again relatively insensitive to this length scale (see Figure 18). Furthermore, for the reaction rate coefficients considered, the results were close to the infinite reaction rate limit, and hence the reactions were diffusion and convection limited.

In order to compare the two-dimensional results with the one-dimensional results, integrated (total) averages were defined by

$$\hat{\bar{C}}(t) = \int_0^{L_z} \bar{C}(\zeta,t)\, d\zeta \tag{38}$$

where $\hat{g}$ defines the integral over all z of the function g, $\bar{f}$ indicates a spatial average of f [see Equation (28)], and the transverse (z) boundaries in

the computational domain are denoted by 0 and L_z. Note that of course for the one-dimensional case, $\bar{f} = f$. Figure 30 gives the time development of the integrated mean product both for the one-dimensional simulations and for Case 1 (the fundamental mode alone) of the two-dimensional simulations, and for three different diffusivities. Comparing a one- and a two-dimensional case for a given diffusivity, we see that for short times the total products are about the same. However, as the mixing layer rolls up in the two-dimensional simulation (at a time of about 8), the total product is greatly increased. The final value of the product for these two-dimensional simulations is also plotted in Figure 17. The enhanced amount of product due to the vortex rollup is evident. Also, the dependence of the results on the diffusivity is significantly different. The velocity field has to some extent exerted a controlling influence on the overall reaction.

Figure 31 gives a similar plot for the integrated mean reaction rate for the same cases. Again, the enhancement of the reaction rate by vortex rollup and the influence of the diffusivity are both evident. It is interesting that, for the two-dimensional simulations, as the diffusivity is decreased, the peak in the integrated reaction rate is delayed somewhat in time. Vortex rollup is stretching the reaction interface and bringing the two species in closer proximity, but diffusion is still necessary to cause the reaction to occur. Also note that, after the rollup has abated (see Figure 25), and the reactants in the middle layer have been greatly consumed, the integrated reaction rate decreases to near the value for the one-dimensional case.

The simplest estimate of the average reaction rate $R\overline{C_A C_B}$, the average of the product of concentrations, is given by the product of the average concentrations $R\bar{C}_A\bar{C}_B$. The usefulness of this estimate can be determined by examining the mixedness parameter M, defined by

$$M = \frac{\overline{C_A C_B}}{\bar{C}_A \bar{C}_B} \tag{39}$$

This quantity is related to the intensity of segregation parameter defined by Danckwerts (1952) in order to determine the degree of spatial segregation of the reacting species. [Related parameters have been defined by, e.g., Sutton (1968) and Donaldson and Hilst (1972).] When M approaches 1, the species do not tend to be spatially segregated, and the product of the averages $R\bar{C}_A\bar{C}_B$ is a

good estimate of the average reaction rate. However, as M becomes small, the reactants are more spatially isolated (at least in the direction of averaging), and the product of the averages becomes a poorer estimate of the average reaction rate. An integrated mixedness parameter $\hat{M}$ can be defined by

$$\hat{M} = \frac{\widehat{\overline{C_A C_B}}}{\widehat{\overline{C_A}\,\overline{C_B}}} \tag{40}$$

where the numerator and denominator are appropriate integrated values. Figure 32 gives plots of the integrated mixedness parameter versus time for the Case 1 simulations and various diffusivities. Because of the initial conditions, $\hat{M}$ is initially 1. As the flow develops in time, $\hat{M}$ decreases as the species become segregated (along the direction of averaging). $\hat{M}$ also decreases with decreasing diffusivity, since sharper reaction zones are defined and the species become more segregated. Note that for larger times, after the maximum layer extent has been attained and collapse has occurred, $\hat{M}$ again approaches 1, since the reactants become more uniformly mixed in the central region (Figure 25). It is clear from these results that the approximation of the average reaction rate by the product of the averages would be a poor estimate for these cases, overestimating the true average reaction rate by a factor of at least 9.

It is also of interest to compare the integrated averages for the various rollup cases, i.e., for the fundamental mode alone (Case 1), the subharmonic mode alone (Case 2), and the fundamental and subharmonic out-of-phase (Case 3). Figure 33 contains plots of the integrated products as functions of time for these cases. In comparing the results for Cases 1 and 3, we see, somewhat surprisingly, that the effect of the second rollup on the integrated product is not apparent until after a time of about 22, when the second rollup has just about reached its maximum (see Figure 22). Apparently, only when the vortex cores begin to merge is the reaction rate enhanced by this second rollup. Also, the subharmonic rollup (Case 2) takes more time to enhance the integrated product. However, its effect is ultimately greater than the effect of the fundamental mode alone, since the subharmonic rollup entrains more reactants into the mixing layer. A tentative conclusion from these figures is that, for the parameter range considered, the straining of the reaction interface is not nearly as important a mechanism in enhancing the reaction rates as is the merging of the species in the vortex core.

The effect of the different rollup cases on the integrated mixedness parameter is shown in Figure 34. We see that the subharmonic rollup and double rollup result in even smaller values of $\hat{M}$, and that these values are maintained for much longer in time, since the collapse and mixing of the central layer take much longer to occur. Again, the product of the average concentrations would give a poor estimate of the average reaction rate.

When the integrated product is divided by a characteristic concentration, say the free-stream concentration of species A, a length scale results which indicates the product thickness. When this length scale is compared to a characteristic scale of the velocity field, a nondimensional estimate of the effectiveness of the mixing layer in enhancing the reaction rate is obtained. Such a quantity has been measured experimentally (Breidenthal, 1978; Mungal, 1983) and is defined by

$$P = \frac{1}{C_{A\infty}} \int_0^{L_z} \overline{C}_P(\zeta,t)\, d\zeta \Big/ \delta_v(t) \tag{41}$$

where the mean vorticity thickness δ_v is defined by

$$\delta_v(t) = U \left\{ \frac{\partial}{\partial z} \overline{U}(z,t) \Big|_{z=0} \right\}^{-1} \tag{42}$$

Figure 35 contains plots of this nondimensional product thickness versus time for the three different cases computed. Of course, the product thickness is initially zero, since the initial product concentration is identically zero. The nondimensional thicknesses increase with time until the collapse of the layer occurs. After collapse, the product thickness continues to grow, whereas the mean vorticity thickness decreases (as does z_M, see Figure 22). Similar results taken from laboratory
data and from three-dimensional simulations are discussed in the next section.

Up to this point we have mainly considered integrated averages, which give information about the overall behavior of the reaction. More insight into the details of the reaction can be gained by examining spatially averaged quantities. For the two-dimensional case, spatial averages are defined [see Equation (28)] as an average in the x-direction for fixed z. As was pointed

out in Section 4, this spatial average is analogous to a time average in a spatially growing mixing layer in the laboratory.

Figure 36 contains plots of the average concentration of species A, $\overline{C}_A$, versus the transverse coordinate z for several different times from Case 1. The growth of the mixing layer in terms of this average concentration is apparent. Note that a fairly uniform region forms in the center, which is probably an indication of the vortex core. Because of the symmetry in this problem, $\overline{C}_B(z) = \overline{C}_A(-z)$, so that the profile for $\overline{C}_B$ can be easily obtained from that for $\overline{C}_A$. When this is done, it becomes apparent that there is a large region of overlap of $\overline{C}_A$ and $\overline{C}_B$, even though the contour plot (Figure 23) indicates that the two species are highly segregated. This is the reason for the large value of the product of the averages, $\overline{C}_A\overline{C}_B$, compared to the average of the product, $\overline{C_AC_B}$. Figure 37 contains plots of the rms values of the concentration fluctuations of species A, $\tilde{C}_A$, versus z for the same case and times. Again, the growth of the mixing layer is apparent from these plots. When the average and rms of the concentrations are compared (Figure 38), it is observed that, in the central core and on the upper side of the layer, the rms is almost equal to the average. This is a characteristic property of highly intermittent processes. Finally, Figure 39 contains plots of the average product concentration versus z for the same case and times. Note that the product field is identically zero at the beginning of the calculation. The growth of the product as the reaction proceeds and also the growth of the mixing layer are apparent in these plots. The results for the same average quantities taken from other two-dimensional cases lend themselves to the same qualitative interpretation.

If we decompose the dependent variables in terms of their average values and fluctuations about the average, e.g.,

$$C = \overline{C} + C' \tag{43}$$

where f' denotes the fluctuation about the average of f, then the average reaction rate can be written as

$$R\overline{C}_A\overline{C}_B = R[\overline{C}_A\overline{C}_B + \overline{C'_AC'_B}] \tag{44}$$

The term $\overline{C'_AC'_B}$, called the concentration correlation function, is clearly the correction needed in the estimate of the average reaction rate by $R\overline{C}_A\overline{C}_B$.

Figure 40 displays these quantities for Case 1 at a time of 12. Note that, as indicated by our results for the mixedness parameter, the average product of the concentrations is much less than the product of the averages. The correlation function is almost equal to the negative of $\bar{C}_A\bar{C}_B$, their small difference giving the average reaction rate. Note that many theories suggest that, in the fast reaction limit, the sum of $\bar{C}_A\bar{C}_B$ and $\overline{C'_A C'_B}$ will be of the order of the second Damkohler number taken to the minus 1 power (see, e.g., Gibson and Libby, 1972). Also note that a good estimation of the correlation function is a necessary ingredient for a useful theory using the moment equations. Again, the same statistics were computed for the other two-dimensional cases, and the results were in qualitative agreement with the above.

Dynamic equations can also be developed for the concentration correlation function and for the mean square concentration fluctuations (see, e.g., Donaldson and Hilst, 1972). When this is done, the following additional terms appear in the equations: $\bar{C}_A\overline{C'_A C'_B}$, $\bar{C}_A\overline{C'^2_B}$, $\overline{C'^2_A C'_B}$, $\bar{C}_B\overline{C'_A C'_B}$, $\bar{C}_B\overline{C'^2_A}$, and $\overline{C'^2_B C'_A}$. Note that, because of the symmetry of our problem, the first, second, and third terms are the symmetric images of the fourth, fifth, and sixth terms, respectively. In the moment equation approach, the triple correlation terms (as well as other turbulent diffusion and concentration dissipation terms) need to be modeled. Figure 41 contains plots of $\overline{C_A C'_A C'_B}$, $\overline{C_A C'^2_B}$, and $\overline{C'^2_A C'_B}$ versus z for Case 1 at a time of 12. The term $\bar{C}_A\,\overline{C'^2_B}$ is large and always positive, since both $\bar{C}_A$ and $\overline{C'^2_B}$ are necessarily nonnegative. On the other hand $\bar{C}_A\,\overline{C'_A C'_B}$ is large and always negative, since $\bar{C}_A$ is nonnegative and $\overline{C'_A C'_B} \approx -\bar{C}_A\bar{C}_B$ appears to be always negative. Finally $\overline{C'_A C'^2_B}$ is roughly asymmetric about the plane of symmetry of the mixing layer. The negative values indicate that fluctuations in C_B are associated with negative values of C_A, while the opposite holds true for the positive values. Again, similar results have been obtained for the other two-dimensional cases.

Even more insight into the reaction process can be obtained by examining the probability density functions (pdf's) for the species concentrations. Because any moment of a random variable can be obtained from its pdf, the pdf contains the entire information about these moments. As discussed in the introduction, pdf's have also become an important theoretical/numerical tool in the understanding and prediction of reacting flows. Therefore, it is useful to examine the behavior of the pdf's for our computed flows. The pdf's are computed from our simulations in the following manner. The range over

which the concentration can vary (in our case from 0 to 1 since the concentrations have been normalized by their free-stream values) is divided into equally spaced bins. At a given value of the transverse coordinate z, and for every grid point in the x-direction, the value of the concentration is tested, and 1/N is added to the appropriate bin, where N is the total number of grid points in the x-direction. The resulting value for the n^{th} bin is just the probability for the concentration to be within the limits defined by that bin.

Figure 42 shows the pdf for the concentration C_A at the transverse distance $\pi/2$ for Case 1 and for various times. We see that for the earliest time shown (t = 6), all of the grid points contain concentrations in the range of 0.9 to 1, since the reaction had not yet reached this level. The reaction zone enters this layer at about a time of 8. At the times of 12 and 18, the probability densities have become rather flat, with large values still in the bin near 1. This latter fact indicates that an appreciable part of this level still contains fluid with only species A. At the time of 24, the probabilities of the larger values of concentration have increased considerably, probably indicating the collapse of the layer.

It is also interesting to examine the spatial behavior of the pdf's. To do this we choose the time of 12, when the mixing layer for this case has reached its maximum extent and has started to collapse. From Figure 23, which contains contour plots of C_A for this case and time, we learn that the mixing layer has rolled up, and that some fluid with only this species has actually penetrated unmixed into the lower region. Strong gradients exist in the braids of the mixing layer, whereas the concentration is more diffuse in the vortex core. Figure 43 displays pdf's at four different positions across the layer at this same time. At the lowest level ($z = -3\pi/4$), all of the concentration values lie near 1, since the reaction zone has not reached this level. At the next higher level ($z = -\pi/2$), the pdf has become flat, with a large value in the bin near 1. For the levels nearer the plane of symmetry, the profiles are flat, but with large values both near 0 and 1. The large value near 0 implies that parts of the fluid at this level contain no species A, while the large value near 1 indicates a region of only species A. The flat portions of the profiles result from the diffusion and reaction zones. These pdf results are entirely consistent with the contour plots and, in some ways, help describe them. Again, similar results have been found for other two-dimensional cases.

6.3 Three-Dimensional Mixing Layer

The third in our series of simulations was the three-dimensional mixing layer. These calculations were intended to simulate three-dimensional turbulent flows with chemical reactions, similar to experiments that have been carried out in the laboratory. The purposes of the simulations were (i) to examine the combined influence of the large-scale structure and smaller-scale three-dimensional turbulence on the chemical reactions, (ii) to compare results of the simulations with applicable theoretical models, and (iii) to determine the validity of the methodology by comparisons with laboratory data.

The initial conditions for the two concentration fields were the same as in the one- and two-dimensional cases [see Equations (17) and (18)]. The velocity field was initialized using the laboratory data of Wygnanski and Fiedler (1970), as discussed in Section 4. A particular realization of the initial flow field was intended to model the turbulent flow, and hence was a somewhat complex three-dimensional flow. When averages in the x-y plane were taken over an initial field [see Equation (28)], some of the resulting average properties of the flow were close approximations to corresponding quantities taken from the laboratory data, in particular, the mean velocity and turbulence intensity profiles and the longitudinal integral scale. Different realizations of the statistically same flow field (i.e., taken from the same ensemble) could be generated, which give an estimate of the statistical scatter in the averaged results. In the following we will often give the results from two independent realizations from the same ensemble in order to indicate the statistical scatter in the results.

In the two-dimensional simulations, in order to obtain a single rollup, either the fundamental or the subharmonic mode was added to the mean velocity to initialize the flow. To obtain multiple rollup, the fundamental and subharmonic were added in, but out-of-phase. In the three-dimensional simulations, in order to obtain only a single rollup, the extent of the computational domain in the x-direction was restricted to be smaller than the wavelength of the subharmonic mode (usually this extent was taken to be equal to the wavelength of the fundamental mode), so that the subharmonic could not develop and a second rollup occur. To compute multiple rollup, the domain length was extended to include the subharmonic mode. (Usually, for the multiple rollup case, the extent of the computational domain was taken to be

the wavelength of the subharmonic mode.) The spectrum of the initial turbulence energy [Equation (25)] is very broad, so that appreciable energy exists in the fundamental and subharmonic modes to cause the vortex rollup.

In the three-dimensional simulations, although energy exists at the wavelength of the most unstable mode (and at the wavelength of its subharmonic when the computational domain is large enough), the most unstable mode itself has not been added to the initial field. Also, this field is random and somewhat isotropic. Therefore, although vortex rollup is expected to occur, it will not take place in as coherent a fashion as in the two-dimensional simulations.

There are a number of ways in which one might generate the initial conditions for a turbulent mixing layer, and the choice of the initial conditions might have a significant influence in determining the outcome of the simulations. For example, it has been found from laboratory experiments that the initial conditions can exert a strong influence on the resulting mixing layer, especially in the near field of the layer (see, e.g., Hussain and Zedan, 1978). Our initial conditions are intended to model a fully developed turbulent mixing layer, or the mixing layer produced by fully turbulent boundary layers coming off a splitter plate. Such a flow might lack the two-dimensional organization which has been observed in many laboratory experiments (see, e.g., Browand and Troutt, 1980), although whether the large-scale features of turbulent mixing layers are strongly two-dimensional is presently very controversial (see, e.g., Dimotakis and Brown, 1976; Chandrsuda et al., 1978). Other possibly reasonable initial conditions include (i) the initial mean velocity given by Equation (20) with a low-level perturbation field, having a fairly broad spectrum, superimposed, and (ii) flows with the same statistical properties as ours in terms of the mean velocity, turbulence intensity, and integral scale, but with strong coherence in the y-direction, so that the flow will be more well-organized two-dimensionally. Case (i) would involve a calculation of transition to turbulence, which is a complete study in itself (see Patera and Orszag, 1981, for simulations of a particular aspect of this transition), while the method of determining the y-coherence in case (ii) is unclear. Since our results for the velocity field were in reasonable agreement with laboratory data using the present initialization method (Riley and Metcalfe, 1980a; Metcalfe and Riley, 1981), we decided to use this method in the present investigation.

Figures 44 and 45 give a temporal sequence of contour plots of the y-component of the vorticity in two different x-z planes that are located a distance $L_y/2$ apart. We see that initially the vorticity is in a fairly narrow region and has a somewhat random orientation. As the flow develops, the vorticity begins to become concentrated in local regions, and by a time of about 16 there is what appears to be vortex rollup. Note however that rollup takes longer to occur than in the two-dimensional simulations (see Figure 19), it does not appear to be as strong, the braids between the vortices are not as distinct, and there is little lateral coherence in the flow. Figure 46 gives a temporal sequence of contour plots of the concentration of species B for reactions occurring on the same velocity field and x-z plane as depicted in Figure 44. Again, the rollup can be observed. However, the concentration gradients do not appear to be as steep as in the two-dimensional case (Figure 23), probably due to the small-scale mixing and to the less vigorous vortex rollup.

We next examine the behavior of various length scales that characterize the mean velocity field and the mean product field. Figure 47 contains results from our simulations for the mean velocity half-width, z_M, the distance from the plane of symmetry to the transverse plane where the mean velocity takes on one-half its free-stream value. Data are presented for two different realizations of the single rollup case and for a double rollup case. Similarity theory (see, Tennekes and Lumley, 1972) suggests that this quantity, or any characteristic length scale, should vary linearly with time. We see that the results are in approximate agreement with this theory. Although not shown explicitly in this figure, in the single rollup case, the results begin to deviate from linearity at a time of about 24, whereas this deviation occurs in the double rollup case for times greater than 36. This is expected since, when the second vortex rollup is inhibited by the lack of a subharmonic, the layer growth rate is substantially reduced, and in fact it can become negative (collapse). These preceding results are consistent with those reported by Riley and Metcalfe (1980a; see also Metcalfe and Riley, 1981). As discussed in Section 3, Riley and Metcalfe (1980a) found that the behavior of z_M was consistent with laboratory data if space and time were assumed to be related by the transformation given by

$$x = \frac{1}{2}(U_1 + U_2)t$$

The present results are also consistent with laboratory data if the same assumption is made. Figure 48 contains similar data for the mean vorticity thickness [see Equation (42)]. We see that again the growth rate is approximately linear, consistent with similarity theory.

The mean product thickness, z_p, defined by

$$z_p = \frac{1}{C_{A\infty}} \int_0^{L_z} \overline{C}_p(\zeta,t)\, d\zeta \tag{45}$$

was also computed from our simulations. Figure 49 contains plots of the mean product thickness versus time. Included are data from two different realizations for the single rollup case, from a double rollup case, from a simulation with the molecular diffusivity D increased by a factor of 2 over its usual value, and for an infinite reaction case. Again, similarity theory suggests that this length scale should increase linearly with time, and again the results are in approximate agreement with the theory. Comparing the results for the two independent realizations, we find that the results deviate by about 5% to 10% at the end of the calculation. A comparison of the results for the two different diffusivities indicates that increasing the diffusivity by a factor of 2 results in a less than 10% increase in the product thickness. In contrast, the theoretical result of Burke and Schumann (1928) for the interdiffusion and reaction of two species with no velocity field predicts an increase of about 40%. Comparing the single and double rollup cases leads to the conclusion that the results are approximately the same up to a time of about 20, when the growth in the single rollup case is inhibited by the lack of a subharmonic. Finally, comparing the results for the infinite reaction case with those for the finite reaction cases, we find that the infinite reaction rate leads to about a 15% increase in the product thickness.

As discussed in the previous subsection, the mean product thickness divided by the mean vorticity thickness is a useful parameter with which to compare experimental data. Figure 50 is a plot, taken from Mungal (1983), of this thickness ratio as a function of the equivalence ratio ($\phi = C_{A\infty}/C_{B\infty}$). These data were taken from experiments performed in a gaseous mixing layer, so the Schmidt number was approximately 1 as in our simulations. For an equivalence ratio equal to 1, which is then the same as in our simulations, Mungal's thickness ratio equals approximately 0.35. Similar data from Wallace

(1981) give a value of about 0.3. Breidenthal (1978) measured the thickness ratio in experiments in water. His Schmidt number was approximately 600, and his equivalence ratio was about 200. If the experiments in water have approximately the same dependence on equivalence ratio as the previously discussed experiments in a gas, then Breidenthal would obtain a thickness ratio of about 0.23 for an equivalence ratio of 1. A recent model by Broadwell and Breidenthal (1982) suggests that the differences between the results of Breidenthal and those of Mungal and Wallace are due to the substantial difference in the Schmidt number.

Figure 51 contains results for the thickness ratio as a function of time from our various three-dimensional simulations. We see that the thickness ratio starts from zero and ultimately attains an approximately constant value of about 0.2 for the finite reaction rate case and 0.22 for the infinite reaction rate case. Thus, the results are very close to those of Breidenthal, but are about 25% to 30% below those of Mungal and Wallace. Since the value of the Schmidt number in our calculations is 1, we would expect better agreement with the latter experiments. However, the above agreement must be considered reasonably good, especially since there are no adjustable parameters in our calculations.

Another nondimensional quantity of interest is the integrated mixedness, defined by Equation (40). Figure 52 contains results for this quantity computed from various three-dimensional simulations. Comparing these results with similar results from two-dimensional simulations (Figure 32), we see that the mixedness in the former case is not as small as in the latter, indicating that the reacting species are not quite as segregated in the three-dimensional case as in the two-dimensional case. This is probably due to the small-scale three-dimensional turbulence and also the lack of coherent vortex rollup in the three-dimensional simulations.

We next examine the behavior of some of the spatially averaged quantities [see Equation (28) for a definition of the spatial average]. Figure 53 contains a sequence of plots of the mean concentration of species A, $\overline{C}_A$, for a number of selected times for the first realization of the double rollup case. The growth of the mixing layer and the depletion of this species by the reaction are evident from this plot. Figure 54 gives a similar sequence for the concentration of species B for the same conditions. Note that, due to the symmetry of this problem, $\overline{C}_B(z) = \overline{C}_A(-z)$ should hold. This is approximately the case, and

the deviation from it gives some indication of the statistical scatter in our results. Note also the large overlap in the profiles for $\bar{C}_A$ and $\bar{C}_B$ for the later times. Figure 55 contains a sequence of plots for $\bar{C}_A$ taken from the second realization at the same times. As described at the beginning of this section, comparing the results again gives a good indication of the statistical scatter in our results.

Figure 56 contains plots of the rms of the fluctuating concentration of species A for the first realization and the same times. Initially, this fluctuating concentration is zero. However, it rapidly grows and attains an approximately constant maximum value of about 0.31 $C_{A\infty}$. The profiles tend to be somewhat skewed to the lower side of the mixing layer, since this is the region containing species A. The growth of the layer is also apparent from this plot. Figure 57 provides the same profiles for species B for the same conditions. Again the symmetry condition $\tilde{C}_B(z) = \tilde{C}_A(-z)$ should hold, which is approximately the case. Figure 58 contains similar profiles for species A taken from the second realization. Again, there is approximate agreement between the results for the two realizations.

Figure 59 contains plots of $R\overline{C_A C_B}$, $R\bar{C}_A\bar{C}_B$, and $R\overline{C'_A C'_B}$ for the first realization at the time 12. From Equation (44) we know that the first term, the mean reaction rate, is equal to the sum of the second two terms. It is clear from the figure that the product of the means is, as in the two-dimensional case, not a good estimate of the mean of the products. These results are typical of our other three-dimensional calculations.

Figure 60 contains plots of $\bar{C}_A\,\overline{C'_A C'_B}$, $\bar{C}_A\,\overline{C'^2_B}$, and $\overline{C'^2_A\,C'_B}$ for the first realization of the time of 12. From symmetry conditions, these should be symmetrically related to $\bar{C}_B\,\overline{C'_A C'_B}$, $\bar{C}_B\,\overline{C'^2_A}$, and $\overline{C'^2_B\,C'_A}$, respectively. Note that, as discussed in the previous subsection, these terms are of importance in the equations for $\overline{C'^2_A}$, $\overline{C'^2_B}$, and $\overline{C'_A C'_B}$. As in the two-dimensional case, the function $\bar{C}_A\,\overline{C'^2_B}$ is large and positive, $\bar{C}_A\,\overline{C'_A C'_B}$ is large and negative, and $\overline{C'^2_B C'_A}$ is roughly asymmetric about the axis of symmetry. The interpretation of these results is qualitatively the same as for the two-dimensional case. Apparently, the two-dimensional dynamics govern the basic behavior of these quantities. Figure 61 contains plots of the same quantities for the second realization at the same time. Note the significant scatter in the result for $\overline{C'^2_A C'_B}$. It is common in analyzing statistical data that the errors increase with the order (power) of the statistical quantity.

A theoretically and experimentally useful method to analyze results for flows with simple geometries is in terms of similarity theory. Similarity theory implies that there is a characteristic length scale (ℓ), velocity scale (U, and hence time scale ℓ/U), and concentration scale (C) which should characterize all of the results of an experiment. (See, e.g., Tennekes and Lumley, 1972, for a lengthy discussion of similarity theory.) For a temporally developing flow, these scales should only depend on time, and, for example, the mean velocity should be given by

$$\bar{u}(z,t)/U(t) = f(z,t) = g[z/\ell(t)] \tag{46}$$

Therefore, when similarity holds, if the mean velocity is normalized by U and the transverse coordinate z by ℓ, then the data should collapse when plotted for various times. In the case of the mixing layer, the characteristic velocity scale should be a constant in time and can be taken to be the velocity difference across the layer, U. The characteristic concentration scale should also be a constant, and can be taken to be the free-stream value of one of the reacting species, e.g., $C_{A\infty}$. The length scale should vary linearly with time and can be taken to be the mean velocity half-width z_M or the mean vorticity thickness δ_v, which should be proportional. It has been found from laboratory experiments for turbulent mixing layers that the statistics of both the velocity field (see, e.g., Wygnanski and Fiedler, 1970; Brown and Roshko, 1974) and the reacting species fields (see, e.g., Konrad, 1977; Mungal, 1983; Batt, 1977) agree well with similarity theory. Because of the theoretical implications of this theory, and also because of the good agreement of this theory with laboratory data, it is important to determine the consistency of our computed results with this theory.

We have already presented data for the time dependence of various length scales in our computed flows. We found that both the mean velocity half-width (Figure 47) and the mean vorticity thickness (Figure 48) vary approximately linearly with time, in agreement with similarity theory. We also found that the product thickness (Figure 49) grew approximately linearly with time, again consistent with the theory. Thus, all three scales remain proportional, and a single scale characterizes the flow field. We have found from previous studies (Riley and Metcalfe, 1980a; Metcalfe and Riley, 1981) that the mean velocity, turbulence intensity, and Reynolds stress were all in approximate

agreement with similarity theory. We next explore whether the results for the concentration fields are consistent with this theory.

Figure 62 contains a sequence of plots of the average concentration of species A plotted in similarity coordinates for various times in a double rollup, finite reaction rate calculation. The concentrations have been scaled by the free-stream value of C_A, while the transverse distance z has been scaled by the mean velocity half-width z_M, computed from the mean velocity profiles. We see that, except for the initial condition, the collapse of the data is excellent. Note that the width of the mixing layer as measured by z_M grows by a factor of more than 5 over the course of this calculation, so that the average concentration itself has changed significantly over this time frame (see Figure 53). Figure 63 is a similar plot for the concentration of species B. Again the collapse of the data using the similarity scaling is very good. Also note that the symmetry in the problem implies that $\overline{C}_B(z,t) = \overline{C}_A(-z,t)$. Comparing Figures 62 and 63, we see that this is approximately the case.

Figure 64 contains a similar sequence of plots of the rms concentration fluctuation of species A taken from the double rollup results. Initially, the concentration fluctuations are zero, due to the initial conditions. However, the concentration fluctuations adjust and become approximately self-similar with a peak value of about 0.29. The profiles tend to be somewhat skewed to the bottom of the mixing layer, the region containing species A. This behavior is qualitatively similar to that for laboratory data (see, e.g., Konrad, 1977). Some insight into these results can be obtained by examining the dynamic equation for the mean square concentration fluctuation, i.e.,

$$\frac{\partial}{\partial t}\left(\frac{\overline{C_A'^2}}{2}\right) + \overline{w'C_A'}\frac{\partial}{\partial z}\overline{C}_A + \frac{\partial}{\partial z}\left(\frac{\overline{w'C_A'^2}}{2} - D_A\frac{\partial}{\partial z}\frac{\overline{C_A'^2}}{2}\right)$$

$$= -R\left(\overline{C}_A\,\overline{C_A'C_B'} + \overline{C_A'^2}\,\overline{C}_B + \overline{C_A'^2C_B'}\right) + D_A\overline{\left(\frac{\partial C_A'}{\partial x_j}\right)^2} \qquad (47)$$

and noting the behavior of the various concentration correlations given above (see Figure 60). We find that the principal generation terms appear to be $\overline{w'C_A'}\frac{\partial}{\partial z}\overline{C}_A$, which can be interpreted as the generation of concentration fluctuations resulting from turbulent diffusion along the mean concentration gradient (a work-like term if the analogy between concentration fluctuations

and turbulence kinetic energy is made), and $R\bar{C}_A\ \overline{C'_A C'_B}$, which also appears as a source term in the equation for $\overline{C'^2_A}$. The term $\overline{w'C'^2_A/2}$ represents the turbulent diffusion of $\overline{C'^2_A}$. $\overline{C'^2_A}$ is dissipated by the last term on the right hand side of Equation (47), the usual turbulence dissipation term, and $R\overline{C'^2_A}\ \bar{C}_B$, which represents the loss of $\overline{C'^2_A}$ resulting from the decrease in C_A due to the chemical reaction. Not that the peak in $\overline{C'^2_A}$ tends to lie near the high gradient region of $\bar{C}_A$ (compare Figures 62 and 64). This indicates that the work-like term, which generally has its maximum near the region with the largest gradient in C_A, is a significant contributor to the generation of $\overline{C'^2_A}$. We hope to further investigate the dynamics of the concentration fluctuations in the future by carefully comparing the various terms in Equation (47). Figure 65 contains similar plots for the concentration fluctuation for species B. Again, the agreement with similarity theory is rather good. From the problem of symmetry, the relation $\tilde{C}_B(z,t) = \tilde{C}_A(-z,t)$ should hold, and comparing Figures 64 and 65 we find that this is approximately the case.

We next examine the behavior of the concentration fluctuation correlation, which is plotted in Figure 66 in similarity coordinates for a sequence of times for the double rollup case. This quantity is also initially zero because of the initial conditions. However, it also becomes approximately self-similar, with a peak value of about -0.03. There is somewhat more scatter in this result, which is expected since the statistical error in computing correlation functions is generally higher than when computing averages and mean squares. Symmetry conditions imply that this correlation function should be an even function of z, which is approximately the case.

It is interesting to examine the effect of the reaction rate on the concentration statistics. Figure 67 contains similarity plots of the average concentration of species A for various times taken from a double rollup, infinite reaction rate calculation. The velocity field used in these calculations was identical to that used in the previous finite rate calculations. We see that the similarity scaling collapses the results very well for this case, and, comparing Figures 62 and 67, that the reaction rate has very little effect on the average concentration. Figure 68 contains a similar plot for the rms concentration fluctuation for the infinite reaction rate case. Again, agreement with similarity scaling is rather good. Comparing

Figures 64 and 68 we see that the rms concentration is about 15% higher in the infinite reaction rate case.

For the infinite reaction rate case, the product field was also computed. Figure 69 contains a sequence of similarity plots of the average concentration of the product for various times taken from the same double rollup calculation as reported above. Initially, the product field is finite and is determined by both the initial conditions on the concentration fields [Equations (17) and (18)] and also the interpretation of the product field in terms of conserved scalars [see Equation (16) and following]. The product field initially adjusts and then shows good agreement with similarity scaling, attaining a peak value of approximately 0.30. The average product profile has an approximately symmetric, Gaussian shape, which is qualitatively similar to laboratory results for experiments with equivalence ratios of about 1 (see Mungal, 1983).

Figure 70 contains similar plots for the product concentration fluctuation. This quantity is initially zero and also becomes approximately self-similar, with peak values of roughly 0.15. Note the double-peaked behavior of the plots, which is consistent with laboratory data (Konrad, 1977; Mungal, 1983). This behavior is probably due to the generation of concentration fluctuations occurring in the region of large gradients of $\overline{C}_P$, and is reflected in the turbulence work-like term $\overline{w'C_P'} \frac{\partial}{\partial z} \overline{C}_P$ in the equation for $\overline{C_P'^2}$.

We find that the results of our simulations allow extensive examination and interpretation, both in terms of contour plots of relevant variables and also in terms of various statistical quantities of interest. The results also show good agreement with similarity theory, as does the laboratory data. This is true even for quantities that are initially far from their similarity values. And, without any adjustment of parameters, the results for the nondimensional product thickness are in rough agreement with laboratory data. We next briefly examine some of the implications on existing theories of the results of our calculations.

One modeling approach using the Reynolds-averaged equations (Donaldson and Hilst, 1972) includes, in addition to the equations for $\overline{C}_A$ and $\overline{C}_B$, also the equations for $\overline{C_A'^2}$, $\overline{C_B'^2}$, and $\overline{C_A'C_B'}$. These equations can be closed by assuming that triple moments such as $\overline{C_A'^2 C_B'}$ are small compared to lower order terms like $\overline{C}_A \, \overline{C_A'C_B'}$ and $\overline{C_B'} \, \overline{C_A'^2}$ [see Equation (47)]. However our results indicate that the triple moments are not small in comparison to the lower order terms (see

Figure 60), indicating that a model based upon this assumption will probably lead to poor predictions.

Another approach to closing the Reynolds-averaged equations is due to Mason and Spaulding (1973), and has been termed the eddy-breakup model. A version of this model which is currently being used by Sturgess (1983) assumes that the average reaction rate term is given by

$$\overline{RC_A C_B} = \min(\overline{C}_A, \overline{C}_B)/T \tag{48}$$

Here $\min(\overline{C}_A, \overline{C}_B)$ is the minimum of $\overline{C}_A$ and $\overline{C}_B$, i.e., the concentration of the lean reactant, and T is a turbulence time scale. Similarity theory predicts that T should be constant across the mixing layer and should increase linearly with time. Figure 71 is a plot of the mean reaction rate divided by the eddy-breakup model prediction as a function of the transverse coordinate z. [No attempt has been made to set the proportionality constant implied by Equation (48).] This result is taken from a double rollup, finite reaction rate simulation at a time of 12 but is typical of results computed at other times and from other simulations. The breakup model predicts that this ratio is constant across the layer. However, the value varies appreciably across the layer, indicating a significant difference between the theory and our calculations. Figure 72 displays a plot of the ratio $\min(\overline{C}_A, \overline{C}_B)/\overline{C_A C_B}$, computed along the centerline of the mixing layer, versus time. Again, the result is taken from the double rollup, finite reaction rate case but is consistent with other simulations. The breakup model predicts that this ratio should vary linearly with time, which is in approximate agreement with our results.

A critical term in closing the equations for the average concentrations is the correlation $\overline{RC_A' C_B'}$. For statistically homogeneous flows, Toor (1969) made assumptions about the probability distributions of the reacting species and found that this correlation was identical for the very fast and very slow reaction limits. He then conjectured that the correlation would be the same for all reaction rates. If this is truly the case, then the correlation for the reacting flow case could be predicted using the correlation for the non-reacting flow case. The latter is much easier to predict. It is of interest to see how well this hypothesis holds up for our (nonhomogeneous) simulations. In addition to simulations for the finite and infinite reaction rate cases, we have also performed simulations for the limiting case of no reaction.

Figure 73 contains plots of the concentration fluctuation correlation taken from two-dimensional, single rollup simulations for a nonreacting case and for a finite reaction case. We see that the agreement between the correlations taken from these two cases is quite good. This result is typical of comparisons taken from the two-dimensional simulations. Figure 74 shows a similar comparison taken from three-dimensional simulations. We see that the agreement is not as good as for the two-dimensional case. However, the results do suggest that the theory still might be useful in predicting the correlation.

7. CONCLUSIONS AND DISCUSSION

The work discussed in this report has involved the following tasks. First of all, two computer codes were developed, a two-dimension plus time computer code and a three-dimension plus time computer code. These codes solve the dynamic equations for the diffusion-reaction problem [Equations (1) to (5)] in two and three dimensions, respectively. Next, these codes were extensively tested to determine the reliability of the numerical methods and the parameter ranges over which accurate solutions could be expected. Finally, the following sequence of problems was computed: (i) reactions on a unidirection (one- dimensional) mixing layer, (ii) reactions on a mixing layer experiencing large-scale, two-dimensional vortex rollup, and (iii) reactions on a three-dimensional turbulent mixing layer.

The numerical testing involved the comparison of computed results with exact solutions for a number of different cases. Both rigid body rotation and vortex rollup flow fields were used. The work greatly extended the results of Orszag (1971) for the advection of a passive scalar on a rigidly rotating flow field (the color problem) to include also diffusion, chemical reaction, and more complex flows. We have found that high accuracy of the spectral methods observed in the advection case is also obtained when these further complications are present. For computing reacting species, it was found useful to introduce a weak spatial filter [Equation (11)] to insure numerical stability. Our results indicate that spectral numerical methods may prove to be useful in the future both for solving the model equations for combustor processes as well as for future studies of chemically reacting turbulent flows employing direct numerical simulations.

The approach of direct numerical simulations allowed extensive examination and interpretation of the reaction process. From the one-dimensional simulations, we found that we could easily compute finite reaction rates near the fast reaction limit, that the results were fairly insensitive to the initial conditions (for the class of initial conditions computed), and that the results were in reasonable agreement with theoretical predictions.

For the two-dimensional simulations, we first examined contour plots of the vorticity and concentration fields. We found that vortex rollup both caused large regions of fluid containing one species to be drawn deeply into

the regions originally containing the other fluid and also significantly stretched the reaction zone. However flame shortening, which to some extent moderated this latter effect, was noticed in the cores of the vortices. In all of the cases computed, the vorticity field and the product field approximately coincided.

From the computation of volume averages, we observed the enhancement of the overall reaction rate due to the vortex rollup. It also appeared that the merging of vortex cores was a more significant mechanism in increasing the overall reaction rate than the straining of the reaction interface. And the value of the nondimensional product thickness, the ratio of the product thickness to the mean vorticity thickness, was found to be about 0.07. From the spatially averaged (in the x-direction) data, the growth of the mixing layer, the depletion of the reactant, and the creation of products were observed. Significant species segregation was apparent, so that, for example, the average of the product of the reactant concentrations was very different from the product of the averages. Instead, the product of the average concentrations was approximately equal to and opposite the correlation between the fluctuating concentrations. Some of the higher order correlations were also examined. Probability density functions were computed, which were found to be useful in interpreting the various concentration fields.

In the three-dimensional simulations, the contour plots indicated that the vortex rollup takes longer to develop, and the vortices and braids are not as distinct as in the two-dimensional case. Also, the vortices that develop are not strongly correlated laterally. Both the contour plots and the statistical results indicated that the spatial segregation was also not as strong as in the two-dimensional case, probably due to the weaker vortex rollup as well as the effects of smaller-scale, three-dimensional turbulence.

Comparisons were made between the simulation results and results using similarity theory. Approximately linear growth rates of various computed length scales, including the mean velocity half-width, the mean vorticity thickness, and the mean product thickness, were obtained and were in agreement with the theory. Similarity scaling was found to collapse quite well the results for the average reactant concentrations, the rms fluctuating reactant concentrations, the concentration correlations, the average product concentrations, and the rms fluctuating product concentrations. This collapse

was attained over a time interval in which the width of the layer grew by a factor of over 5, even though the initial conditions for these quantities differed significantly from the similarity values.

Some limited comparisons were made with laboratory data. Of course, the agreement with similarity theory is consistent with the laboratory results, since the laboratory data also agree very well with the theory. Computed profiles that were qualitatively similar to corresponding laboratory profiles were obtained for the average reactant concentrations, the rms fluctuating reactant concentrations, the average product concentrations, the rms fluctuating product concentrations, and the concentration correlations. Finally, the nondimensional thickness ratio was computed to be approximately 0.22 for the infinite reaction case. This is to be compared to the value of 0.3 and 0.35 computed from the data of Wallace (1981) and Mungal (1983), respectively, for flows with Schmidt numbers of order 1, and 0.23 estimated from the data of Breidenthal (1978) for a flow with a very large Schmidt number. Since our Schmidt number is equal to 1, we would expect better agreement with the former results. The agreement must be considered reasonably good, since there were no adjustable parameters in the simulations.

We have made some comparisons with existing theories. Donaldson and Hilst (1972) have suggested, in addition to using the equations for the average concentrations, including the equations for the concentration fluctuations and correlation. These equations can be closed by neglecting certain triple moments when compared to certain lower order terms. However, our results indicate that the triple moment terms are as important as other terms in the equations, so that an assumption of this type will probably lead to poor predictions. Mason and Spaulding (1973) have proposed a model for the mean reaction term, suggesting that it will be proportional to the average concentration of the lean species divided by a turbulent time scale. We have found that such an assumption will only be moderately successful if applied to our case. Finally Toor (1969) has suggested estimating the concentration correlation of the reacting species in terms of that for the nonreacting case, which is much easier to model. Although this was proposed mainly for statistically homogeneous flows, we find that it is a reasonable approximation for our reacting flow simulations.

While our present results inspire optimism in the application of the techniques of direct numerical simulations to chemically reacting turbulent flows, one should still keep in mind the potential differences between our computed flow fields and laboratory experiments. First of all, our simulations have been carried out at a rather low turbulent Reynolds number [R_λ of about 50 compared with values of several hundred for the laboratory experiments (see, e.g., Mungal, 1983)]. Since the Reynolds number is significantly lower, the rate of fluid surface (and hence reaction interface) stretching, which depends directly on the small-scale vorticity field, is diminished. This latter fact implies that the reaction interface does not increase as rapidly in our simulations as in the laboratory experiments, thus possibly decreasing the overall reaction rate. Most theories imply, however, that if the Reynolds number is large enough, the overall reaction rate should not depend on the Reynolds number but only on the rate at which the large-scale structures bring the two species together. The recent theory by Broadwell and Breidenthal (1982) suggests in addition that the overall reaction rate should also depend on the Schmidt number. The question remains as to whether the Reynolds number in our simulations is high enough for Reynolds number similarity to be valid. Previous computations of (nonreacting) wakes (Riley and Metcalfe, 1980b) and mixing layers (Riley and Metcalfe, 1980a; Metcalfe and Riley, 1981) indicated that Reynolds number similarity is at least approximately attained in these simulations. However, a higher Reynolds number may be needed for similarity in reacting flows.

It must also be remembered that our calculations are for the temporally growing mixing layer, whereas all of the reacting flow experiments have been for a spatially growing layer. This difference can be exemplified by the entrainment ratio, defined by Konrad (1977) to be the average amount of fluid entrained into the mixing layer from the high-speed side divided by the average amount of fluid entrained from the low-speed side. For constant density flow with a free-stream velocity ratio of 0.38, Konrad estimated that the entrainment ratio was approximately 4:3, so that 4 parts of fluid from the high-speed layer are entrained into the mixing layer for every 3 parts of fluid from the low-speed layer. Of course, in the temporally growing layer, because of the symmetry in the problem, the entrainment ratio is 1.

The initial (upstream) conditions for our flow fields may be considerably different from those in the reported laboratory experiments, perhaps causing a significantly different flow field to develop. Our initial flow is rather randomly distributed in space (see Figures 44 and 45), whereas in the laboratory, the flow just downstream of the splitter plate is somewhat two-dimensional, even if the boundary layer on the plate is very turbulent, since the splitter plate itself is two-dimensional. It has been established that initial conditions in the mixing layer can have a significant effect on the subsequent layer development, especially in the near field (see, e.g., Hussain and Zedan, 1978). This effect can become more pronounced as more sensitive statistical quantities are examined. The comparisons of our computed results with laboratory data for the case of the mean velocity, turbulence intensities, and Reynolds stress (see Riley and Metcalfe, 1980a; Metcalfe and Riley, 1981) have indicated that the initial conditions were adequate to model the essential physics leading to these quantities. However, it is possible that the reaction rates are more sensitive to the initial conditions.

In order to further explore the effects of initial conditions, simulations with different initial conditions should be computed. Two possible candidates, as discussed in Section 6.3, are the following: (i) the initial mean velocity given by Equation (20) with superposition of a low-level perturbation field, which has a relatively broad spectrum, and (ii) flows with the same statistical properties as ours, but with stronger coherence in the lateral direction, so that the flows will be more well-organized in that direction. Based upon laboratory experiments (Konrad, 1977), case (i) should produce vortex rollup followed by a three-dimensional breakdown consisting of longitudinally oriented vortices. Some simulations of this type (for nonreacting flows) have been carried out by Patera and Orszag (1981). For case (ii), the lateral coherence introduced should be consistent with the results on lateral coherence presented by Browand and Troutt (1980).

In addition to further work on initial conditions, more comparisons with laboratory data are needed in order to determine the level of confidence of the simulation methodology. In particular, detailed comparisons of mean and fluctuating concentration profiles (for both the reactant and the products) should be made. During the course of this study, data could not be found with

which to make such comparisons. However, it appears that if the data of Konrad (1977) and Mungal (1983) are analyzed properly, then such comparisons can be made. Also, some ongoing experiments by Choudbury et al. (1983) may produce results against which to compare our numerical simulations.

Additional simulations can also be performed to learn more about the effects of turbulence on the reaction process. For example, the dynamics of the reaction can be examined in more detail by computing the various terms in the appropriate dynamic equations [for example in Equation (47)] and determining which of the terms are dominant and, thus, which effects are of importance and should be included in any model. Furthermore, calculations can be performed for different choices of parameters. For example, the effects of differences in the diffusivities of the two reacting species could be explored, problems with nonstoichiometric free-stream conditions could be studied, and cases with low- to moderate-speed reactions could be computed. Of additional importance would be to examine cases with more complex reactions, possibly with several reactants and the reactions proceeding in both directions. Use could be made of the scalar approach to compute cases where equilibrium chemistry is assumed (Bilger, 1980).

Finally, of utmost importance is to relax the assumption of no heat release and compute cases where the heat release is allowed to effect both the flow field and the reaction rates. This should probably initially be done in the low Mach number limit so that acoustic waves can be filtered out of the problem (see, e.g., Oran and Boris, 1981). The advantages of this approach are that the numerical time stepping is then not controlled by the acoustic waves, so that the time steps can be increased significantly, and that no radiation boundary conditions are needed. However, the basic physics of interest, the effects of heat release on the turbulence and reaction rates, is retained.

APPENDIX A

NUMERICAL RESOLUTION PROBLEMS

In reacting flows of the type addressed in this report, i.e., mixing layers, that involve the interdiffusion and reaction of nonpremixed species and in which the reaction rate is fast relative to the species diffusion, i.e.,

$$\frac{RL^2C_A}{D} >> 1$$

(see Table 1 for definition of the parameters), very steep gradients can develop in the concentration fields, even from smooth initial conditions. Of course, in the limit of an infinite reaction rate, the reacting species become segregated, and the spatial derivatives of the concentrations are discontinuous at the interface between the species. These steep gradients cause several numerical problems. First of all, the number of modes or grid points necessary to resolve a concentration field to a certain level of accuracy increases with the steepness of the gradients in the field (assuming other factors, such as the size of the computational domain, remain constant). Thus, a calculation can be started with adequate resolution for all the initial fields, but can quickly break down as steep gradients develop. Since the extent to which this happens can depend strongly on the evolution of the flow field, its occurrence can be very difficult to predict a priori. Therefore, a number of calculations may have to be made with increasing spatial resolution to determine if an accurate calculation is possible for a particular flow and species field configuration with a given choice of parameters (e.g., R and D).

An attempt to resolve concentration fields with steep gradients can lead to a second problem, which can also have a detrimental effect on the accuracy of the calculation. Near a region where the concentration field C_A increases rapidly from a value of zero, the numerical approximation can produce a "ringing" or Gibbs phenomenon effect (cf. Wengle and Seinfeld, 1978; McRae et al., 1982) that results in spurious negative values of C_A. As can be seen by an examination of the diffusion-reaction equations [Equations (1) and (2)], if this occurs where C_B is positive, as it might near a reaction zone,

the net effect is an artificial production of C_B and an artificial destruction of the product. While this effect may be somewhat mitigated by the tendancy of the C_A equation to drive C_A back toward zero, if the steep gradient and hence the negative overshoot of C_A persists, a significant error can accumulate over a long time integration. The problem becomes more serious if spurious negative regions of C_A and C_B overlap. For example, neglecting advection and diffusion, and assuming $C_A = C_B < 0$ and $R = 1$, Equation (1) behaves like

$$\frac{dC_A}{dt} = -C_A^2 \tag{A1}$$

or

$$C_A = \frac{C_{A_o}}{(C_{A_o} t + 1)} \tag{A2}$$

where C_{A_o} is the initial value of C_A. This becomes singular when

$$t = -\frac{1}{C_{A_o}}$$

Several approaches have been suggested to address this problem. Cullen (1976) and Raymond and Gardner (1976) have added diffusive or dissipative terms to the equations, and Storch (1978) has added high wave number filtering to damp out the oscillations. Forester (1977) has devised a spatially local nonlinear filtering scheme to decrease the amplitude of the oscillations. A number of other alternatives are discussed by McRae et al. (1982). The most direct approach is to simply enforce the condition [Equation (11)]

$$C(\underset{\sim}{x},t) = \begin{cases} \tilde{C}(\underset{\sim}{x},t) & \tilde{C} > 0 \\ 0 & \tilde{C} < 0 \end{cases} \tag{A3}$$

where $\tilde{C}$ is the value of the concentration prior to applying the restriction. Although this has the apparent disadvantage of violating mass conservation, to the extent that the calculation is accurately resolving the steep concentration gradients, the net effect should be small. In fact, if the results of the simulation are significantly dependent on the filtering or smoothing scheme chosen, the spatial resolution in the calculation may well be inadequate.

In our simulations, we have found that the application of condition (A3) every 5 to 10 time steps works very well in preventing the solutions from diverging, and that the results are quite insensitive to whether the condition is applied every time step or every 10 steps. This suggests that, with the high accuracy of the spectral methods we have employed and in the parameter ranges we have chosen, the approximation errors introduced by the Gibbs phenomenon are small. Also, the most important objective under these conditions is to employ a simple scheme that prevents these small errors from amplifying over the course of the simulation. We have found that our 3D simulations with a turbulent velocity field are less sensitive to the effects of oscillation errors near the interface than are the 2D simulations. For example, we have performed run JN20B both with and without the application of condition (A3) and the energies and other moments differ by less than 0.1% between the two runs. A possible explanation for this is that in a highly structured, coherent flow field like that in our 2D mixing layer simulations, it is possible for regions of overlapping spurious negative concentrations to persist for some time and thus cause the calculation to diverge. In the 3D simulations, however, such regions and the steep gradients that generate them are being advected and deformed much more drastically by the turbulent flow field. The turbulent diffusion acts both to decrease the steepness of the concentration gradients and to prevent possible negative concentration regions from overlapping for a sufficiently long time interval to destabilize the calculation.

APPENDIX B

THE RELATIONSHIP BETWEEN MONTE-CARLO METHODS AND DIRECT NUMERICAL SIMULATIONS

The basic ideas for the application of Monte-Carlo methods to probability density function (pdf) equations stem from the theory of Markov processes and, in particular, Brownian motion (see, e.g., Wax, 1954). A dynamic system is assumed to be described by the following equation:

$$\frac{dv}{dt} + v = f \tag{B1}$$

where v(t) is, for example, the speed of a particle, and f(t) is a forcing function. Here, f is assumed to be a known white noise process, so that v is a stochastic process. The equation for the pdf of the displacement x can be found to be:

$$\frac{\partial P}{\partial t} = D \frac{\partial^2 P}{\partial x^2} \tag{B2}$$

This equation is often referred to as the Fokker-Planck equation, and the dynamic equation is called the Langevin equation. If one is interested in solving an equation of the form given by Equation (B2), then the Monte-Carlo approach is to numerically solve Equation (B1) a large number of times for random, independently selected initial conditions, and to compute the pdf or its moments by averaging over the ensemble of solutions. Note that Equation (B1) is of lower dimension than Equation (B2) and, thus, is generally significantly easier to solve numerically.

Applying these concepts to the pdf equations for reacting turbulent flows, the pdf equation is analogous to the Fokker-Planck equation. What is then needed is an analogous Langevin system. In coalescence-dispersion modeling, this system was invented by Curl (1963), and Monte-Carlo methods have been used to solve for the pdf's and their moments (e.g., Spielman and Levenspiel, 1965; Pratt, 1976). Several authors (see, e.g., the review by O'Brien, 1981) have derived more rigorous pdf equations describing reacting turbulent flows, although adhoc assumptions are still required. Pope (1979) has devised an analogous system for one of these approximate pdf equations, making the application of Monte-Carlo methods again possible.

Of course, the analogous Langevin system for the exact (unmodeled) pdf equations is just the coupled Navier-Stokes and diffusion-reaction equations. A Monte-Carlo solution to the exact pdf equations would require solving this coupled system of equations many times and taking averages over the computed ensemble. However, for a dynamic system that is statistically homogeneous in either space or time, spatial or temporal averages are, under usual conditions, equivalent to ensemble averages. Thus, direct numerical simulations can be considered as a type of Monte-Carlo method, where spatial (or temporal) averages, sometimes supplemented by ensemble averaging over a small number of realizations, are used instead of ensemble averages. Direct numerical simulations have the advantage of a more exact Langevin system than the approaches of Curl or Pope, so that the physical system is modeled better. However, they have the disadvantage of a much more difficult numerical calculation than the previous approaches, so that, in particular, they are more difficult to apply to complex problems.

APPENDIX C

LIST OF SYMBOLS

C_i	molar concentration of species i
$C_{i\infty}$	free-stream value of C_i
C_P	molar concentration of product
D	reactant diffusivity
D_I	first Damkohler number
D_{II}	second Damkohler number
I	species conservation invariant
$\underset{\sim}{K}$	truncation wave number vector
$\underset{\sim}{k}$	wave number vector
L	length nondimensionalization factor = UT
L_x	length of computational domain in streamwise (x) direction
L_y	length of computational domain in lateral (y) direction
L_z	length of computational domain in transverse (z) direction
M	mixedness parameter
N	number of Fourier modes in each spatial direction
n	stoichiometric coefficient
N_x	number of grid points in x-direction
N_y	number of grid points in y-direction
p	pressure
R	reaction rate constant
r	instantaneous reaction rate
Re	Reynolds number
R_L	Reynolds number = UL/ν
R_λ	turbulent Reynolds number = $\tilde{u}\lambda/\nu$
Sc	Schmidt number
T	time nondimensionalization factor = $(dU/dz)^{-1}$
t	time
T_a	activation temperature
T_c	temperature
U	velocity difference across mixing layer

$\tilde{u}$	turbulence intensity
$\underset{\sim}{u}$	velocity field
U_1	free-stream speed of high-speed layer
U_2	free-stream speed of low-speed layer
(x,y,z)	streamwise, lateral, and spanwise coordinates
(u,v,w)	corresponding velocity components
x_o	initial concentration field scaling factor
z_o	initial concentration field scaling factor
z_M	mixing layer half-width
z_P	mean product thickness
Γ	circulation of the vortex
δ_v	mean vorticity thickness
θ	conserved scalar defined in Equation (12)
Λ	longitudinal integral scale
λ	Taylor microscale
ν	kinematic viscosity
ρ	density of fluid
ϕ	conserved scalar defined in Equation (16)
ψ	stream function
ψ_H	stream function for most unstable mixing layer mode
ψ_{SH}	stream function for subharmonic of most unstable mixing layer mode
Ω	angular velocity
ℓ	characteristic length scale

ACKNOWLEDGEMENTS

This work was supported by the NASA Lewis Research Center under Contract No. NAS3-23531. The code used in the 3D simulations was developed in collaboration with Dr. Steven A. Orszag. The work benefited from discussions with Professor R. E. Breidenthal and Dr. W.-H. Jou.

REFERENCES

Acton, E. 1976. "The Modeling of Large Eddies in a Two-Dimensional Shear Layer", J. Fluid Mech., Vol. 76, Part 3, pp. 561-592.

Ashurst, W. T., and P. K. Barr. 1981. "Lagrangian-Eulerian Calculation of Turbulent Diffusion Flame Propagation", presented at the Third Symp. Turb. Shear Flows, pp. 3.44-3.49, University of California, Davis.

Batt, R. G. 1977. "Turbulent Mixing of Passive and Chemically Reacting Species in a Low-Speed Shear Layer", J. Fluid Mech., Vol. 82, Part 1, pp. 53-95.

Bilger, R. W. 1980. "Turbulent Flows with NonPremixed Reactants", in Turbulent Reacting Flows, edited by P. A. Libby and F. A. Williams, Springer-Verlag.

Borghi, R. 1974. "Chemical Reactions Calculations in Turbulent Flow", Adv. Geophysics, Vol. 18B, pp. 349-365.

Breidenthal, R. E., Jr. 1978. "A Chemically Reacting, Turbulent Shear Layer", Ph.D. Thesis, California Institute of Technology.

Broadwell, J. E., and R. E. Breidenthal, Jr. 1982. "A Simple Model of Mixing and Chemical Reaction in a Turbulent Shear Layer", J. Fluid Mech., Vol 125, pp. 397-410.

Browand, F. K., and C.-M. Ho. 1983. "The Mixing Layer: An Example of Quasi Two-Dimensional Turbulence", to appear in J. de Mechanique.

Browand, F. K., and T. R. Troutt. 1980. "A Note on Spanwise Structure in the Two-Dimensional Mixing Layer", J. Fluid Mech., Vol. 97, pp. 771-781.

Brown, G. L., and A. Roshko. 1974. "On Density Effects and Large Structure in Turbulent Mixing Layers", J. Fluid Mech., Vol. 64, pp. 775-816.

Burke, S. P., and T. E. Schumann. 1928. "Diffusion Flames", Ind. Eng. Chem., Vol. 120, p. 998.

Chandrsuda, C., R. D. Mehta, A. D. Weir, and P. Bradshaw. 1978. "Effects of Free-Stream Turbulence on Large Structure in Turbulent Mixing Layers", J. Fluid Mech., Vol. 85, pp. 693-704.

Chorin, A. J. 1973. "Numerical Studies in Slightly Viscous Flow", J. Fluid Mech., Vol. 57, pp. 785-796.

Choudbury, P. R., M. Gerstein, and J. S. Cho. 1983. "A Novel Technique of Concentration Measurement in a Turbulent Reacting Medium", unpublished manuscript.

Cullen, H. J. P. 1976. Quart. J. Roy. Meteorol. Soc., 102, p. 77.

Curl, R. L. 1963. "Dispersed Phase Mixing: 1. Theory and Effects in Simple Reactors", AIChE Journal, Vol. 9, pp. 175-181.

Danckwerts, P. V. 1952. Appl. Sci. Res., Vol. 3, pp. 279-296.

Deardorff, J. W. 1970. "A Numerical Study of Three-Dimensional Turbulent Channel Flow at Large Reynolds Numbers", J. Fluid Mech., Vol. 41, pp. 453-480

Deardorff, J. W. 1974. "Three-Dimensional Numerical Study of the Height and Mean Structure of a Heated Planetary Boundary Layer", Bound. Layer Met., Vol. 7, pp. 81-106.

Dimotakis, P., and G. L. Brown. 1976. "The Mixing Layer at High Reynolds Number: Large-Structure Dynamics and Entrainment", J. Fluid Mech., Vol. 78, pp. 535-560.

Donaldson, C. duP., and G. R. Hilst. 1972. "Effect of Inhomogeneous Mixing on Atmospheric Photochemical Reactions", Env. Sci. Tech., Vol. 6, pp. 812-816.

Donaldson, C. duP., and A. K. Varma. 1976. "Remarks on the Construction of a Second-Order Closure Description of Turbulent Reacting Flows", Comb. Sci. Tech., Vol. 13, pp. 55-78.

Dopazo, C. 1976. "A Probabilistic Approach to Turbulent Flame Theory", Acta Astronautica, Vol. 3, pp. 853-878.

Forester, C. K. 1977. J. Comp. Phys., Vol. 23, p. 1.

Ghoniem, A. F., A. J. Chorin, and A. K. Oppenheim. 1982. "Numerical Modelling of Turbulent Flow in a Combustion Tunnel", Phil. Trans. R. Soc. Lond., Ser. A, Vol. 304, pp. 303-325.

Gibson, C. H., and P. A. Libby. 1972. Comb. Sci. Tech., Vol. 6, pp. 29-35.

Haidvogel, D. B., A. R. Robinson, and E. D. Schulman. 1980. "The Accuracy, Efficiency, and Stability of Three Numerical Models with Application to Open Ocean Problems", J. Comp. Phys., Vol. 34, pp. 1-34.

Herring, J. R. 1974. "Approach of Axisymmetric Turbulence to Isotropy", Phys. Fl., Vol. 30, pp. 859-872.

Herring, J. R., J. J. Riley, G. S. Patterson, Jr., and R. H. Kraichnan. 1973. "Growth of Uncertainty in Decaying Isotropic Turbulence", J. Atmos. Sci., Vol. 30, pp. 303-325.

Hill, J. C. 1979. "Simulation of Chemical Reaction in a Turbulent Flow", in Proc. Second B. F. Ruth Chem. Eng. Res. Symp., pp. 27-53, Iowa State University.

Ho, C.-M., and L.-S. Huang. 1982. "Subharmonics and Vortex Merging in Mixing Layers", J. Fluid Mech., Vol. 119, pp. 443-473.

Hussain, A. K. M. F., and M. F. Zedan. 1978. "Effects of the Initial Condition on the Axisymmetric Free Shear Layer: Effects of the Initial Momentum Thickness", Phys. Fl., Vol. 21, pp. 1100-1112.

Janicka, J., and W. Kollman. 1979. "Prediction Model for the PDF of Turbulent Temperature Fluctuations in a Heated Round Jet", presented at the 2nd Symp. Turb. Shear Flows, Imperial College, London, pp. 1.7-1.11.

Jones, W. P., and J. H. Whitelaw. 1982. "Calculation Methods for Reacting Turbulent Flows: A Review", Combustion and Flame, Vol. 48, pp. 1-26.

Karagozian, A. R. 1982. "An Analytical Study of Diffusion Flames in Vortex Structures", Ph.D. Thesis, California Institute of Technology.

Konrad, J. H. 1977. "An Experimental Investigation of Mixing in Two-Dimensional Turbulent Shear Flows with Applications to Diffusion-Limited Chemical Reactions", Ph.D. Thesis, California Institute of Technology.

Libby, P. A., and F. A. Williams. 1981. "Some Implications of Recent Theoretical Studies in Turbulent Combustion", AIAA Journal, Vol. 19, pp. 262-274.

Mansour, N. N., P. Moin, W. C. Reynolds, and J. H. Ferziger. 1979. "Improved Methods for Large-Eddy Simulations of Turbulence", in Turbulent Shear Flows I, p. 386, Springer-Verlag.

Marble, F. E. 1982. "Growth of a Diffusion Flame in the Field of a Vortex", to appear in Luigi Crocco Anniversary Volume.

Marble, F. E., and J. E. Broadwell. 1977. "The Coherent Flame Model for Turbulent Chemical Reactions", TRW Report 29314-6001-RU-00.

Mason, H. B., and D. B. Spaulding. 1973. "Prediction of Reaction Rates in Turbulent Premixed Boundary Layer Flows", in Proc. First Symp. (European) on Comb., pp. 601-606, Academic Press.

McRae, G. J., W. R. Goodin, and J. H. Seinfeld. 1982. "Numerical Solution of the Atmospheric Diffusion Equation for Chemically Reacting Flows", J. Comp. Phys., Vol. 45, pp. 1-42.

Mellor, A. M., and C. R. Ferguson. 1980. "Practical Problems in Turbulent Reacting Flows", in Turbulent Reacting Flows, editied by P. A. Libby and F. A. Williams, Springer-Verlag.

Metcalfe, R. W., and S. A. Orszag. 1974. "Numerical Simulation of Turbulent Jet Noise -- Part 1", Flow Research Report No. 53.

*Metcalfe, R. W., and J. J. Riley. 1981. "Direct Numerical Simulations of Turbulent Shear Flows", in Proc. Seventh Conf. Num. Methods in Fl. Dyn., pp. 279-284, Springer-Verlag.

Michalke, A. 1964. "On the Inviscid Instability of the Hyperbolic-Tangent Velocity Profile", J. Fluid Mech., Vol. 19, pp. 543-556.

Moin, P., and J. Kim. 1982. "Numerical Investigation of Turbulent Channel Flow", J. Fluid Mech., Vol. 118, pp. 341-377.

Mularz, E. J. 1983. "New Trends in Combustion Research for Gas Turbine Engines", presented at the 6th Intern. Symp. Air Breath. Engines; also NASA T 83338; also AVRADCOM TR 83-C-1.

Mungal, M. G. 1983. "Experiments on Mixing and Combustion with Low Heat Release in a Turbulent Shear Flow", Ph.D. Thesis, California Institute of Technology.

Mungal, M. G., P. E. Dimotakis, and J. E. Broadwell. 1983. "Turbulent Mixing and Combustion in a Reacting Shear Layer", AIAA Paper No. 83-0473.

Nielsen, K. A., and J. C. Hill. 1977. "Numerical Simulation of Turbulent Mixing with Chemical Reaction", 70th Annual AIChE Mtg.

Norton, O. P. 1983. "The Effects of a Vortex Field on Flames with Finite Reaction Rates", Ph.D. Thesis, California Institute of Technology.

O'Brien, E. E. 1969. "Postulate of Statistical Independence of Decaying Reactants in Homogeneous Turbulence", Phys. Fl., Vol. 12, pp. 1999-2005.

O'Brien, E. E. 1971. "On Turbulent Mixing of Two Rapidly Reacting Chemical Species", Phys. Fl, Vol. 14, pp. 1326-1331.

O'Brien, E. E. 1981. "Statistical Methods in Reacting Turbulent Flows", AIAA Journal, Vol. 19, pp. 366-371.

Oran, E. S., and J. P. Boris. 1981. "Detailed Modeling of Combustion Systems", Prog. Energy Combust. Sci., Vol. 7, pp. 1-71.

Orszag, S. A. 1971. "Numerical Simulation of Incompressible Flows within Simple Boundaries: Accuracy", J. Fluid Mech., Vol. 49, pp. 75-112.

Orszag, S. A., and Y.-H. Pao. 1974. "Numerical Computation of Turbulent Shear Flows", Adv. Geophysics, Vol. 18A, pp. 225-236.

Orszag, S. A., and G. S. Patterson, Jr. 1972. "Numerical Simulation of Turbulence", in Statistical Models and Turbulence, p. 127, Springer-Verlag.

Patera, A. T., and S. A. Orszag. 1981. "Transition and Turbulence in Planar Channel Flows", in Proc. Seventh Conf. Num. Methods in Fl. Dyn., pp. 329-335, Springer-Verlag.

Peyret, P., and T. D. Taylor. 1983. Computational Methods for Fluid Flows, Springer-Verlag.

Pope, S. B. 1979. Phil. Trans. Roy. Soc. Lond., Ser. A, Vol. 291, pp. 529.

Pratt, D. T. 1976. "Mixing and Chemical Reaction in Continuous Combustion", Prog. Energy Comb. Sci., Vol. 1, pp. 73-86.

Raymond, W. H., and Gardner, A. 1976. Monthly Weather Rev., 104, p. 1583.

Riley, J. J., and R. W. Metcalfe. 1978. "The Direct Numerical Simulations of the Turbulent Wakes of Axisymmetric Bodies -- An Interim Report", Flow Research Report No. 135, NASA-CR-152282.

*Riley, J. J., and R. W. Metcalfe. 1980a. "Direct Numerical Simulations of a Perturbed, Turbulent Mixing Layer", AIAA Paper No. 80-0274.

*Riley, J. J., and R. W. Metcalfe. 1980b. "Direct Numerical Simulations of the Turbulent Wake of an Axisymmetric Body", in Turbulent Shear Flows II, pp. 78-93, Springer-Verlag.

Riley, J. J., and G. S. Patterson, Jr. 1974. "Diffusion Experiments with Numerically Integrated Isotropic Turbulence", Phys. Fl., Vol. 17, pp. 292-297

Schumann, V., and G. S. Patterson, Jr. 1978. "Numerical Study of the Return of Axisymmetric Turbulence to Isotropy", J. Fluid Mech., Vol. 88, pp. 711-735.

Spielman, L. A., and O. Levenspiel. 1965. "A Monte-Carlo Treatment for Reacting and Coalescing Dispersed Phase Systems", Chem. Eng. Sci., Vol. 20, pp. 247-254.

Storch, H. 1978. Beiträge Phys. Atmosphare, 51, p. 189.

Sturgess, G. J. 1983. "Aerothermal Modeling -- Phase I", United Technologies Report CR 168202.

Sutton, G. W. 1968. AIAA J., Vol. 6, pp. 1403-1405.

Tennekes, H., and J. L. Lumley. 1972. A First Course in Turbulence. MIT Press.

Toor, H. L. 1962. "Mass Transfer in Dilute Turbulent and Nonturbulent Systems with Rapid Irreversible Reactions and Equal Diffusivities", AIChE Journal, Vol. 8, pp. 70-78.

Toor, H. L. 1969. "Turbulent Mixing of Two Species With and Without Chemical Reactions", Ind. Eng. Chem. Fundam., Vol. 8, pp. 655-659.

Wallace, A. K. 1981. "Experimental Investigation of the Effects of Chemical Heat Release in the Reacting Turbulent Plane Shear Layer", Ph.D. Thesis, The University of Adelaide.

Wax, N., Editor. 1954. Selected Papers on Noise and Stochastic Processes. Dover Publications, Inc.

Wengle, H., and Seinfeld, J. 1978. "Pseudospectral Solution of Atmospheric Diffusion Problems", J. Comp. Phys., Vol. 26, pp. 87-106.

Williams, P. A. 1965. Combustion Theory. Addison-Wesley.

Wygnanski, I., and H. E. Fiedler. 1970. "The Two-Dimensional Mixing Region", J. Fluid Mech., Vol. 41, pp. 327-361.

Wygnanski, I., D. Oster, and H. Fiedler. 1980. "A Forced, Plane, Turbulent Mixing-Layer; A Challenge for the Predictor", in Turbulent Shear Flows II, pp. 314-326, Springer-Verlag.

Zalesak, S. T. 1979. "Fully Multidimensional Flux-Corrected Transport Algorithms for Fluids", J. Comp. Phys., Vol. 31, pp. 335-362.

*Reprints available from the authors c/o Flow Research Company, Kent, Washington 98032.

TABLE 1. SIMULATION PARAMETERS*

Two-dimensional simulations

Run No.	ε_H	ε_{SH}	z_o	D	R	ν	Box
MR01A	0.1	0	1.00	0.100	1.00	0.003	2 π
MR01B	0	0	1.00	0.100	1.00	0.003	2 π
MR02A	0.1	0	0.25	0.100	1.00	0.003	2 π
MR02B	0	0	0.25	0.100	1.00	0.003	2 π
MR03A	0.1	0	0.25	0.200	1.00	0.003	2 π
MR03B	0	0	0.25	0.020	1.00	0.003	2 π
MR03C	0.1	0	0.25	0.010	1.00	0.003	2 π
MR03D	0	0	0.25	0.010	1.00	0.003	2 π
MR04A	0.1	0	0.25	0.005	1.00	0.003	2 π
MR04B	0	0	0.25	0.005	1.00	0.003	2 π
MR04C	0.1	0	0.25	0.020	2.00	0.003	2 π
MR04D	0	0	0.25	0.020	2.00	0.003	2 π
MY12B	0.1	0	0.25	0.005	0	0.003	2 π
MY25A	0.1	0	0.25	0.005	1.00	0.003	4 π
MY25B	0.1	0.1	0.25	0.005	1.00	0.003	4 π
MY25C	0	0.1	0.25	0.005	1.00	0.003	4 π
AG10A	0.1	0	0.25	0.005	∞	0.003	2 π

Three-dimensional simulations

Run No.	Realization	z_o	D	R	ν	Box
JN20B	I	0.25	0.005	1.00	0.003	2 π
JN24A	I	0.25	0.01	1.00	0.003	2 π
JL18A	I	0.25	0.005	1.00	0.003	4 π
JL26A	II	0.25	0.005	1.00	0.003	4 π
AG13A	I	0.25	0.005	0	0.003	2 π
AG13B	I	0.25	0.005	∞	0.003	2 π

* The quantities in this table are nondimensionalized by ΔU, the mean velocity difference across the mixing layer, $T = (dU/dz)^{-1}|t = 0$, the inverse mean velocity gradient at the centerline, and by the length scale $L = UT$. The columns ε_H and ε_{SH} specify whether the most unstable mode and/or its subharmonic was introduced in the initial conditions. The value $\varepsilon_H = 0.1$ produced an initial velocity field with $w' = 0.071$ U at the centerline. The initial concentration profile length scale is z_o [see Equations (17) and (18)], D is the reactant diffusivity, R the reaction rate coefficient, ν the kinematic viscosity, and Box is the length of a side of the computational domain, which was the same in all spatial directions. $Re = Uz_o/\nu$ is the Reynolds number, $Sc = n/D$ is the Schmidt number, $D_I = z_o RC_\infty/U$ and $D_{II} = Rz_o^2 C_\infty/D$ are the Damkohler numbers, DT is the time-step increment, and N is the number of Fourier modes in each spatial direction. Runs with $\varepsilon_H = \varepsilon_{SH} = 0$ correspond to laminar, unidirectional (one-dimensional) flow.

TABLE 1. SIMULATION PARAMETERS (Cont.)

Two-dimensional simulations

Run No.	Re	Sc	D_I	D_{II}	DT	N
MR01A	333	0.030	1.00	10.000	0.05	64
MR01B	333	0.030	1.00	10.000	0.05	64
MR02A	83	0.030	0.25	0.625	0.05	64
MR02B	83	0.030	0.25	0.625	0.05	64
MR03A	83	0.015	0.25	0.313	0.05	64
MR03B	83	0.150	0.25	3.125	0.05	64
MR03C	83	0.300	0.25	6.250	0.05	64
MR03D	83	0.300	0.25	6.250	0.05	64
MR04A	83	0.600	0.25	12.500	0.05	64
MR04B	83	0.600	0.25	12.500	0.05	64
MR04C	83	0.150	0.50	6.250	0.05	64
MR04D	83	0.150	0.50	6.250	0.05	64
MY12B	83	0.600	0	0	0.05	64
MY25A	83	0.600	0.25	12.500	0.025	128
MY25B	83	0.600	0.25	12.500	0.025	128
MY25C	83	0.600	0.25	12.500	0.025	128
AG10A	83	0.600	0	0	0.05	64

Three-dimensional simulations

Run No.	Re	Sc	D_I	D_{II}	DT	N
JN20B	83	0.600	0.25	12.500	0.05	64
JN24A	83	0.600	0.25	12.500	0.05	64
JL18A	83	0.600	0.25	12.500	0.05	64
JL26A	83	0.600	0.25	12.500	0.05	64
AG13A	83	0.600	0	0	0.05	64
AG13B	83	0.600	∞	∞	0.05	64

1906R/1872R

Figure 1a t = 0

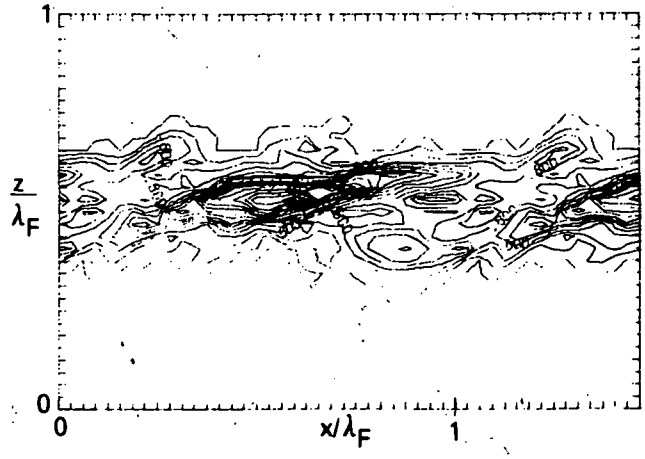

Figure 1b t = 8

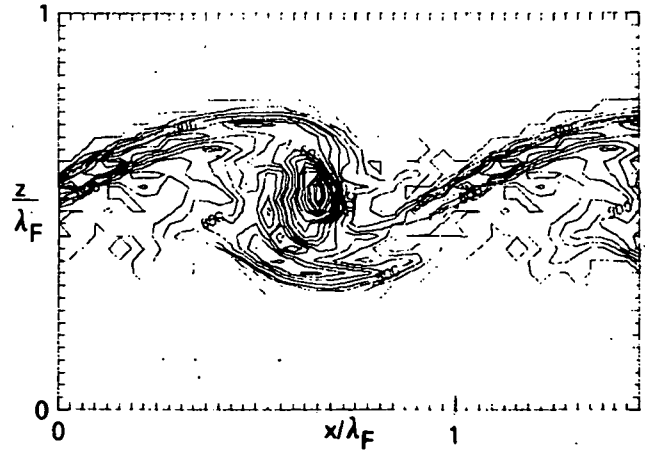

Figure 1c t = 16

Figure 1. Plots of Lateral (y) Vorticity in an x-z Plane (Taken from Riley and Metcalfe, 1980a)

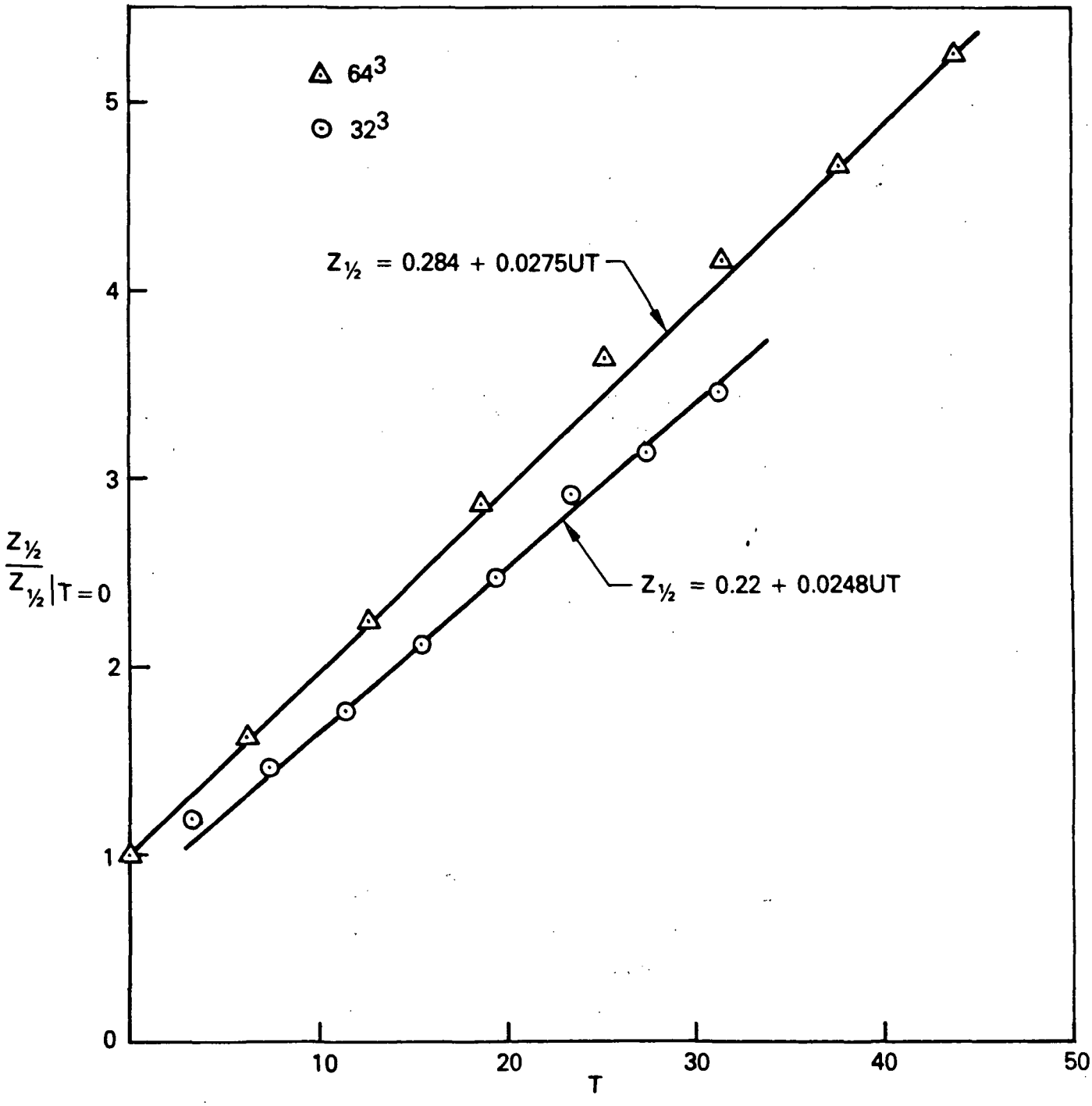

Figure 2. The Mixing Layer Half-Width, z_M (= $z_{1/2}$), Versus Time (Taken from Metcalfe and Riley, 1981)

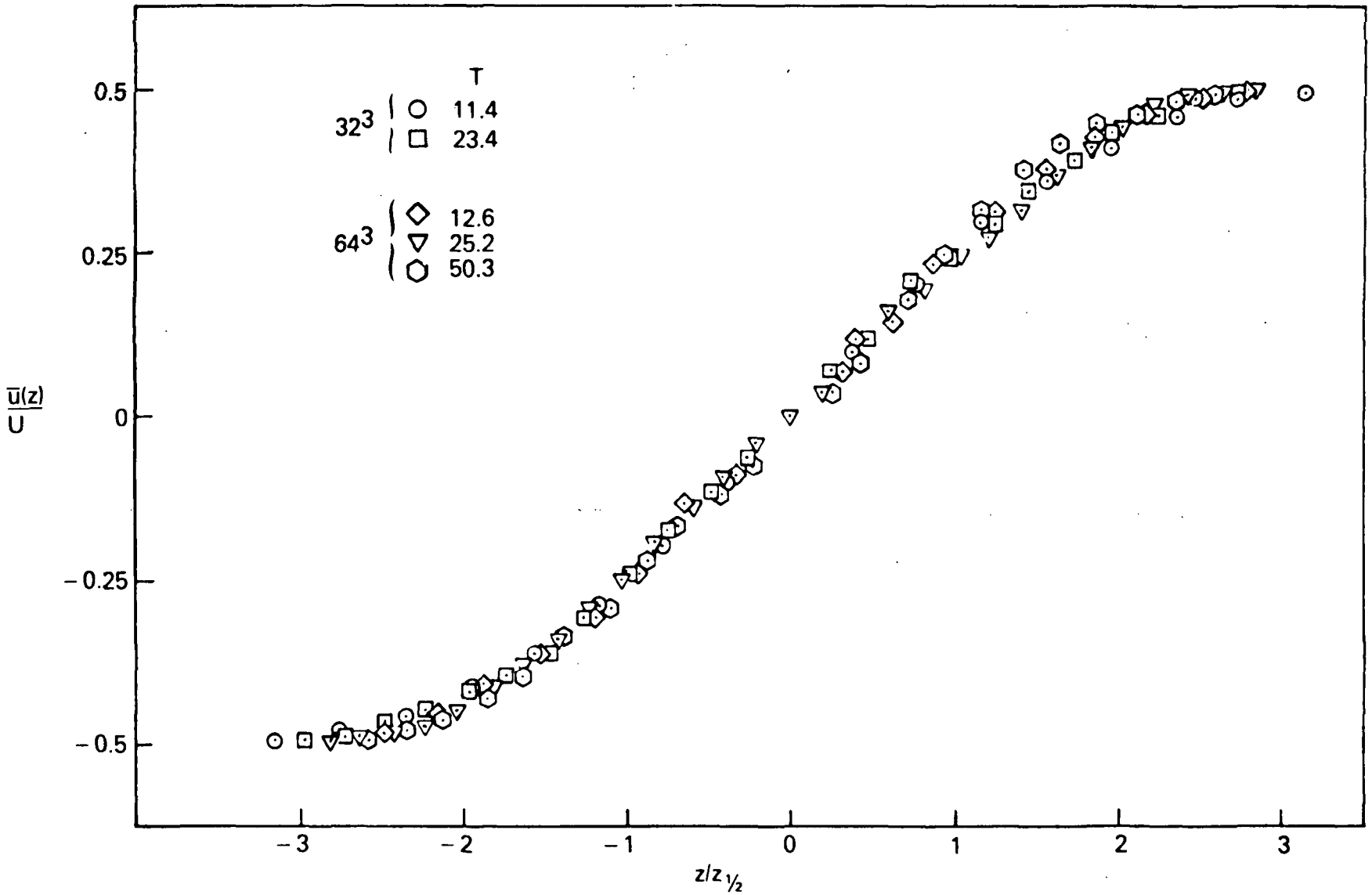

Figure 3. Similarity Plots of $\bar{u}/U$ Versus z/z_M (= $z/z_{1/2}$) (Taken from Metcalfe and Riley, 1981)

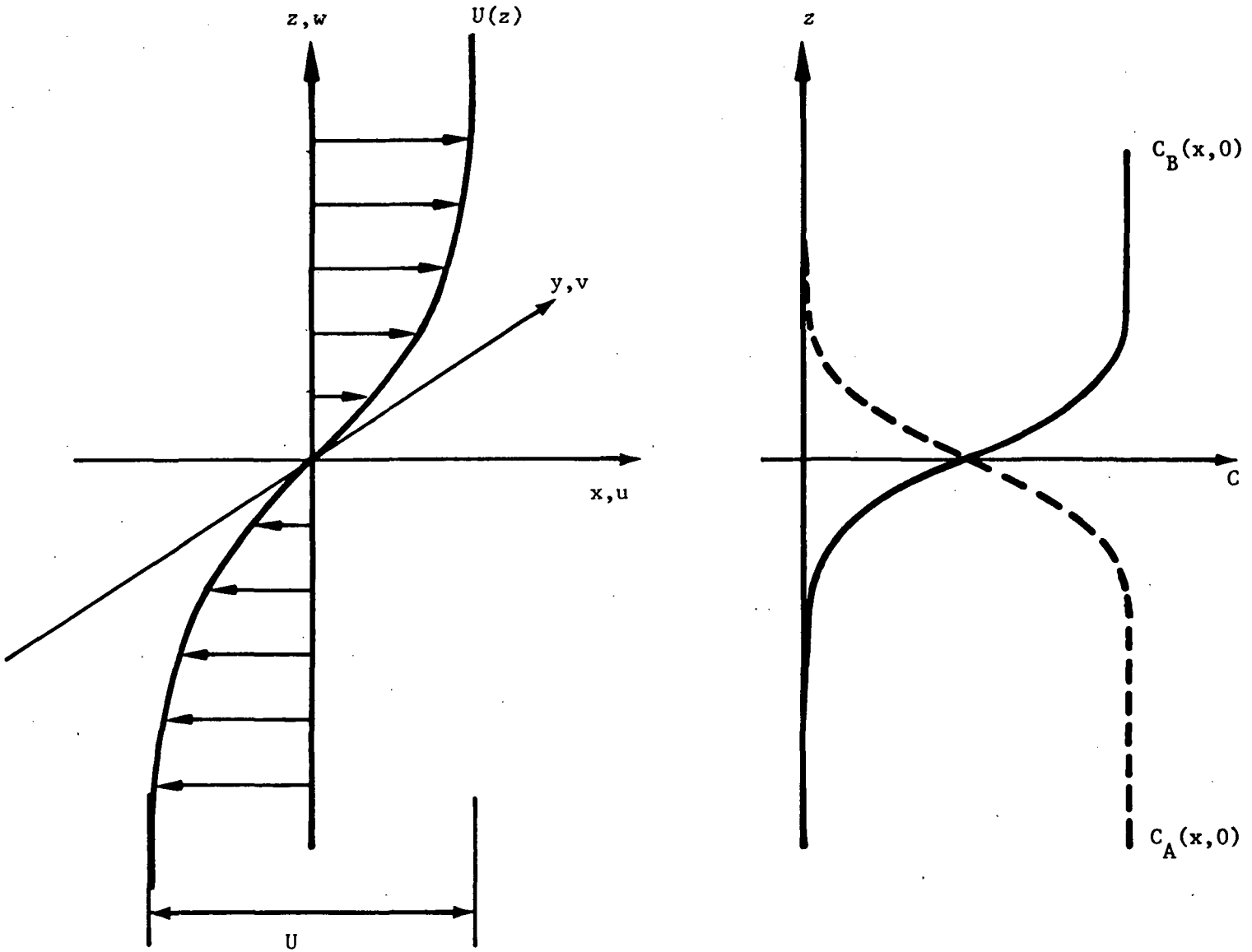

Figure 4. Problem Geometry - Initial Conditions

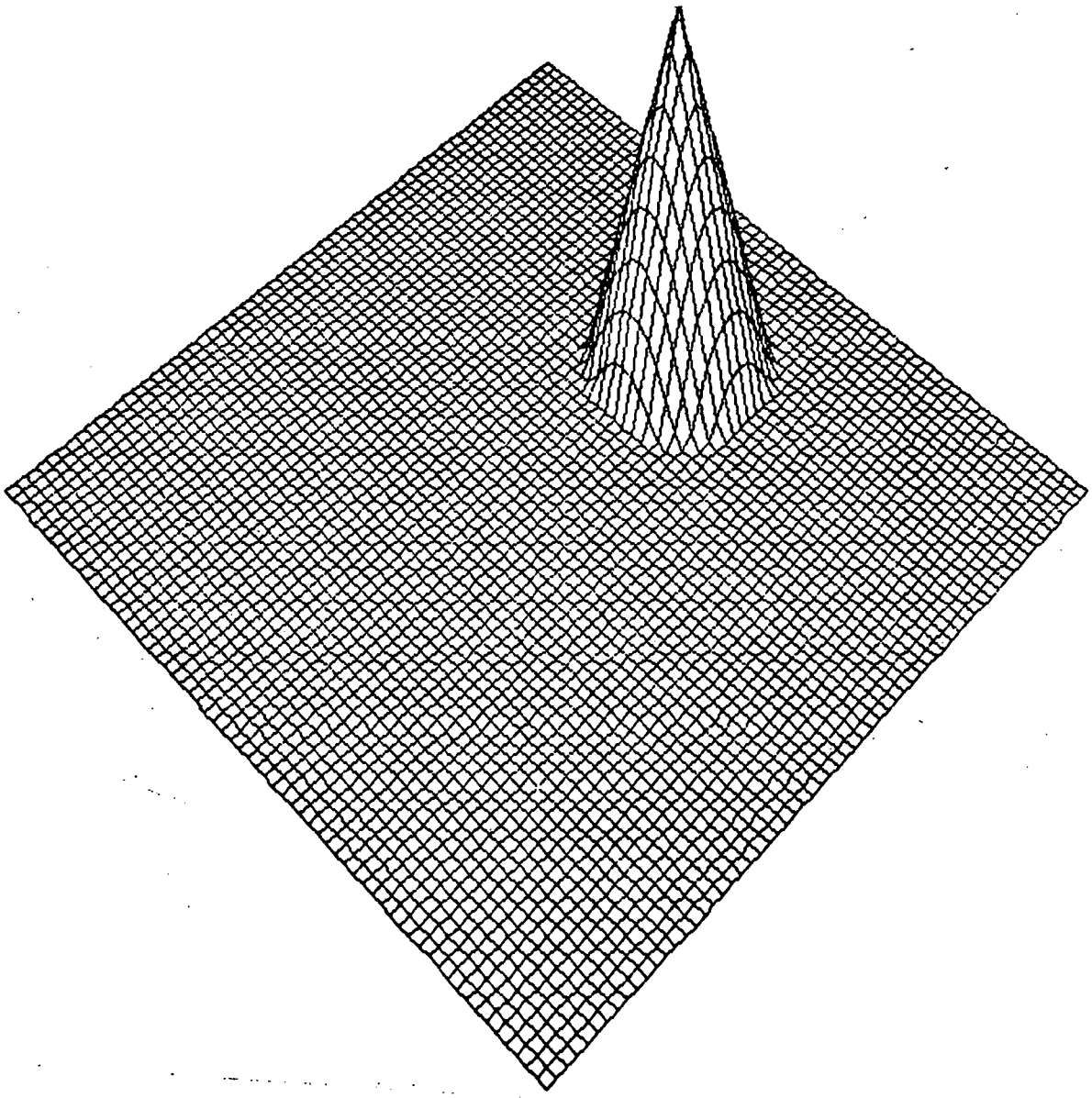

Figure 5. Initial Concentration Field for Color Problem Tests

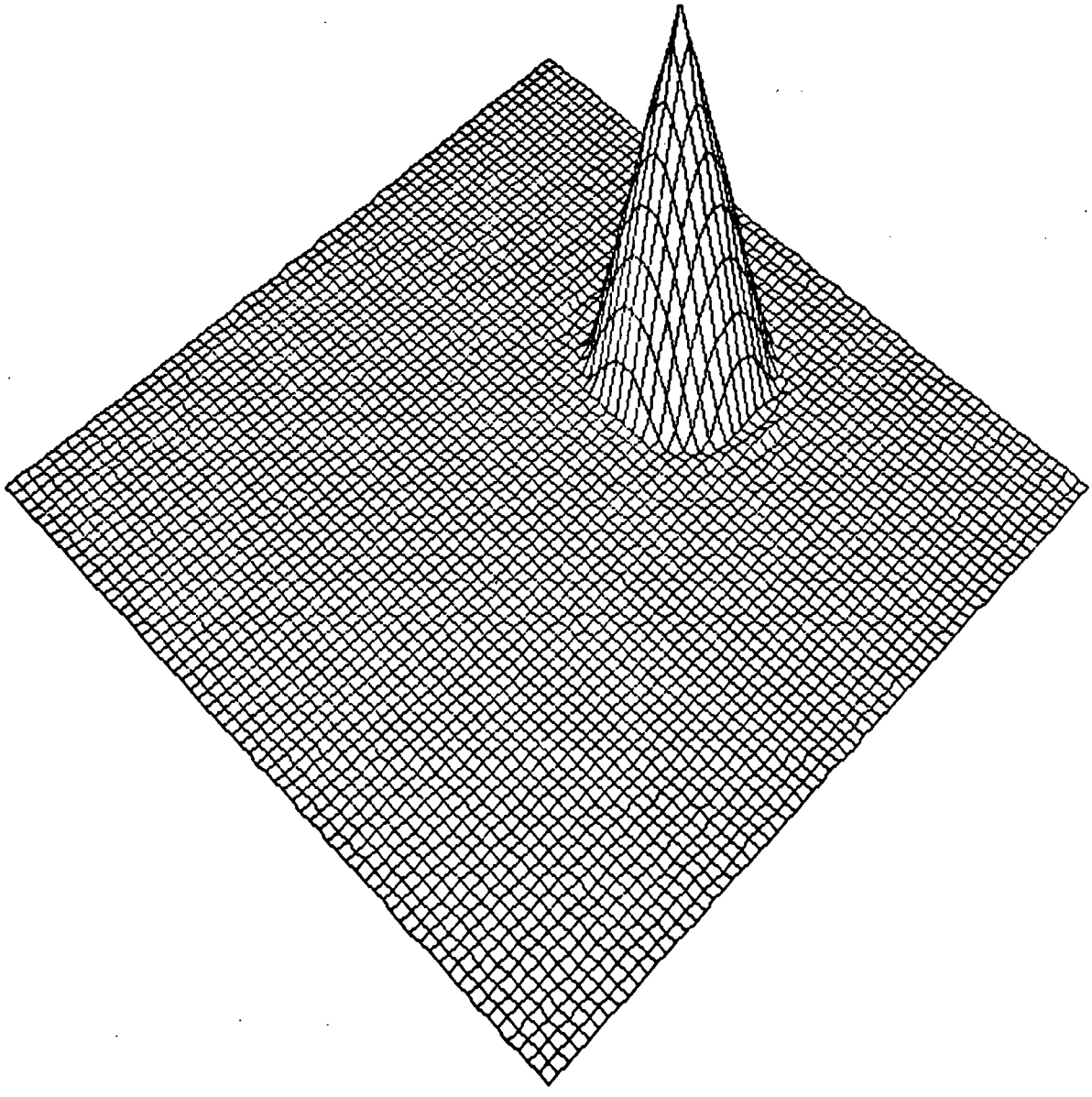

Figure 6. Computed Concentration Field After One Revolution - No Diffusion or Reaction

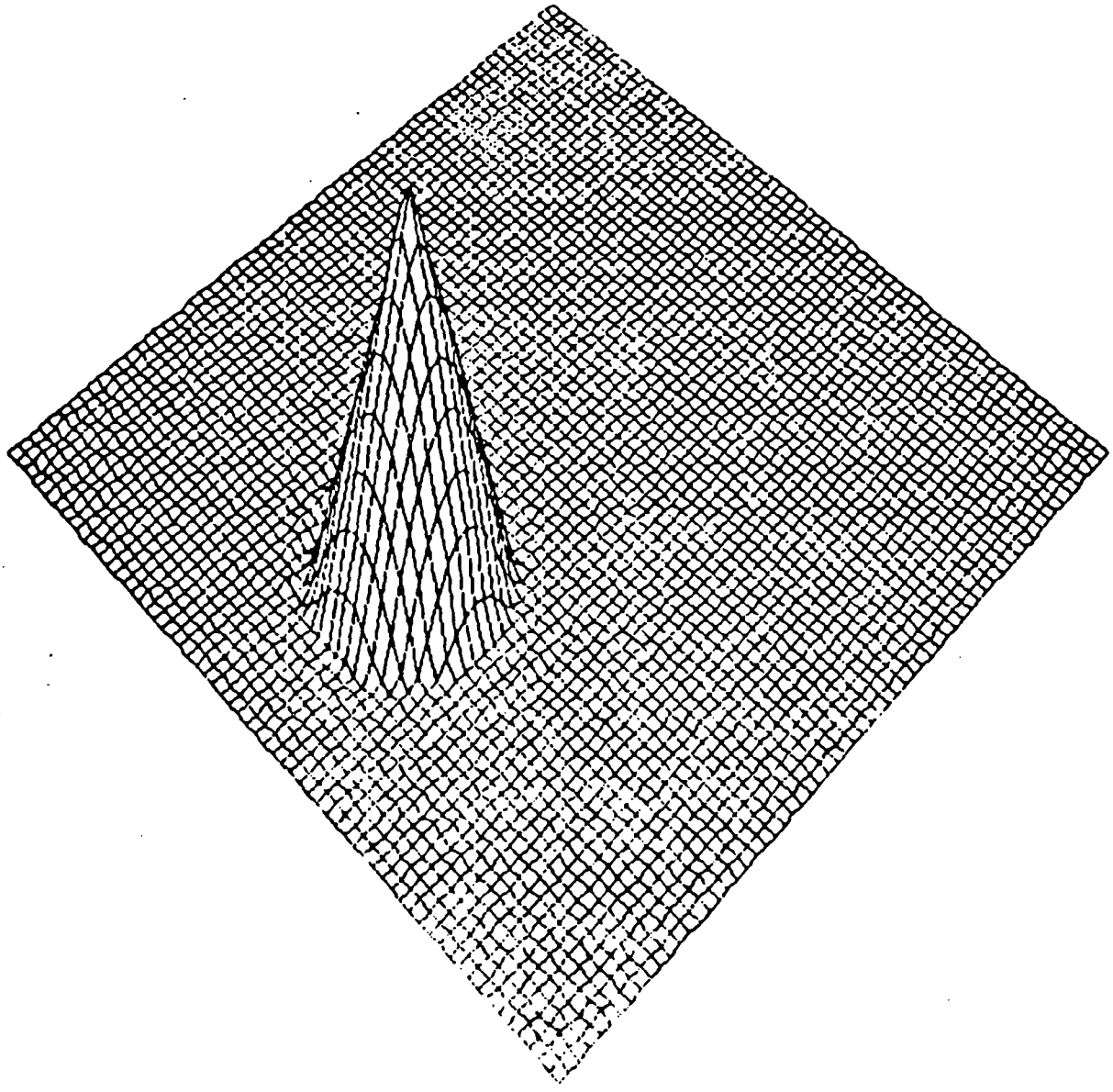

Figure 7. Computed Concentration Field After One-Half Revolution - No Diffusion or Reaction

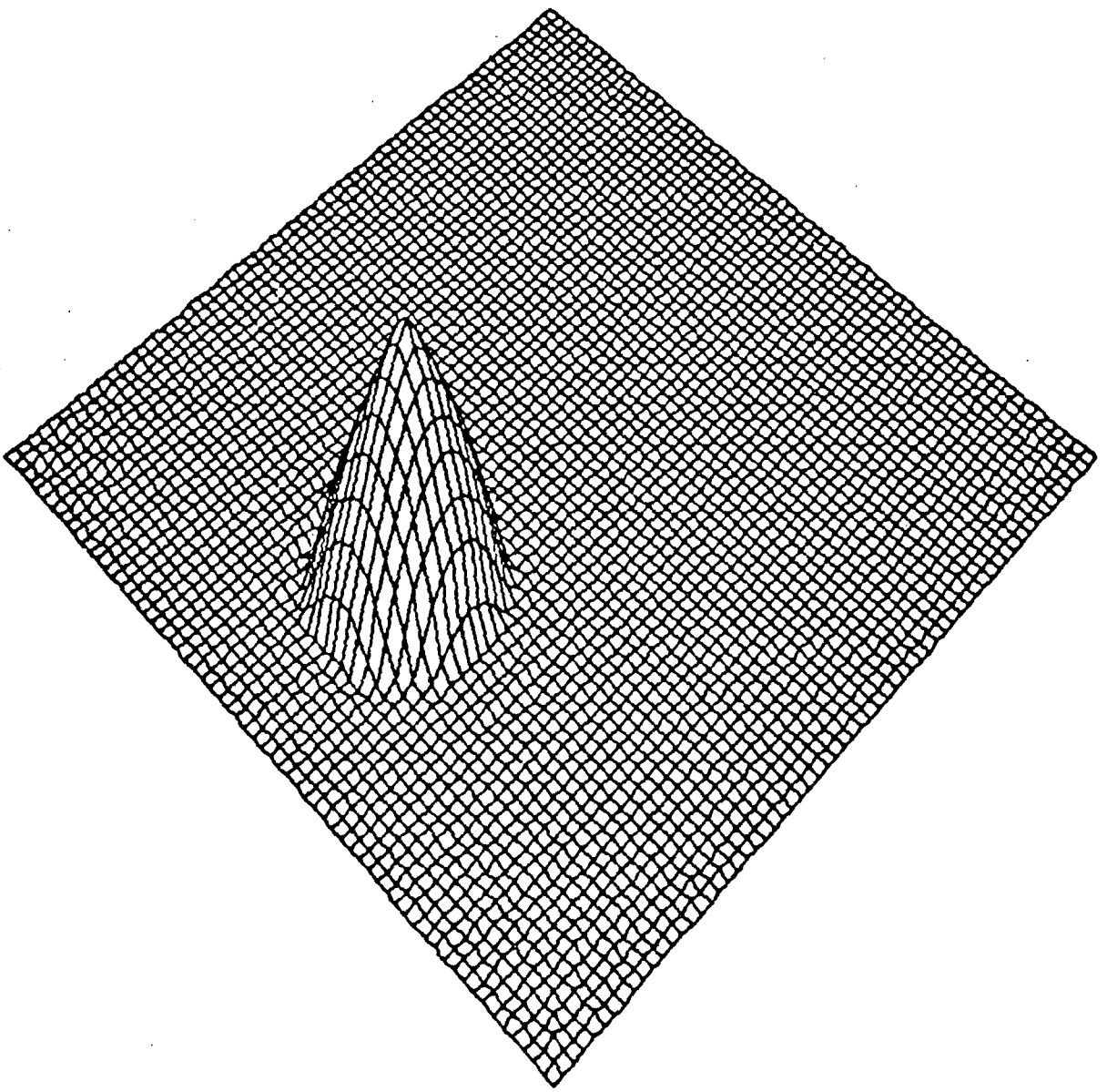

Figure 8. Computed Concentration Field After One-Half Revolution - No Diffusion, R = 1.0

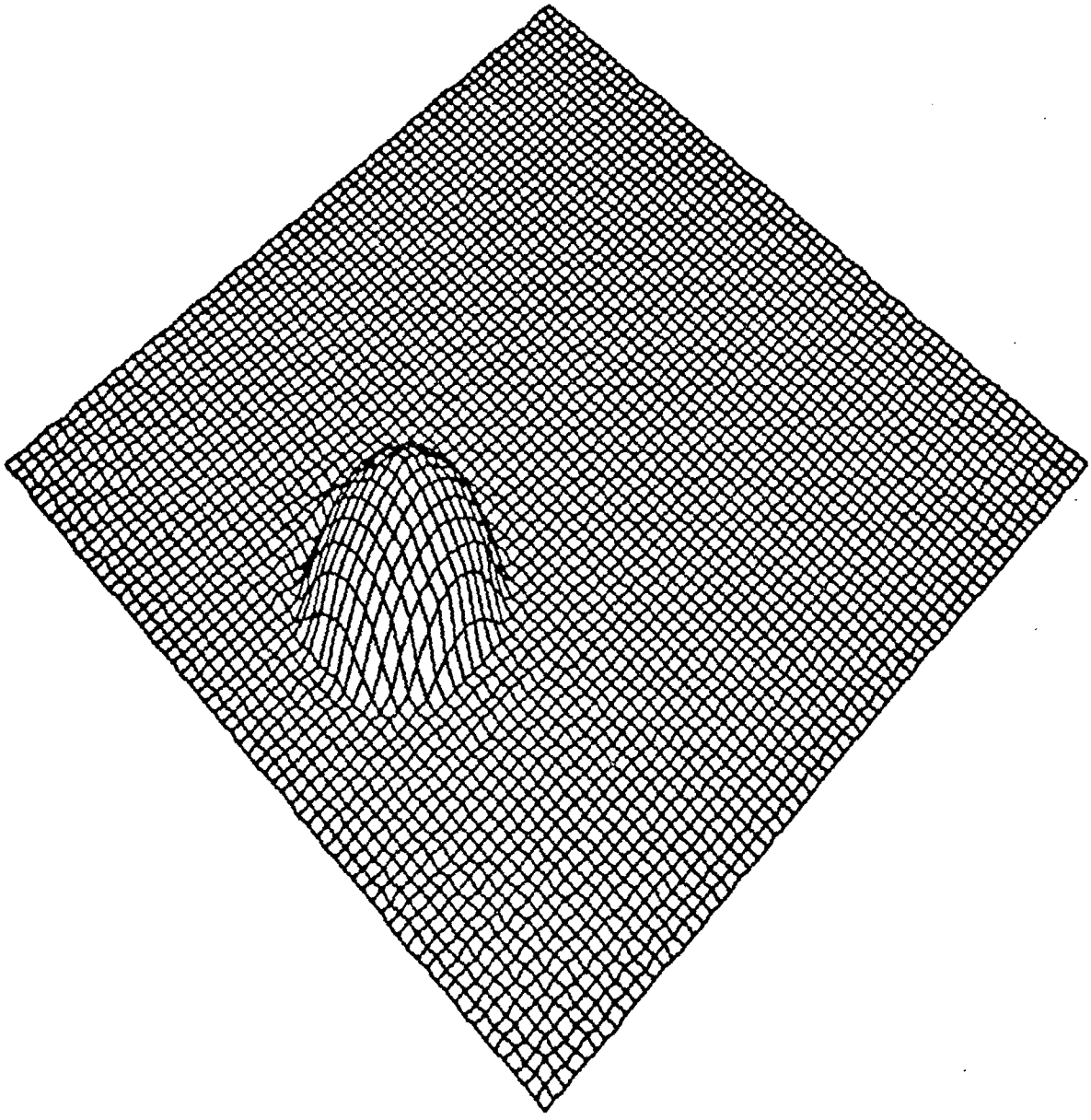

Figure 9. Computed Concentration Field After One-Half Revolution - No Diffusion, R = 4.0

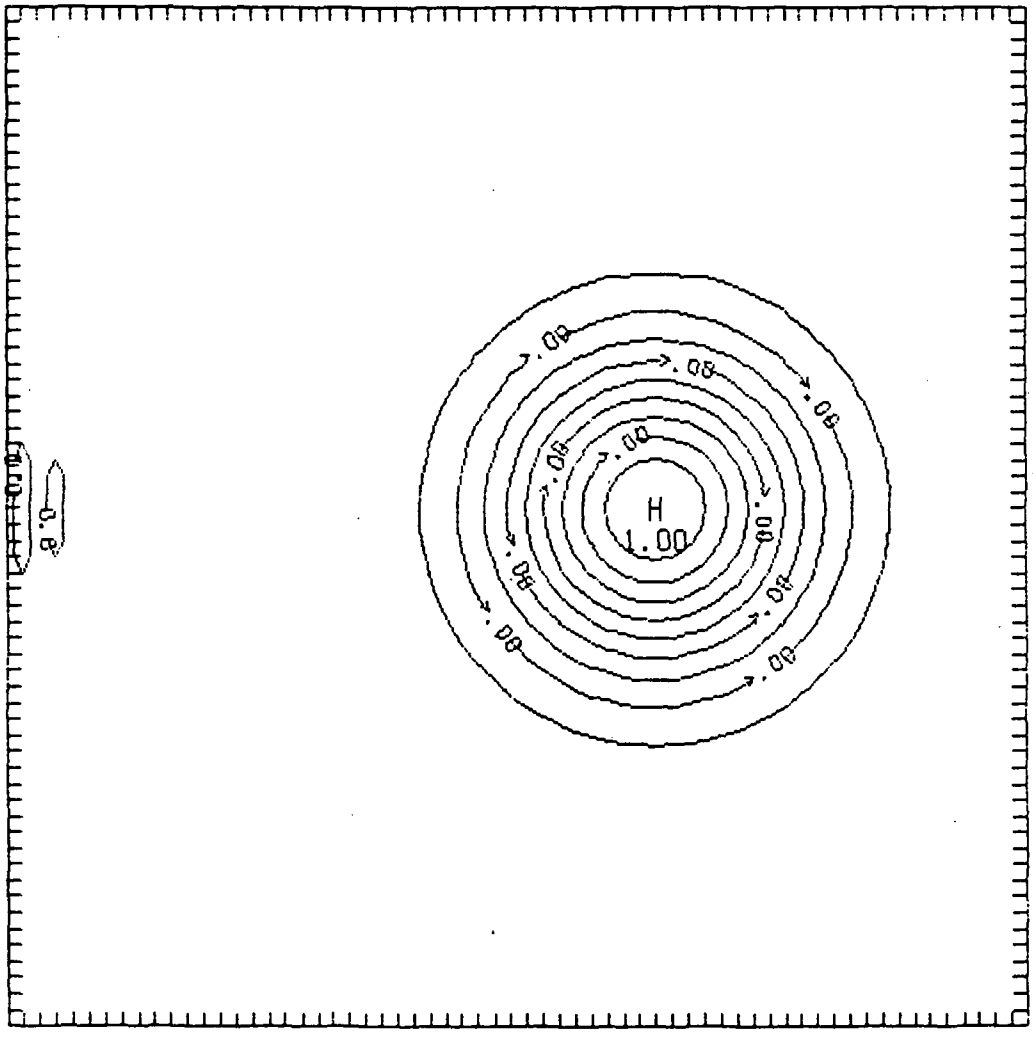

Figure 10. Constant Contour Plot of Initial Concentration Field Given by Equation (31)

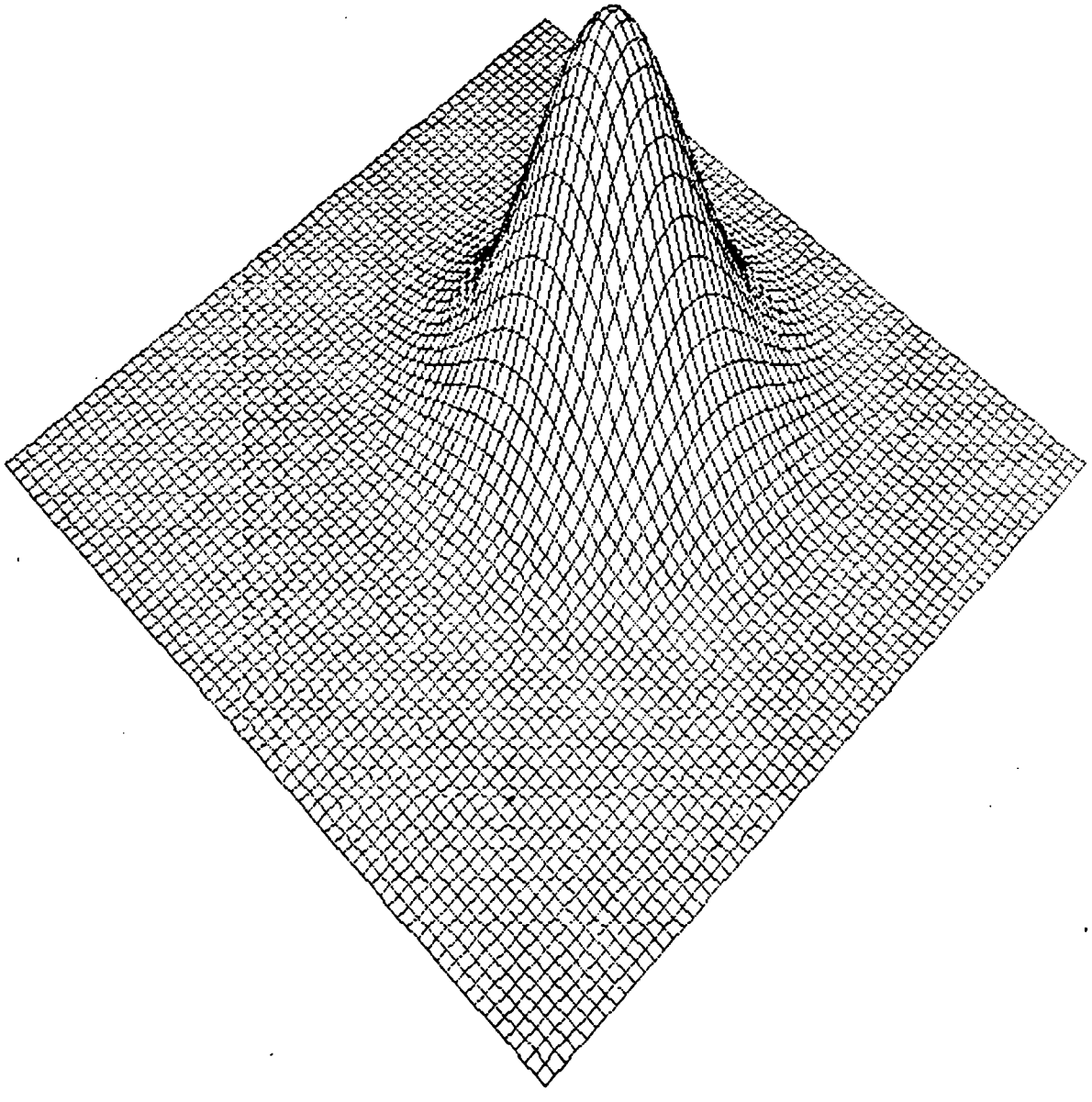

Figure 11. Perspective Plot of Initial Concentration Field Given by Equation (31)

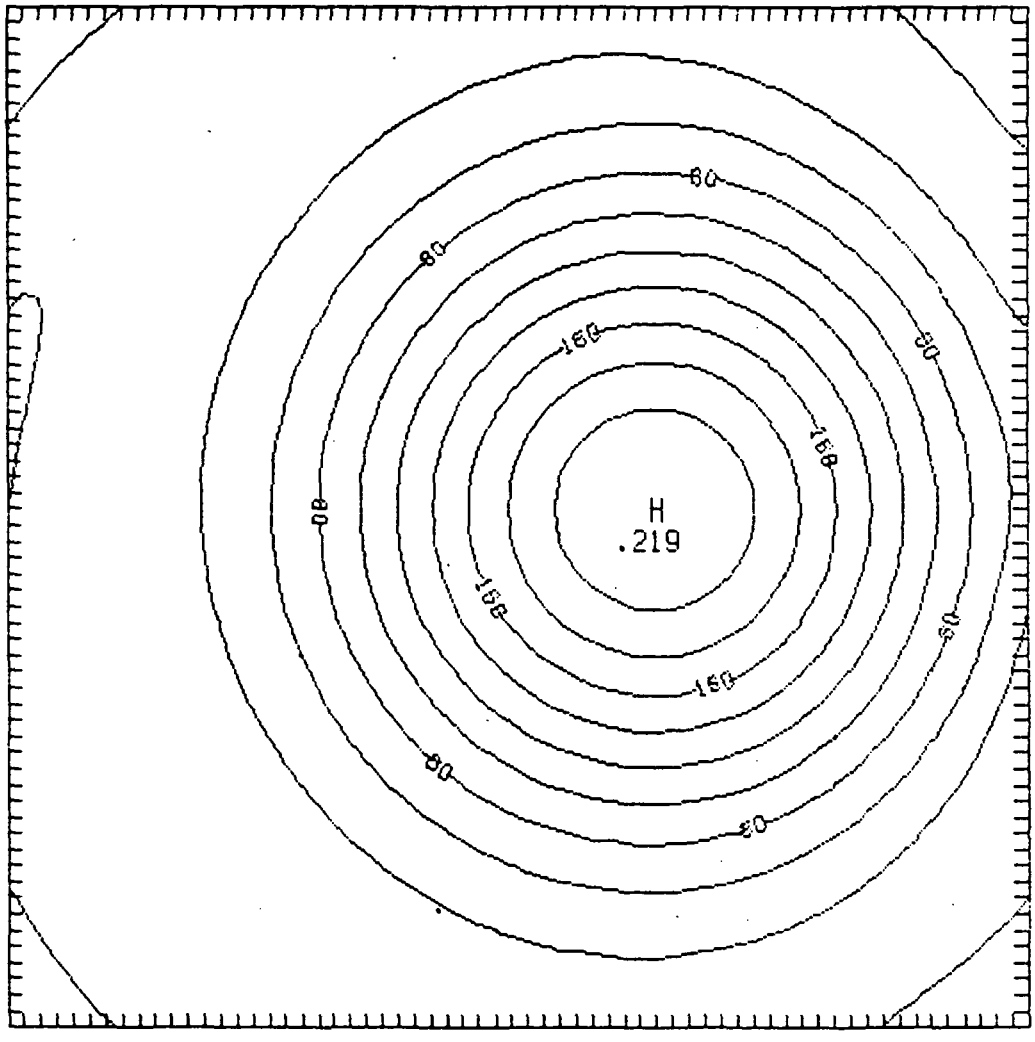

Figure 12. Constant Contour Plot of Computed Concentration Field After One Revolution - Diffusion but No Reaction

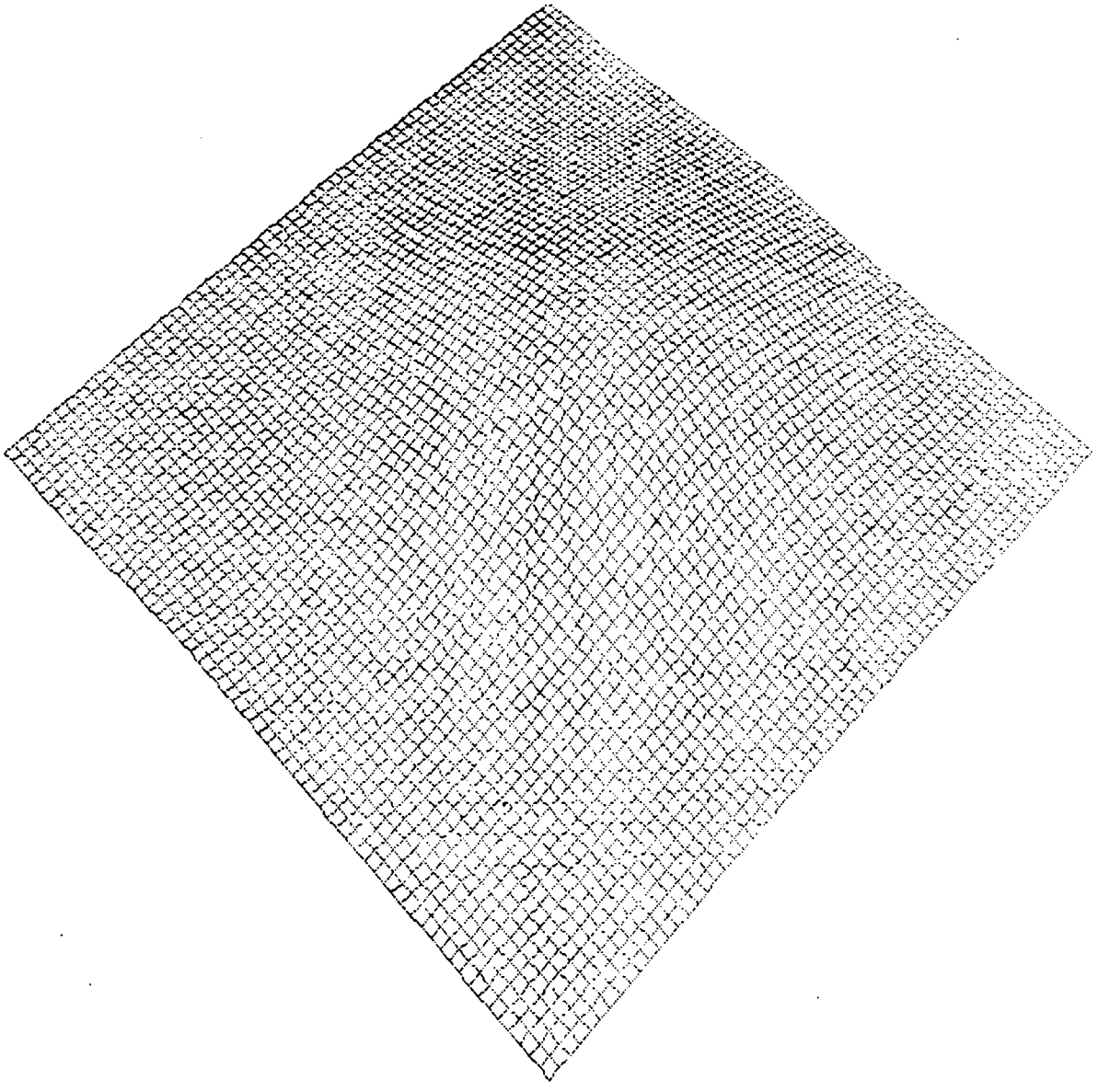

Figure 13. Perspective Plot of Computed Concentration Field After One Revolution - Diffusion but No Reaction

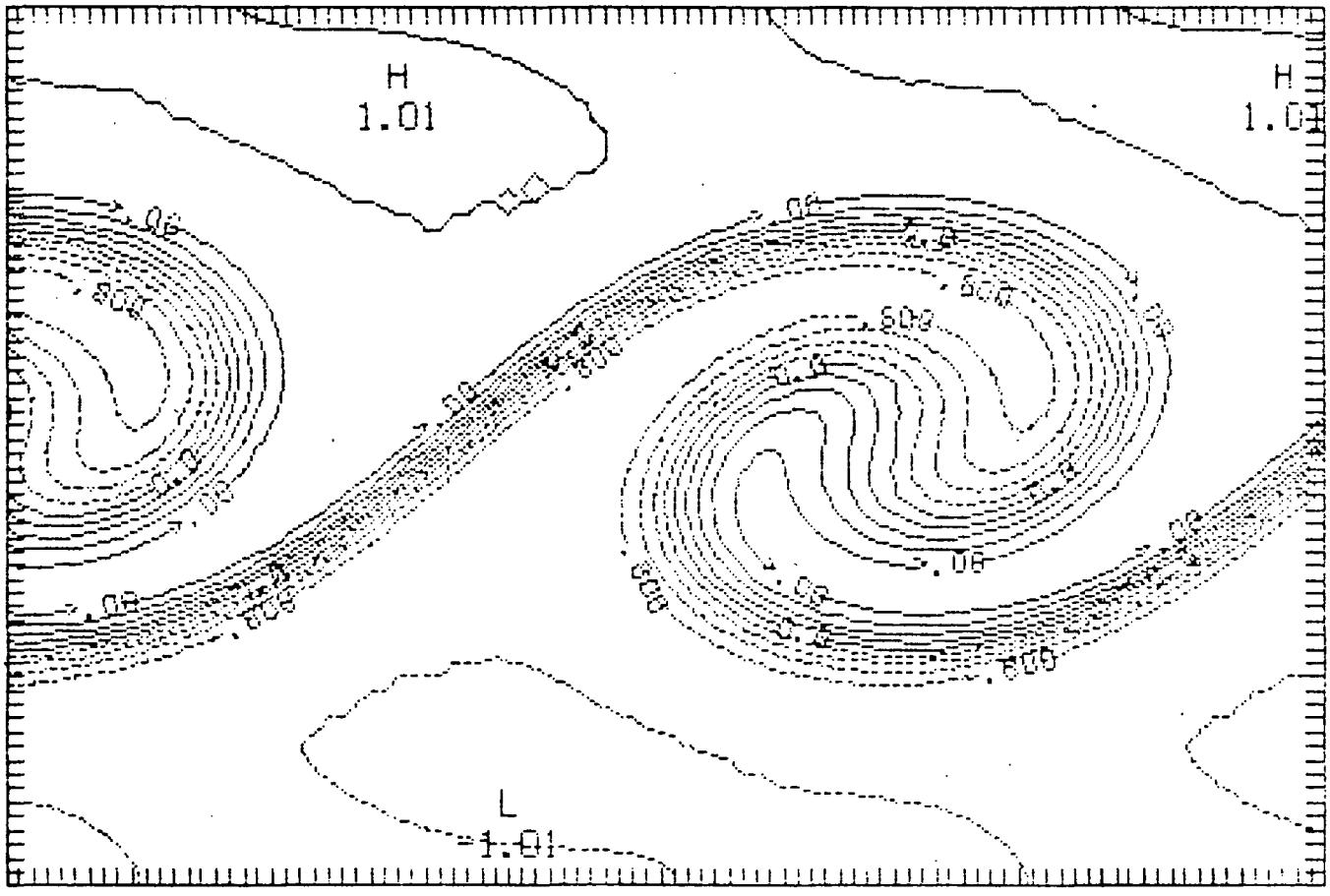

Figure 14. Constant Contour Plot of Conserved Scalar Computed Indirectly from the Difference Between the Species Concentrations - t = 12

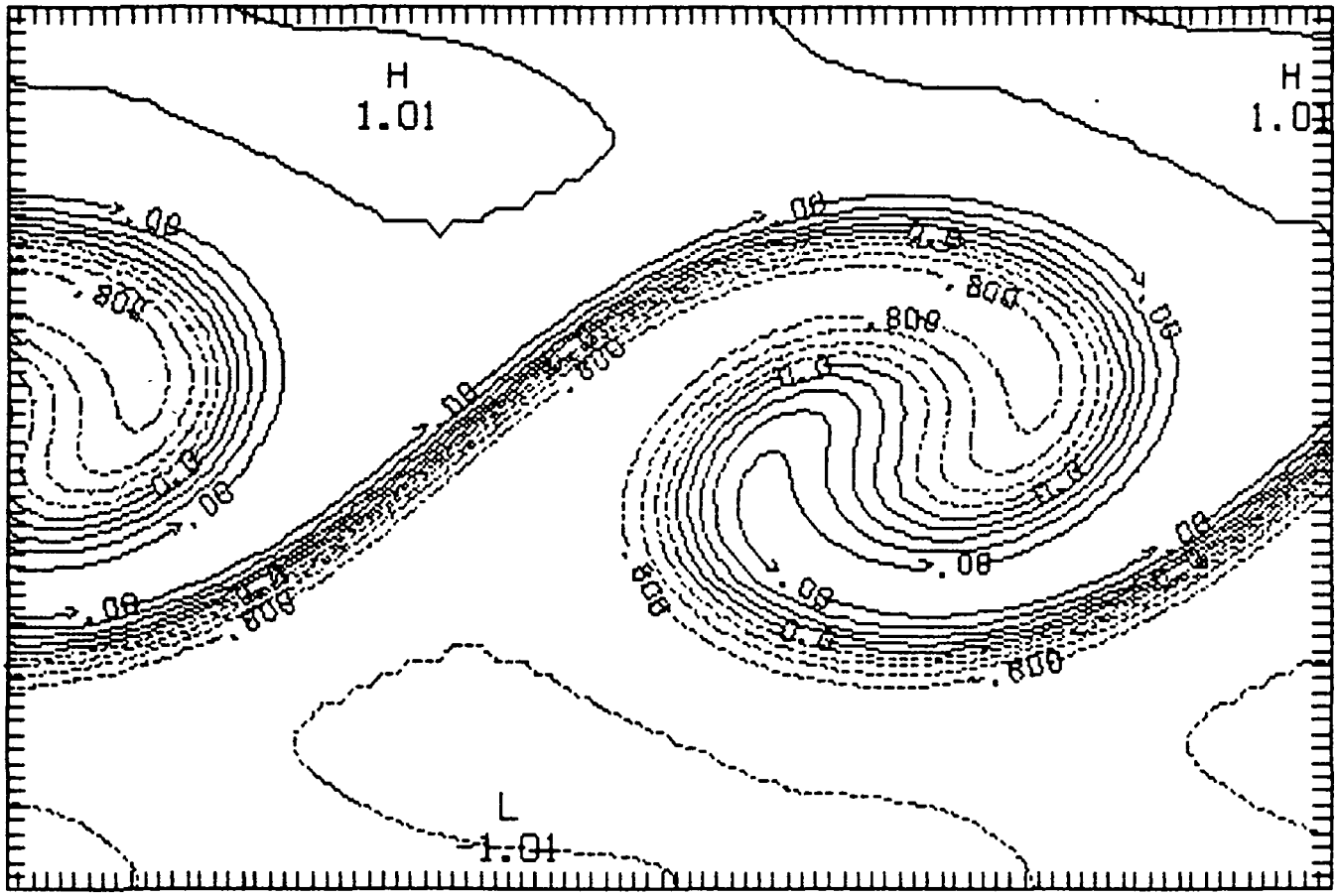

Figure 15. Constant Contour Plot of Conserved Scalar Computed Directly from the Difference Between the Species Concentrations - t = 12

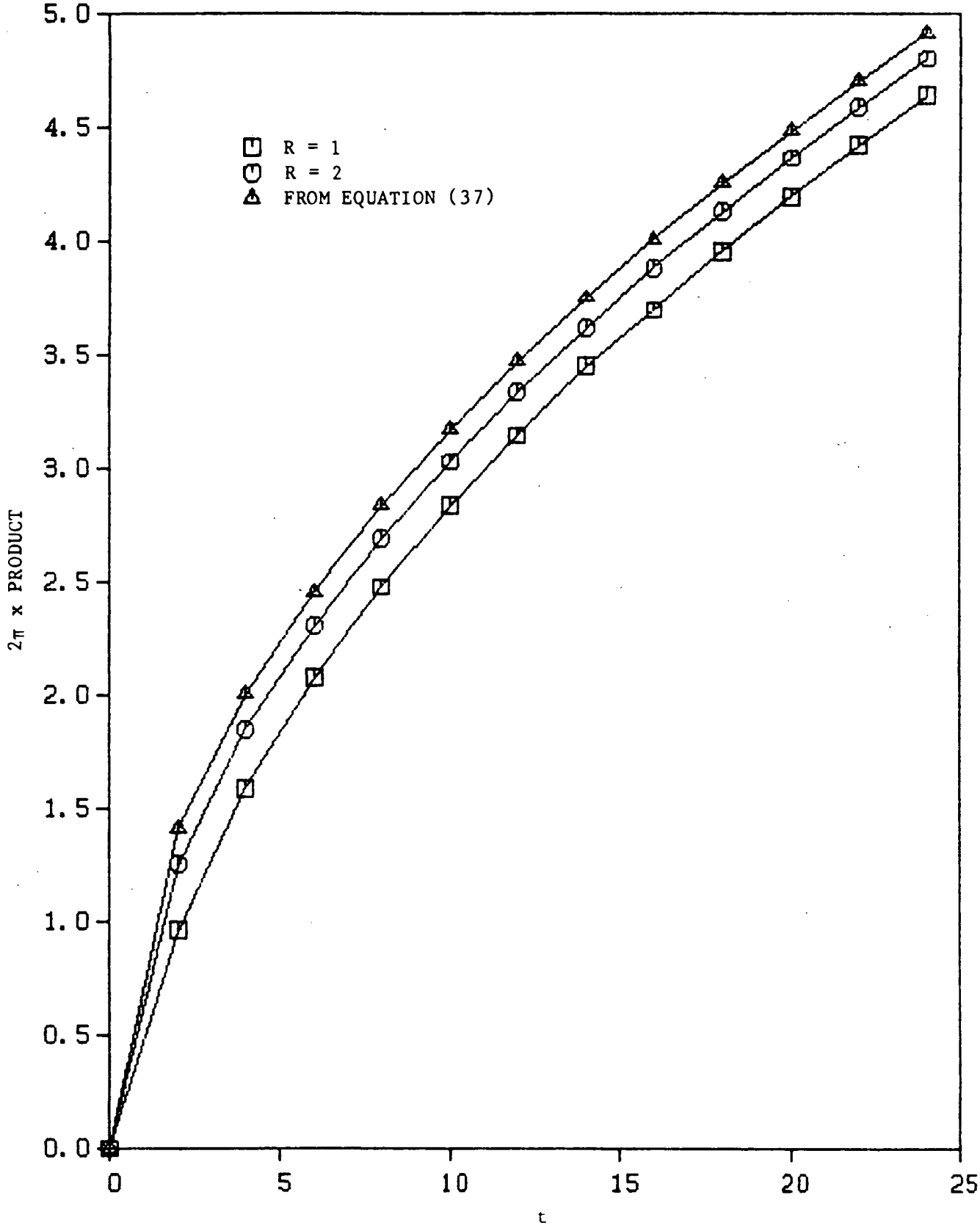

Figure 16. Total Product Versus Time for Two Different Values of the Reaction Rate Coefficient R - One-Dimensional Simulations. Also Shown Is the Infinite Reaction Rate Solution [Equation (37)]

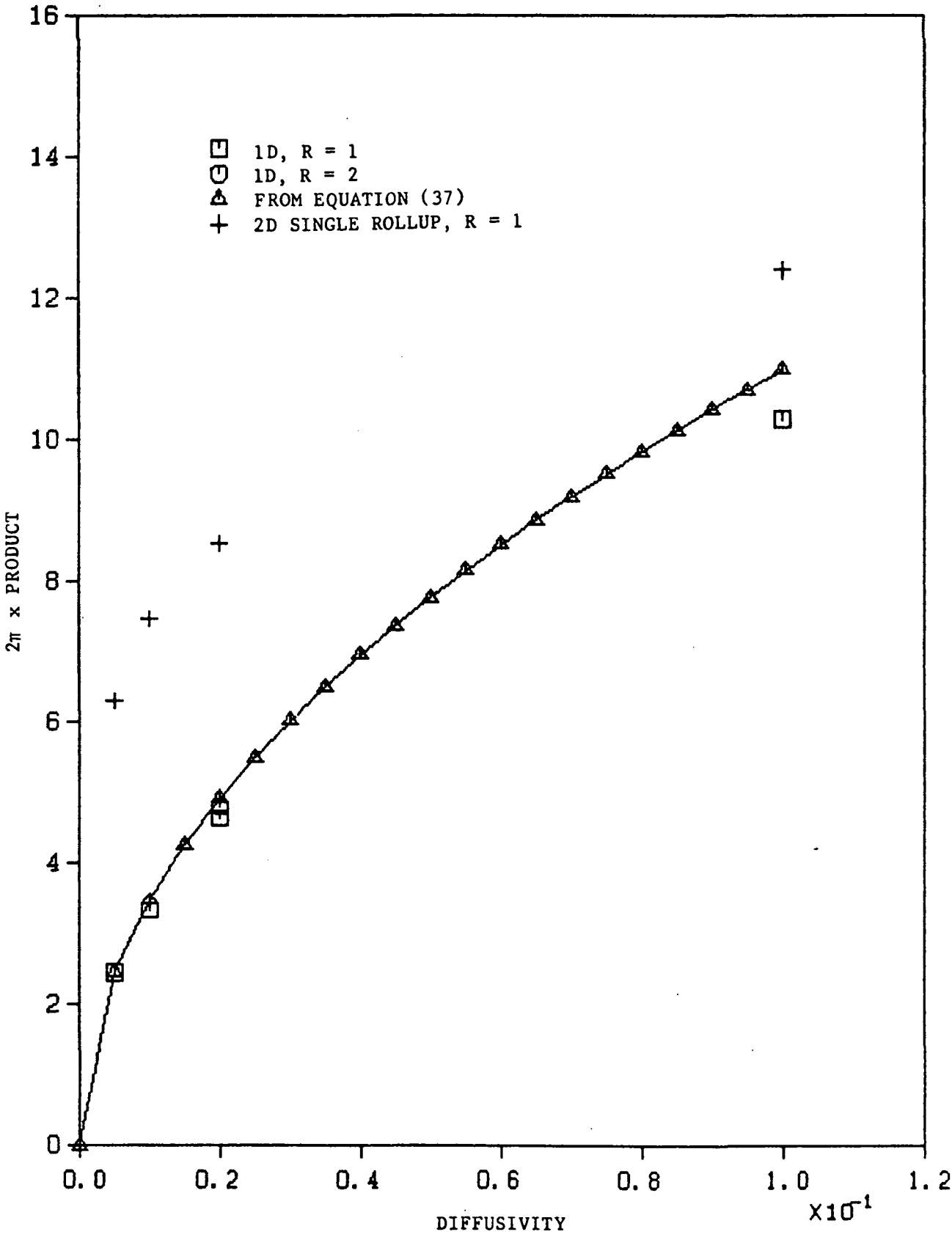

Figure 17. Total Product Versus Diffusivity for a Fixed Time (t = 24) - One- and Two-Dimensional Single Rollup Simulations. Also Shown Is the Infinite Reaction Rate Solution [Equation (37)]

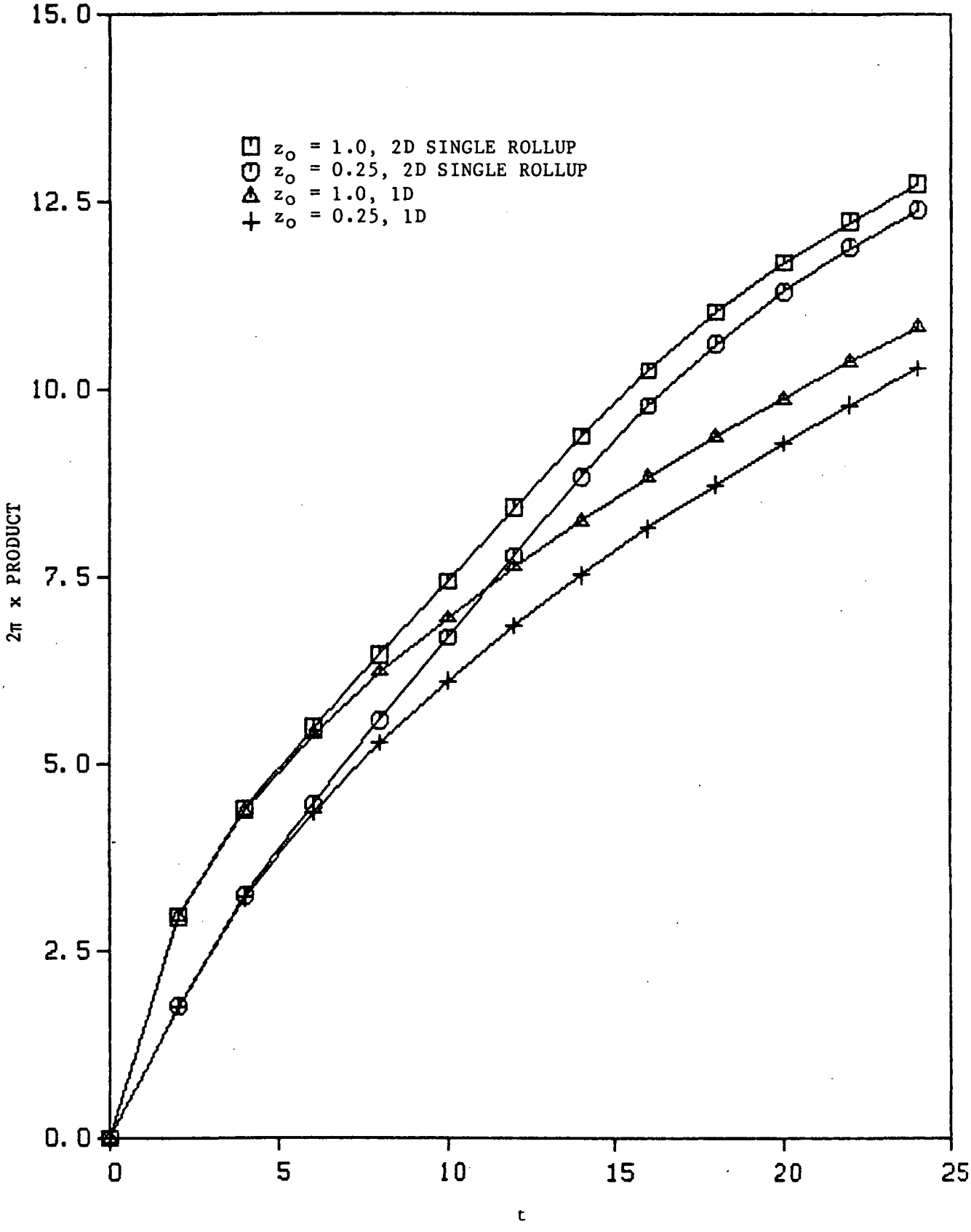

Figure 18. Total Product Versus Time for Two Different Initial Concentration Profiles - One- and Two-Dimensional Single Rollup Simulations

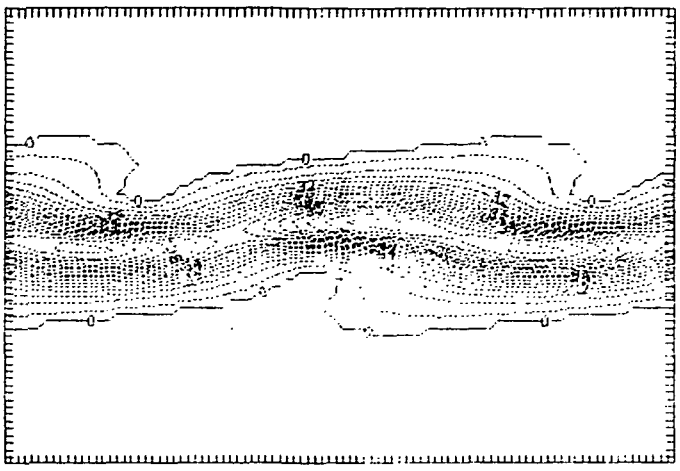

Figure 19a t = 0

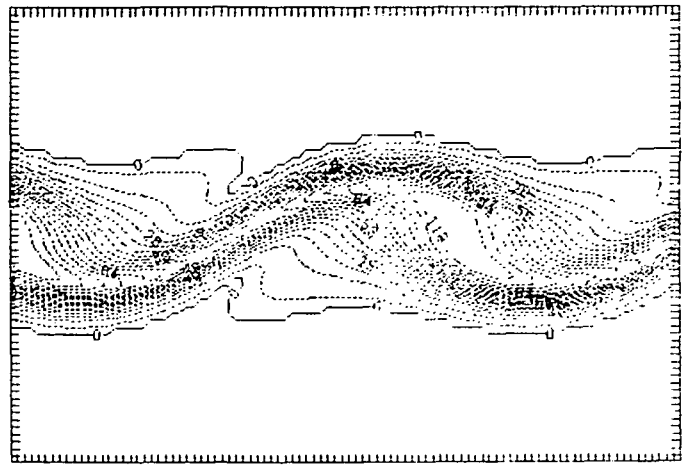

Figure 19b t = 4

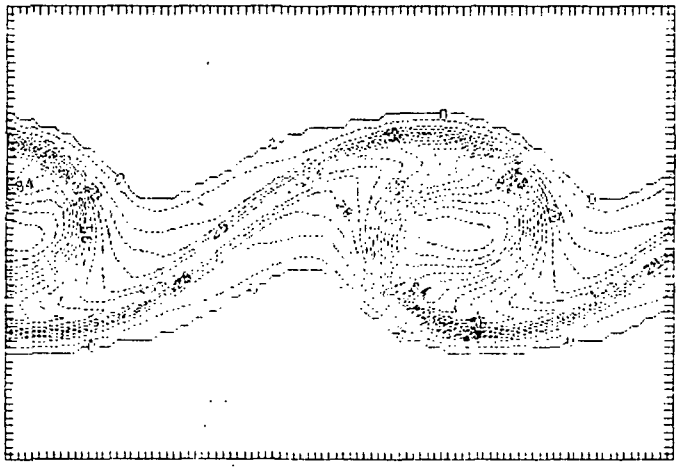

Figure 19c t = 8

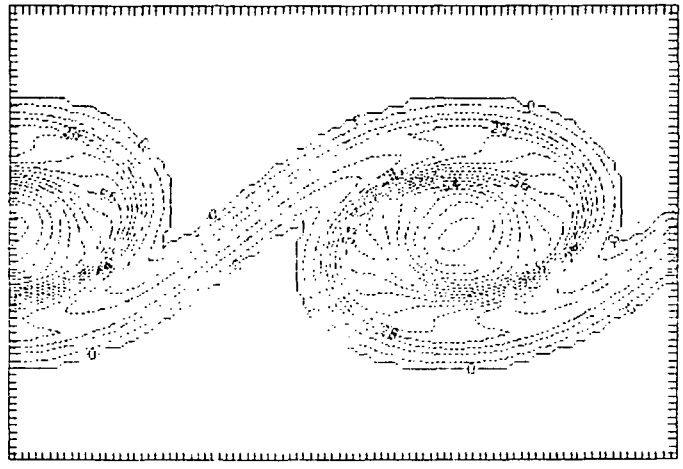

Figure 19d t = 12

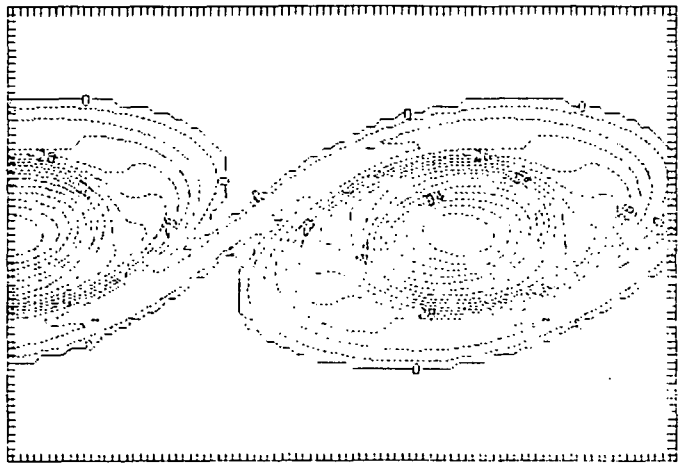

Figure 19e t = 16

Figure 19. Plots of Vorticity Contours for a Sequence of Times - Case 1 (Fundamental Mode Alone)

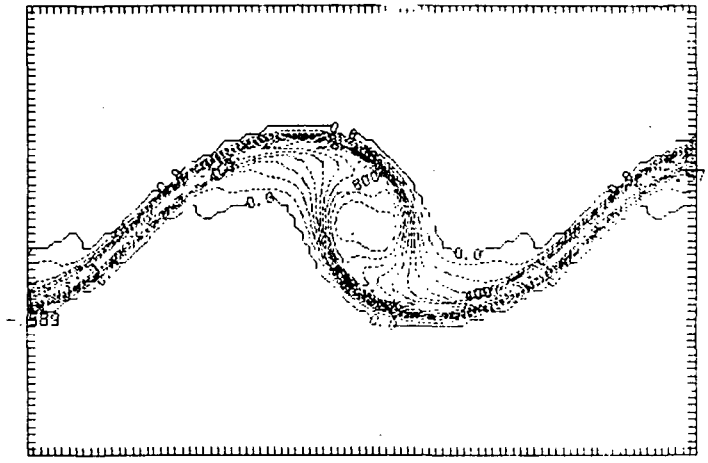

Figure 20a t = 12

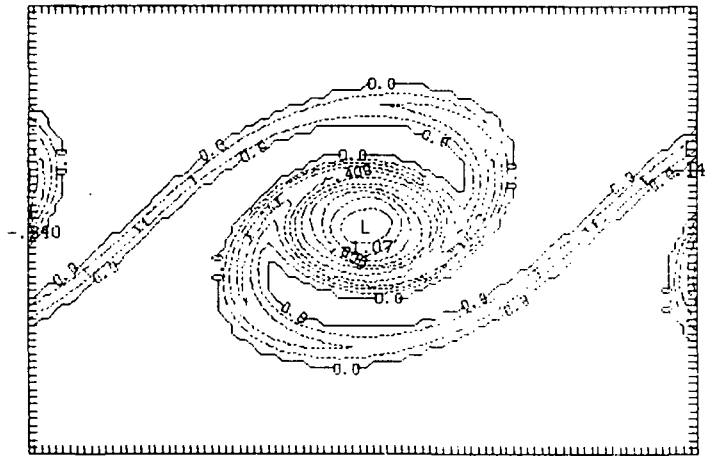

Figure 20b t = 24

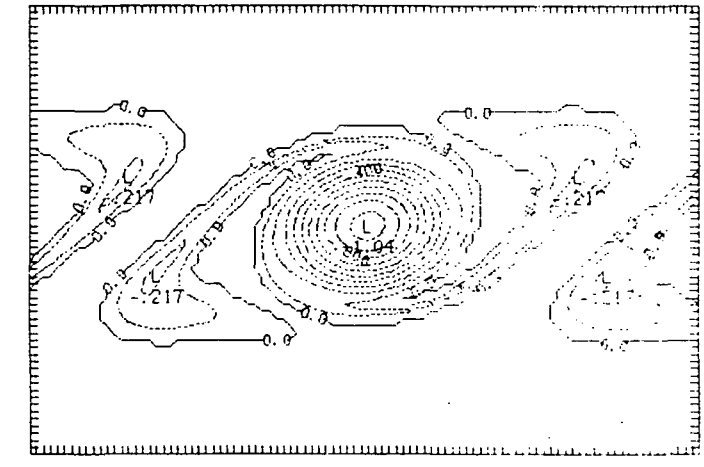

Figure 20c t = 36

Figure 20. Plots of Vorticity Contours for a Sequence of Times - Case 2 (Subharmonic Mode Alone)

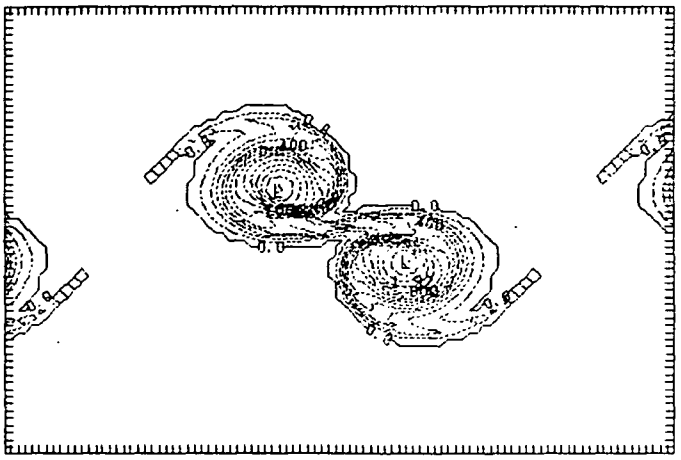

Figure 21a t = 12

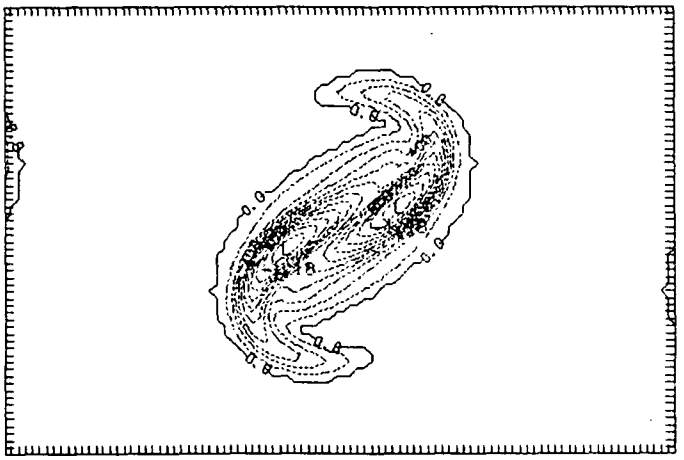

Figure 21b t = 24

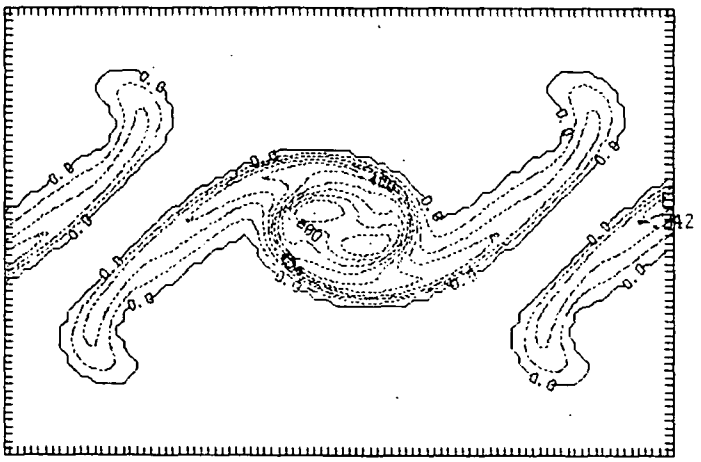

Figure 21c t = 36

Figure 21. Plots of Vorticity Contours for a Sequence of Times - Case 3 (Fundamental and Subharmonic Added Together Out-of-Phase)

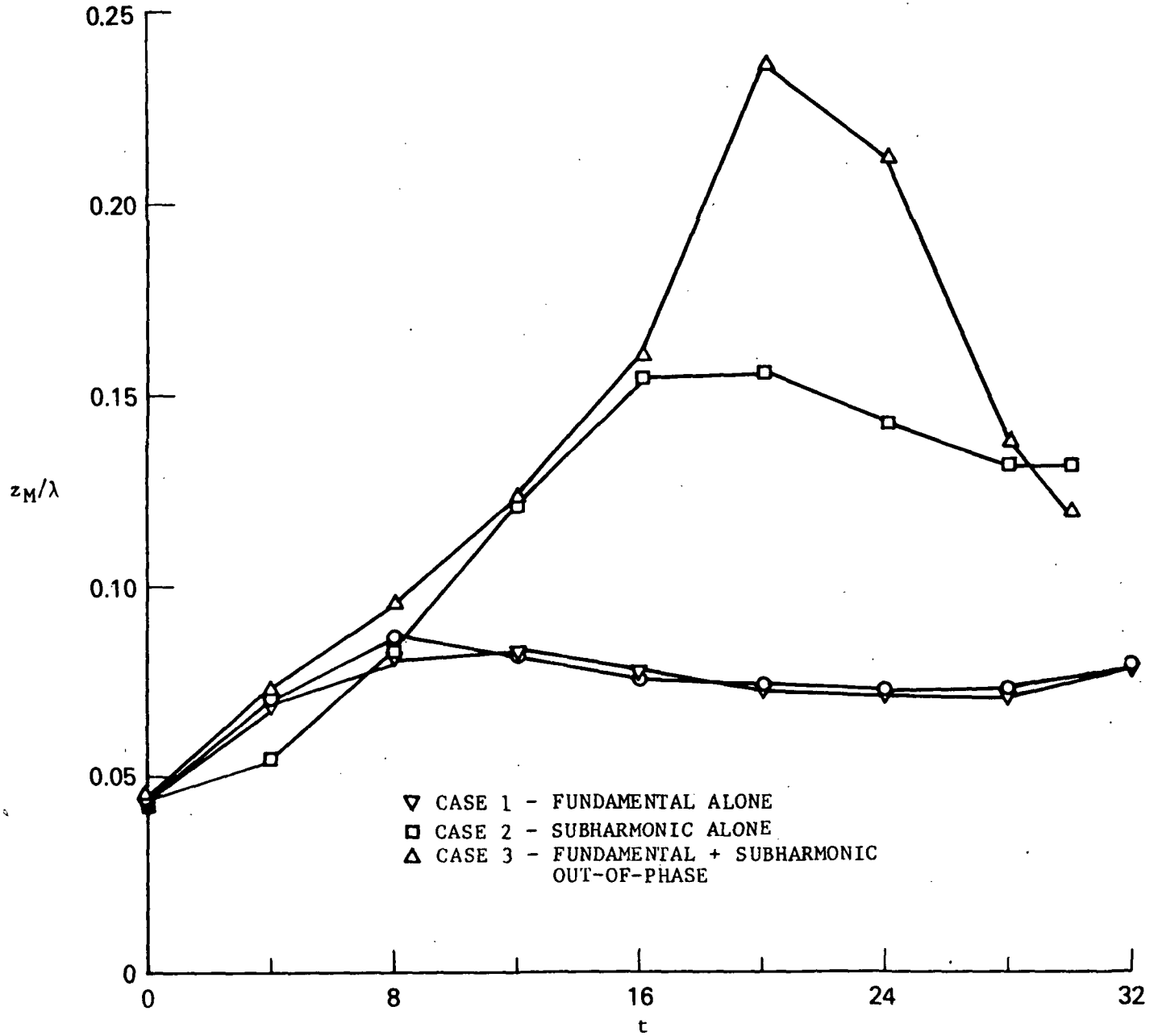

Figure 22. Mean Velocity Half-Width, z_M (= $z_{1/2}$), Versus Time - Two-Dimensional Simulations (λ Is the Wavelength of the Most Unstable Mode)

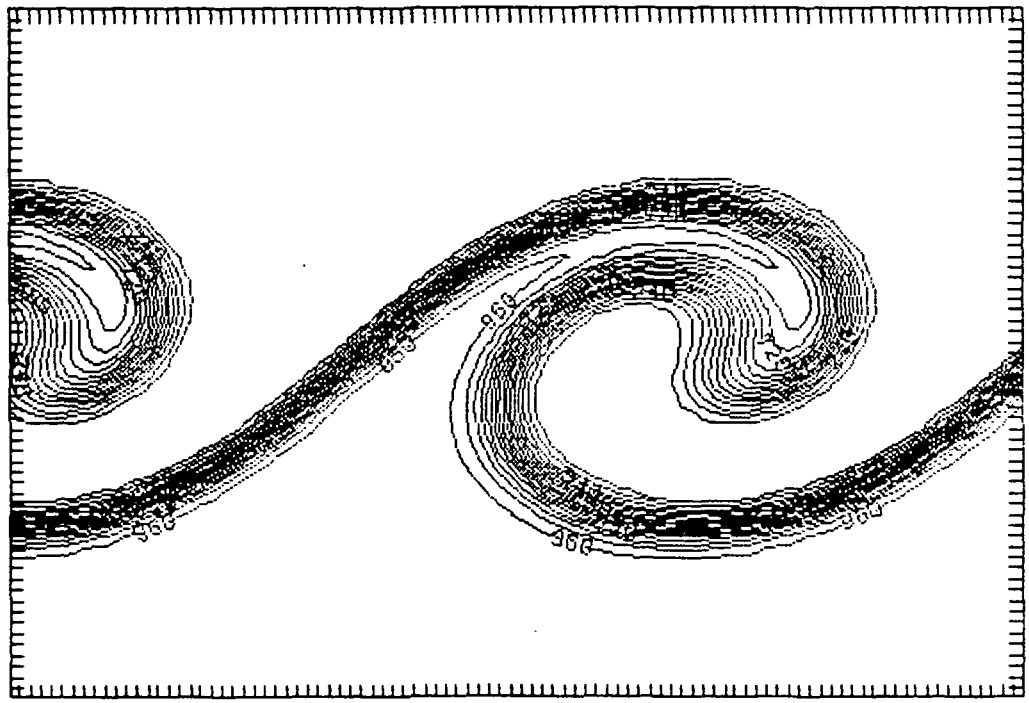

Figure 23a Species A

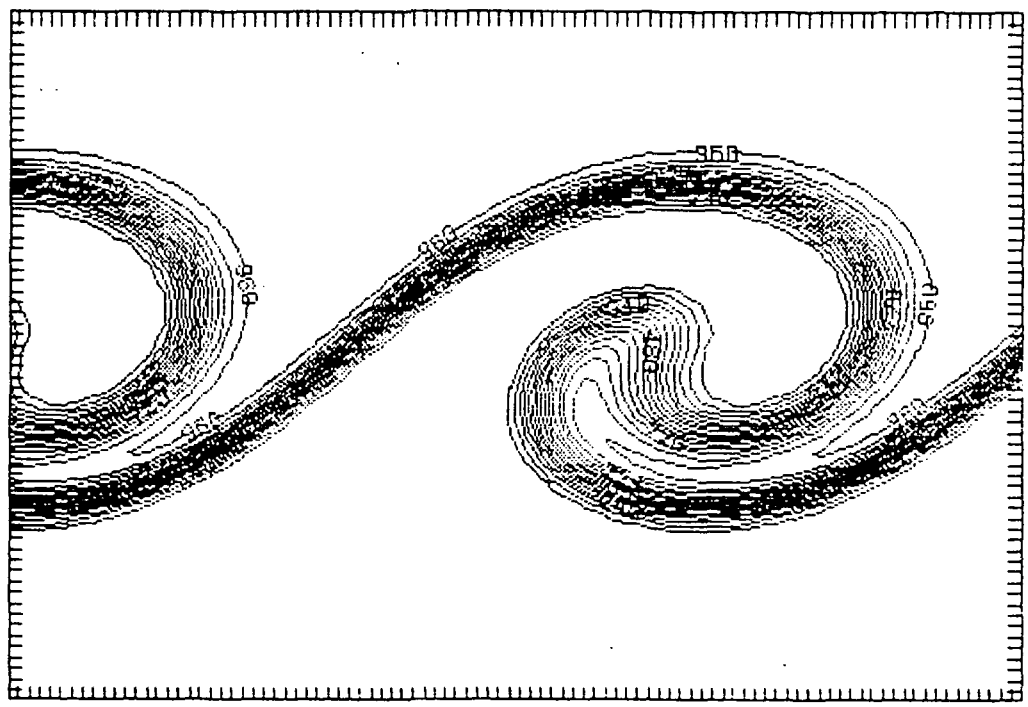

Figure 23b Species B

Figure 23. Plots of Concentration Contours for Species A and B at t = 12 for Case 1 (Fundamental Mode Alone) - Two-Dimensional Simulations

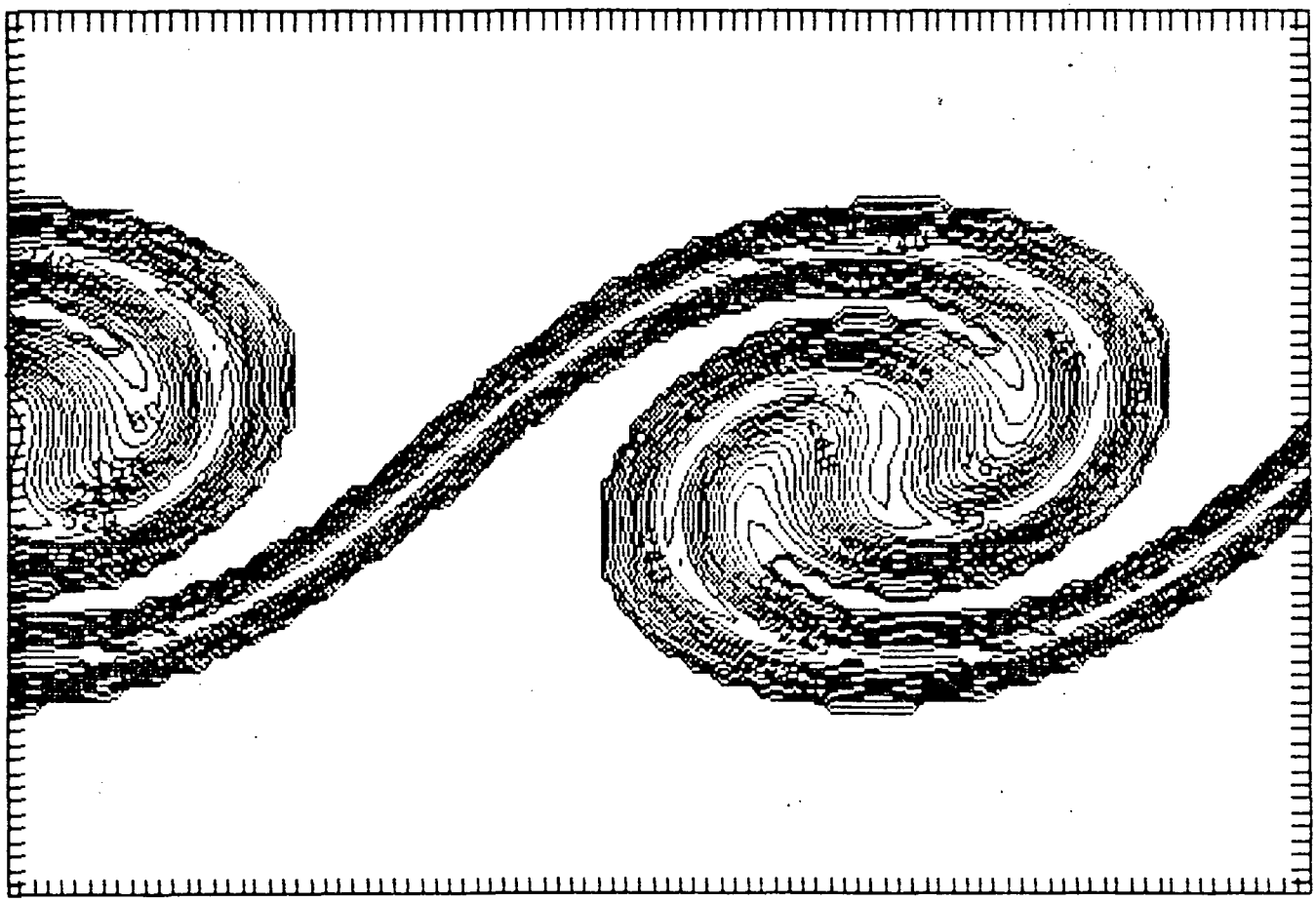

Figure 24. Plot of Product Concentration Contours at t = 12 for Case 1 (Fundamental Mode Alone) - Two-Dimensional Simulations

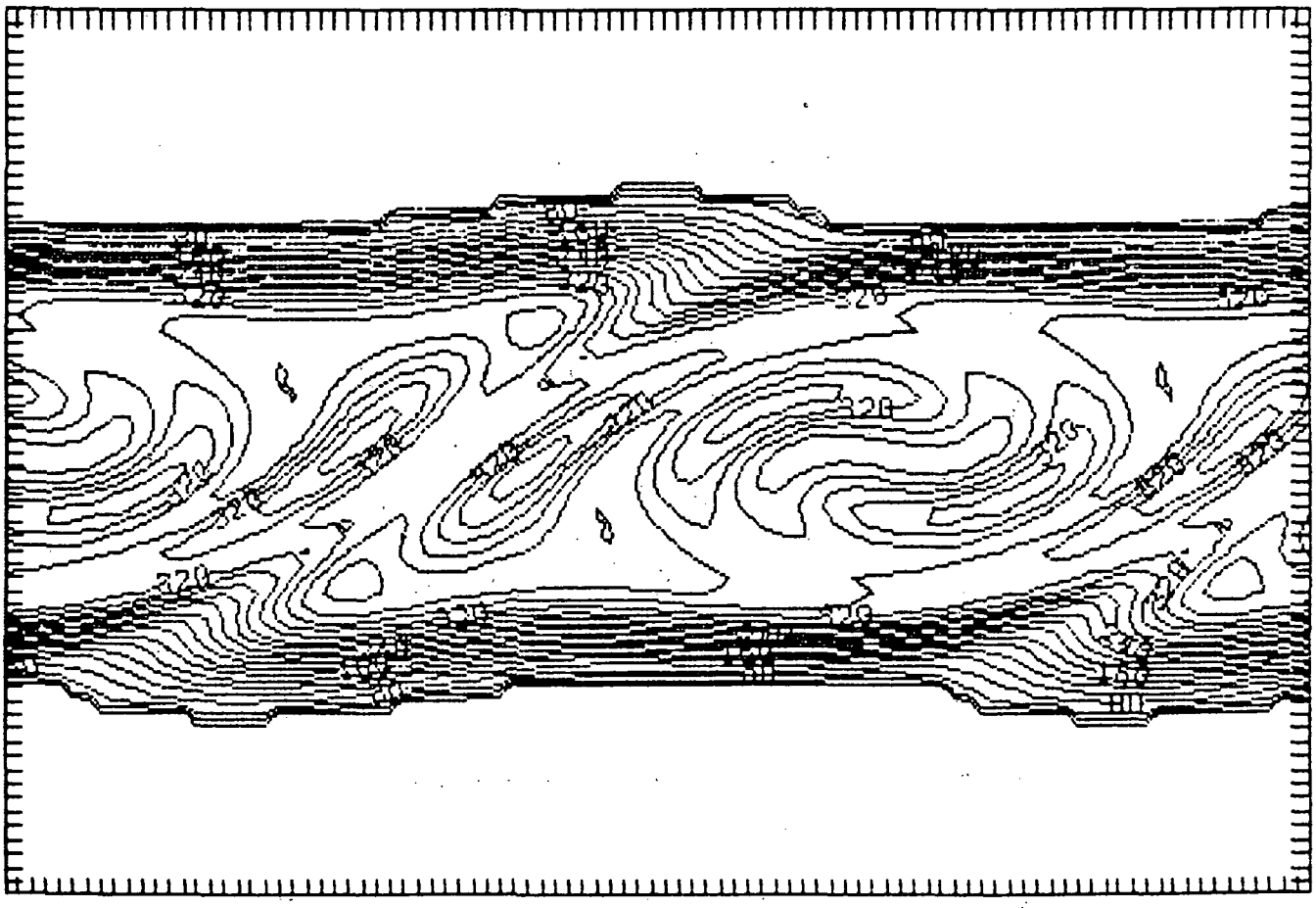

Figure 25. Plot of Product Concentration Contours at t = 24 for Case 1 (Fundamental Mode Alone) - Two-Dimensional Simulations

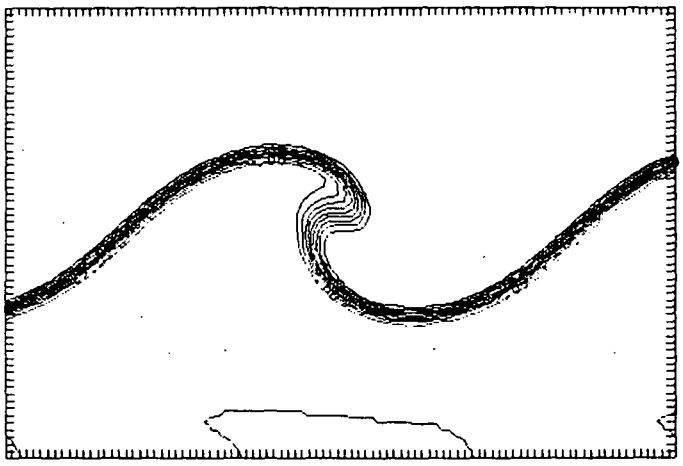

Figure 26a t = 12

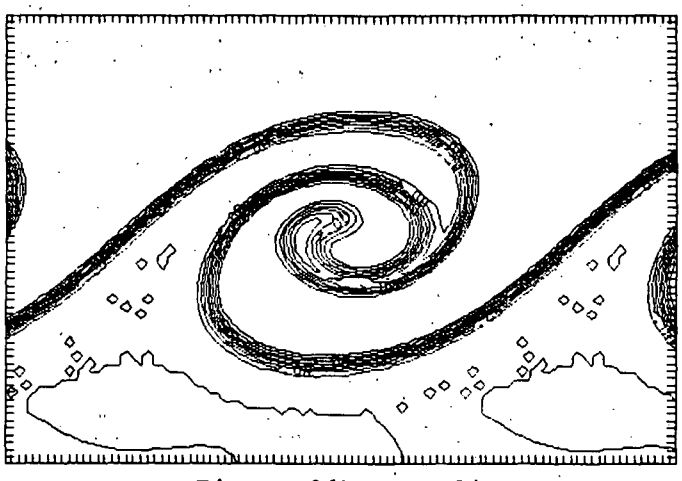

Figure 26b t = 24

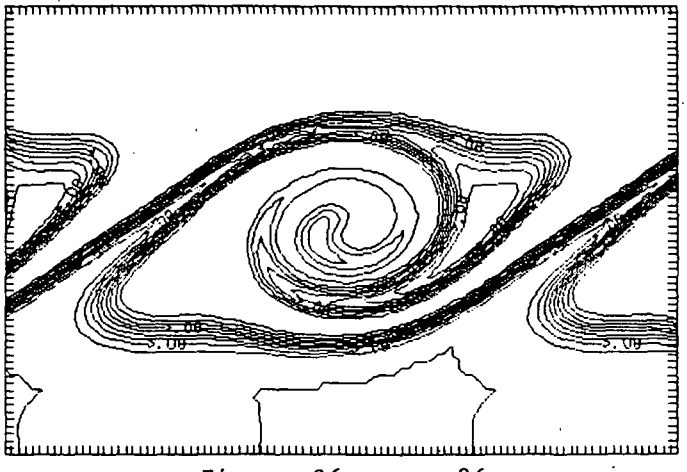

Figure 26c t = 36

Figure 26. Plots of Concentration Contours for Species A for a Sequence of Times for Case 2 (Subharmonic Mode Alone) - Two-Dimensional Simulations

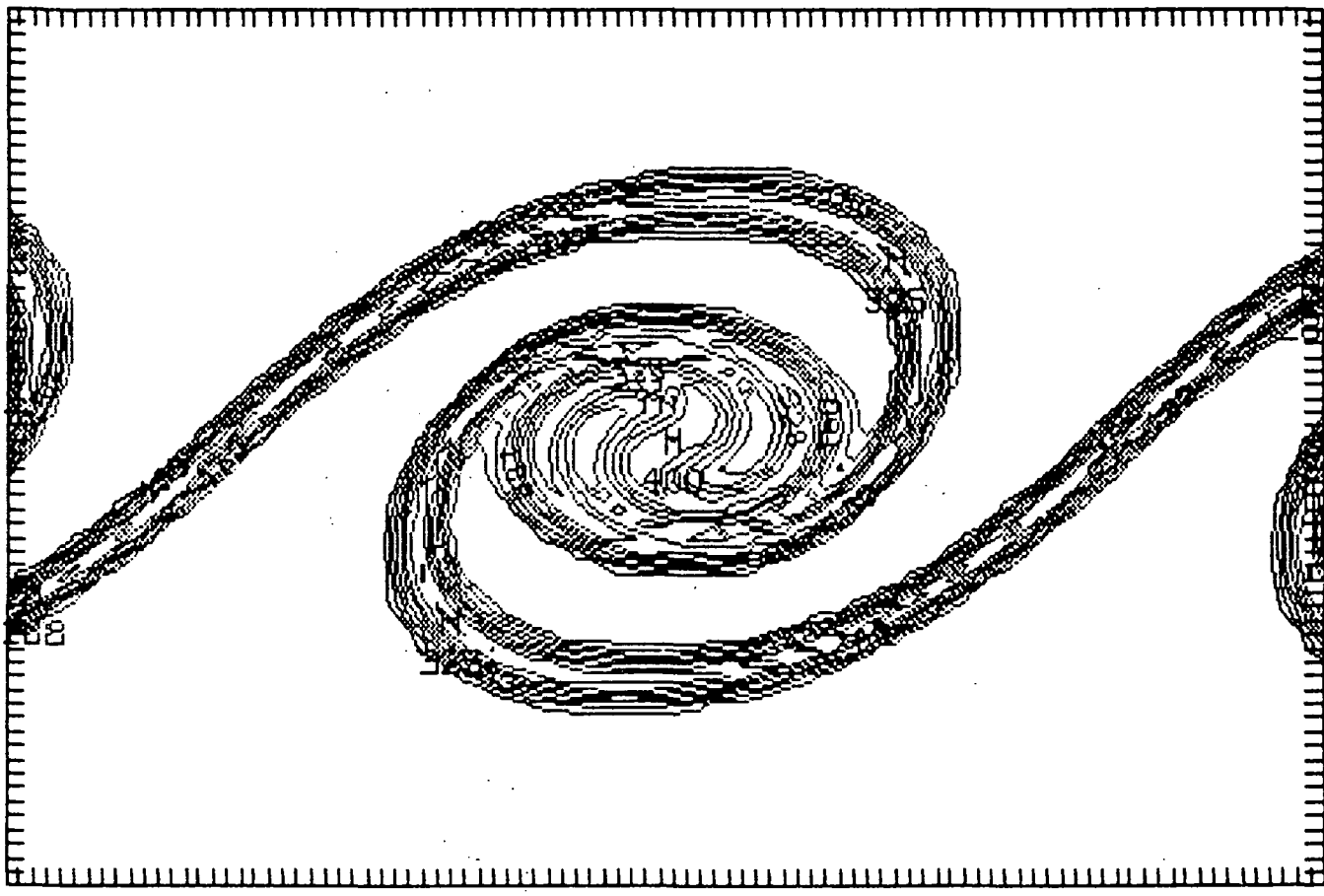

Figure 27. Plot of Product Concentration Contours at t = 24 for Case 2 (Subharmonic Mode Alone) - Two-Dimensional Simulations

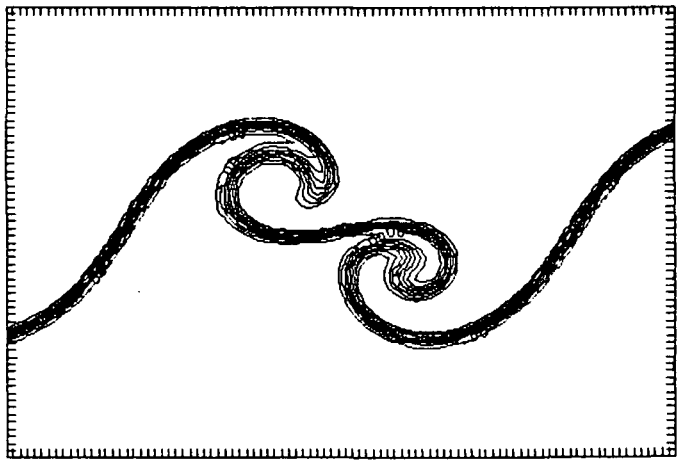

Figure 28a t = 12

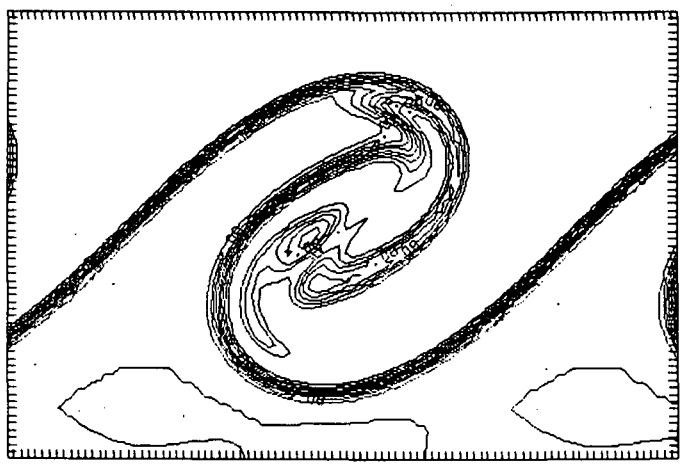

Figure 28b t = 24

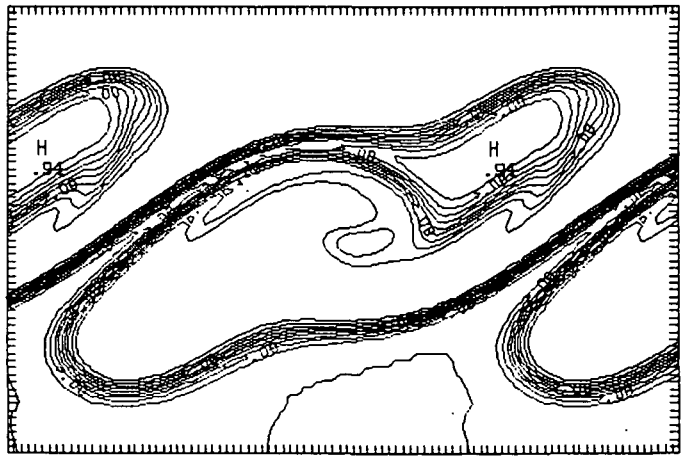

Figure 28c t = 36

Figure 28. Plots of Concentration Contours for Species A for a Sequence of Times for Case 3 (Fundamental and Subharmonic Added Together Out-of-Phase) - Two-Dimensional Simulations

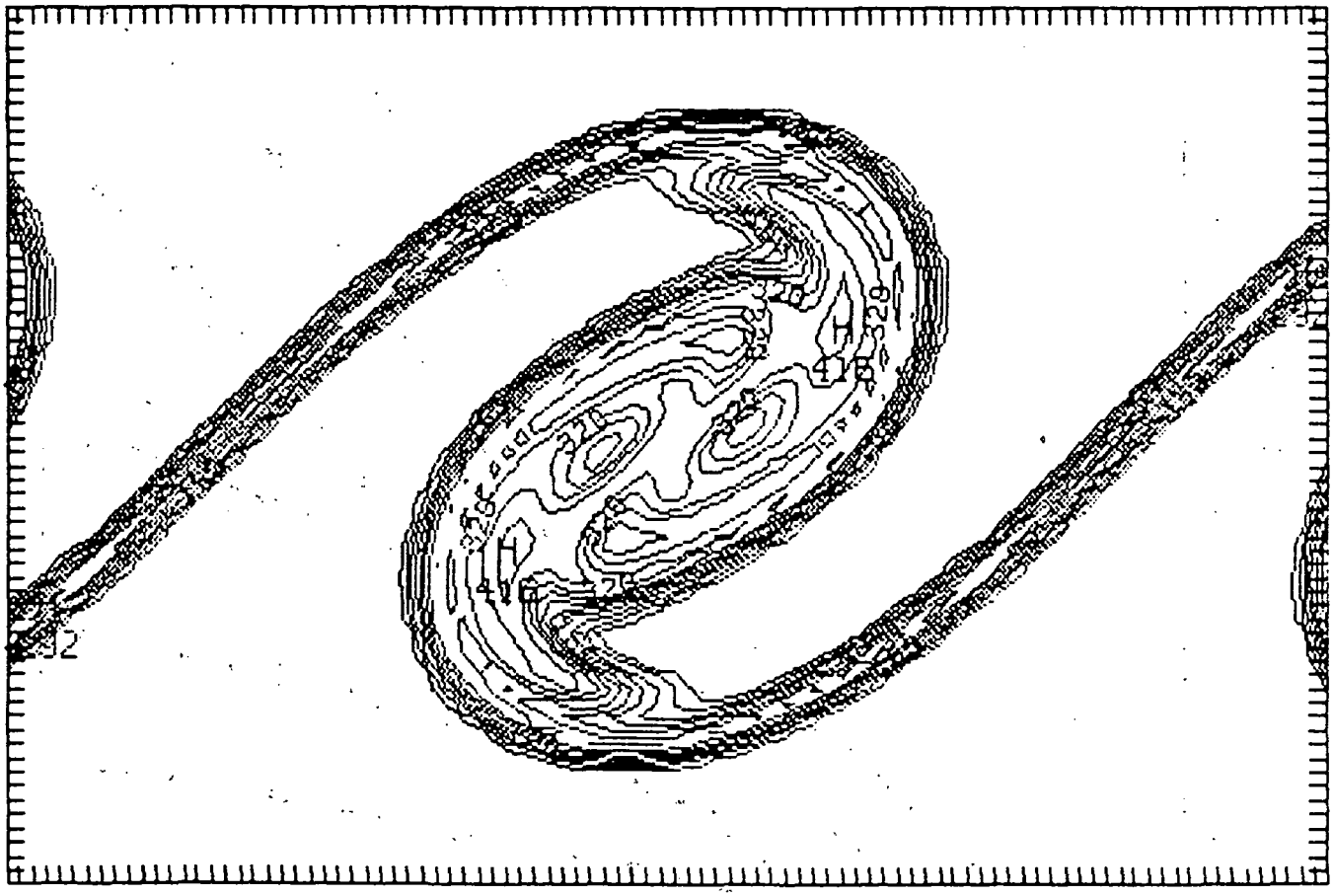

Figure 29. Plot of Product Concentration Contours at t = 24 for Case 3 (Fundamental and Subharmonic Added Together Out-of-Phase) - Two-Dimensional Simulations

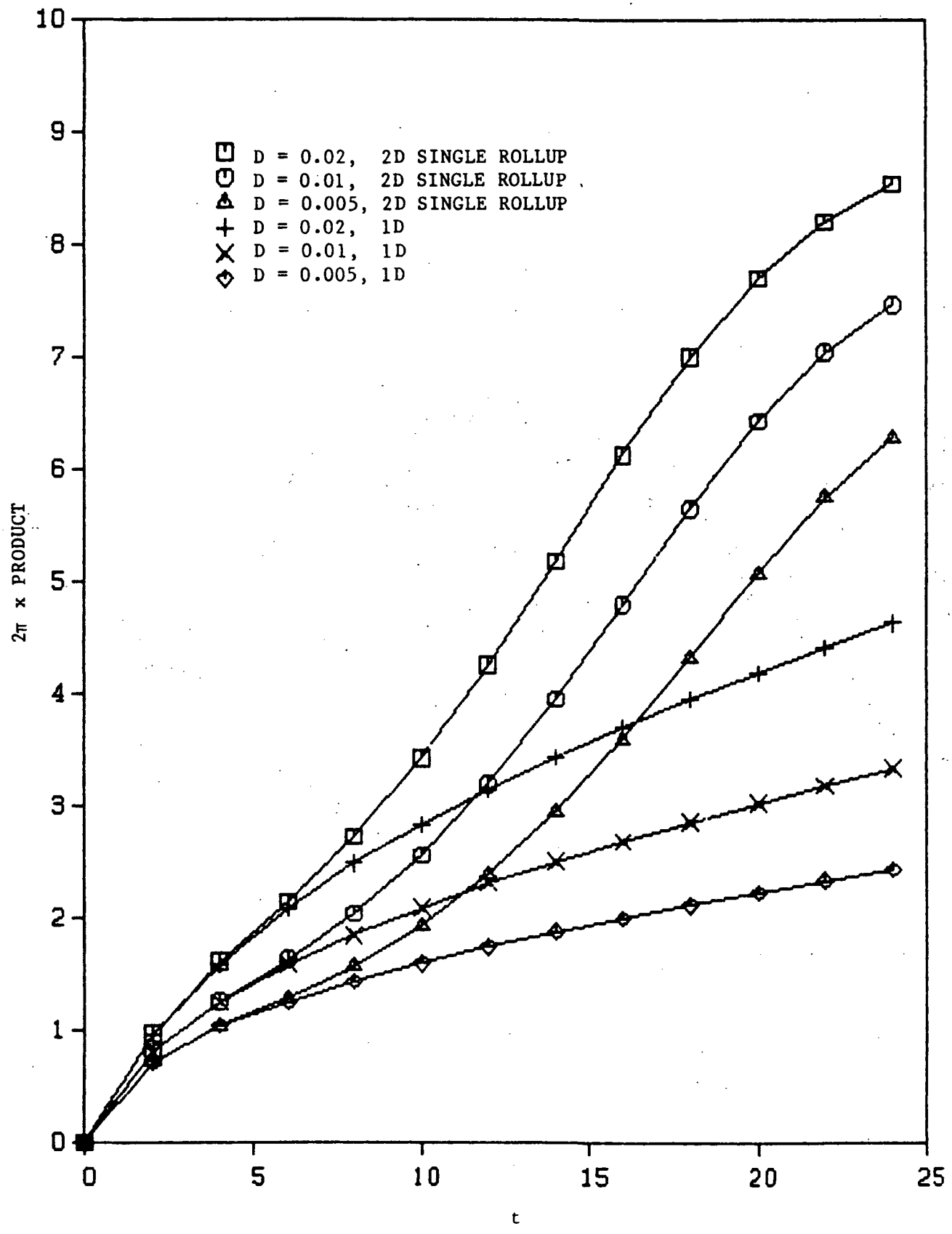

Figure 30. Total Product Versus Time for Different Diffusivities - One- and Two-Dimensional Simulations

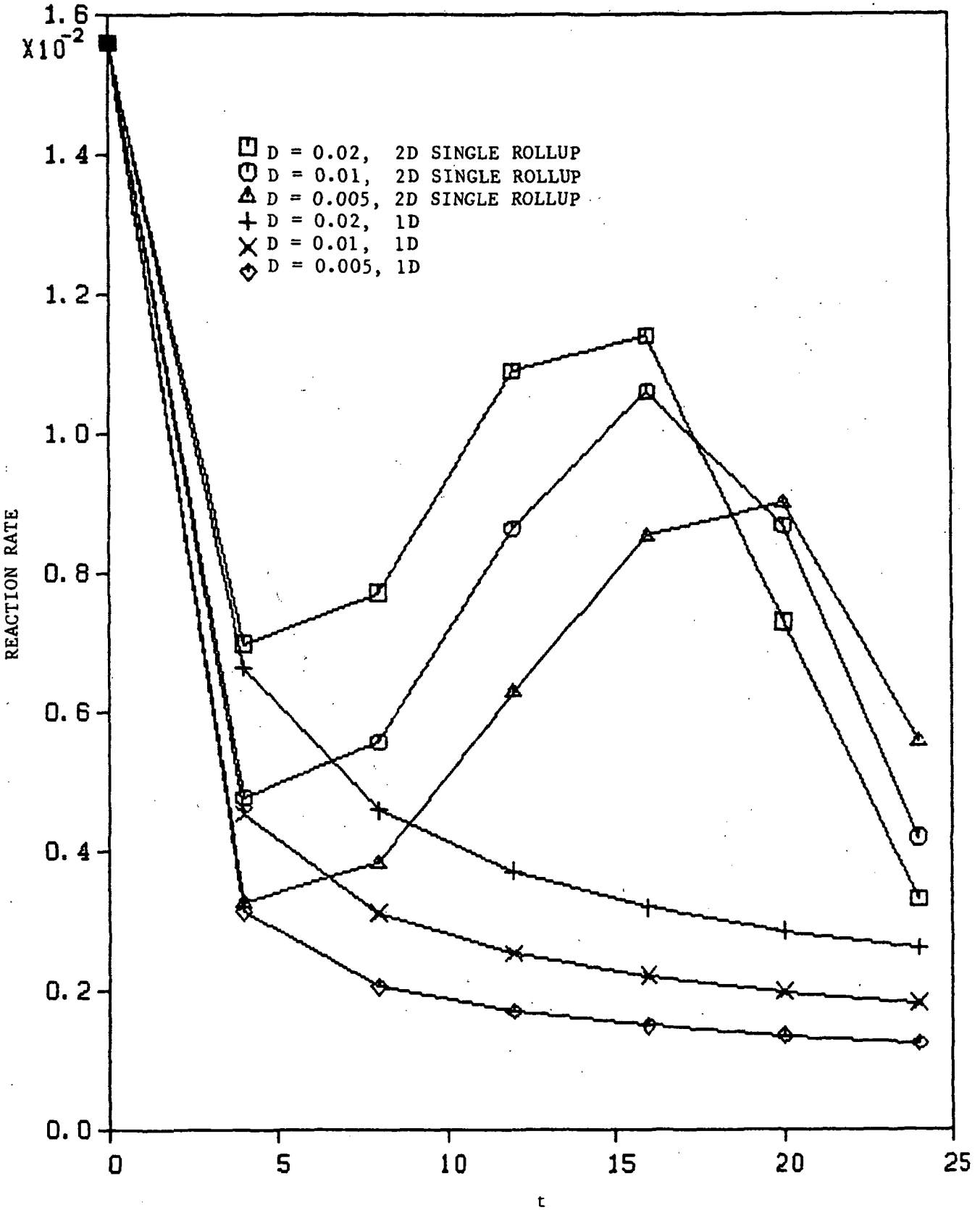

Figure 31. Total Reaction Rate Versus Time for Different Diffusivities - One- and Two-Dimensional Simulations

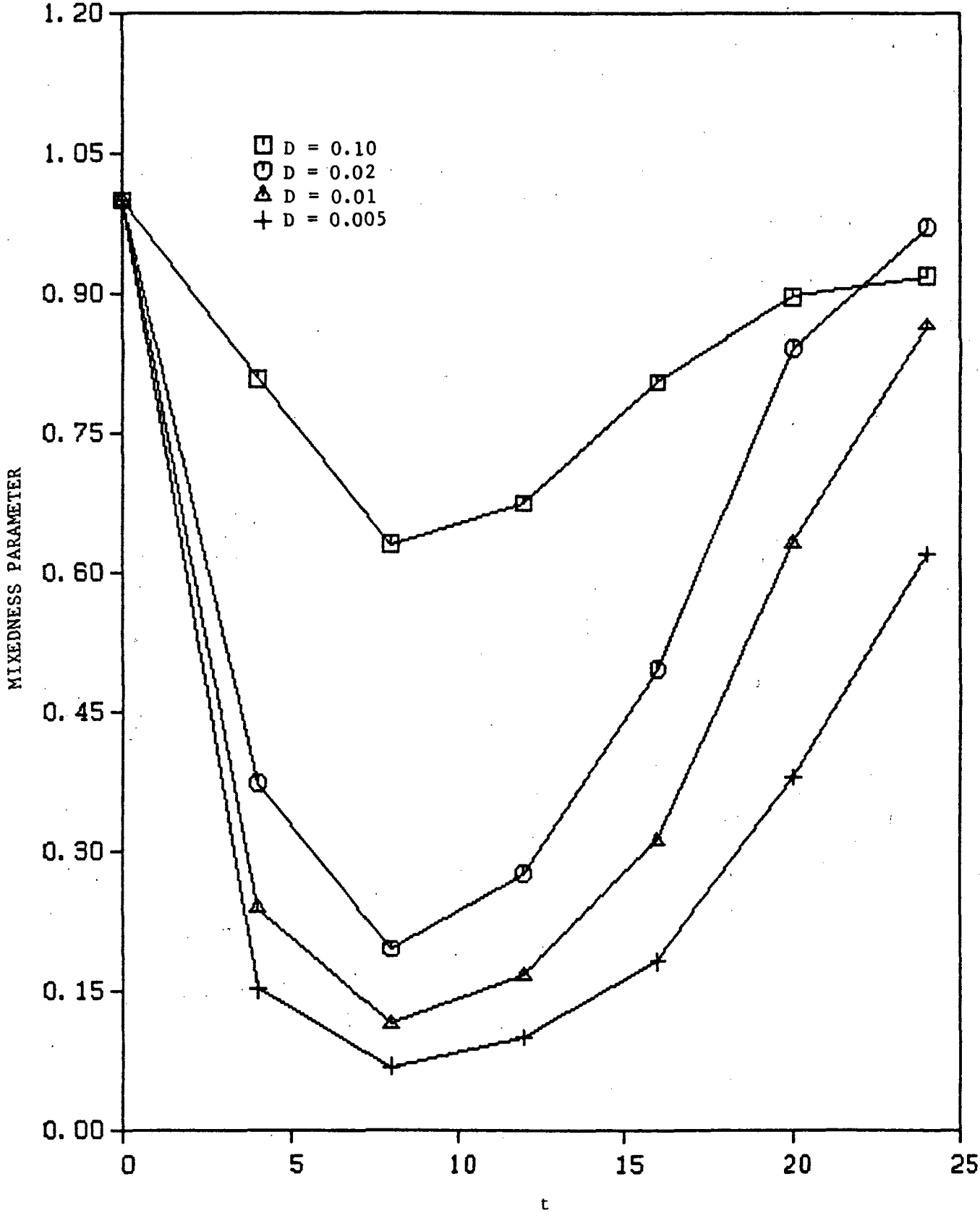

Figure 32. Mixedness Parameter Versus Time for Different Diffusivities - Case 1 (Fundamental Mode Alone), Two-Dimensional Simulations

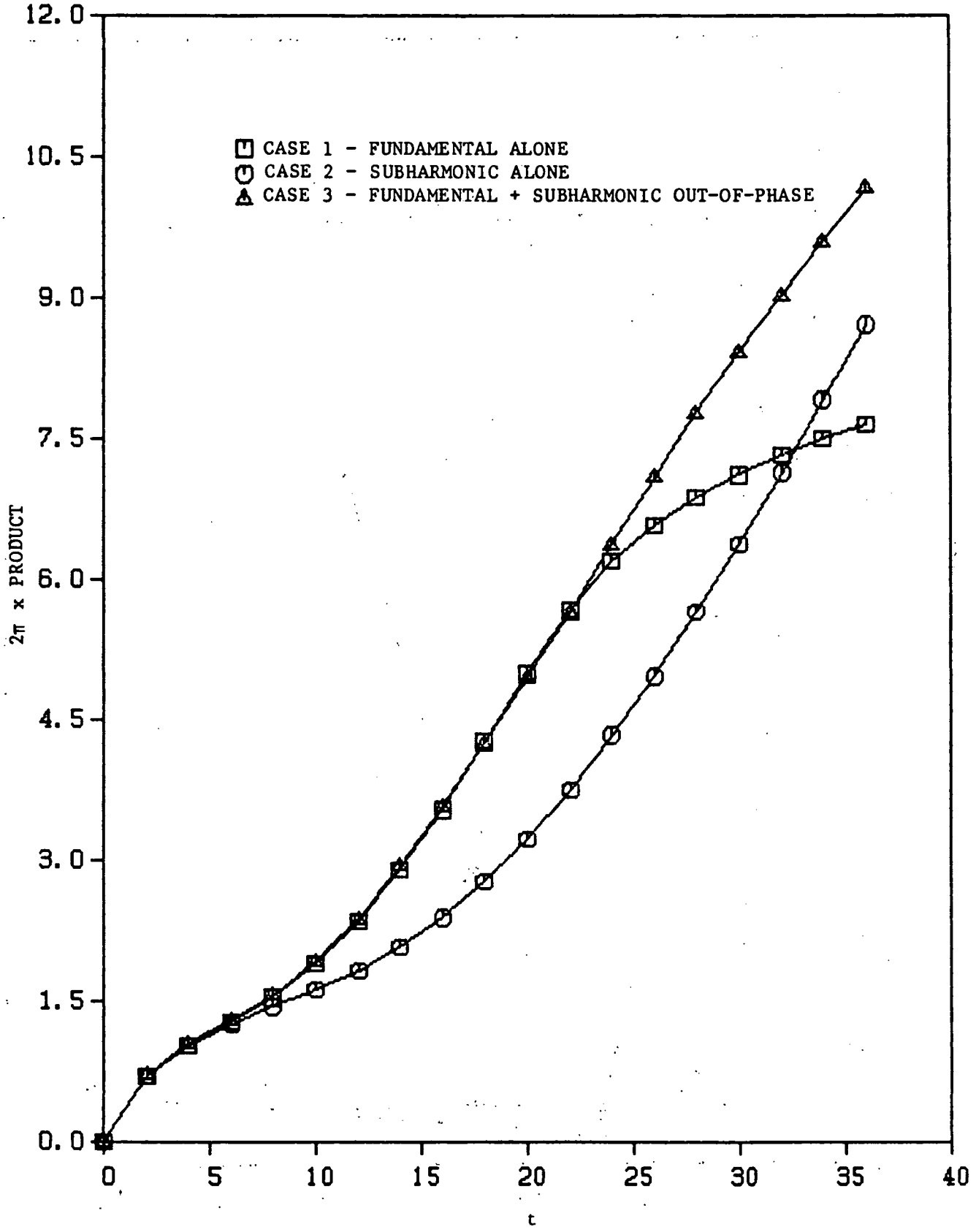

Figure 33. Total Product Versus Time - Two-Dimensional Simulations

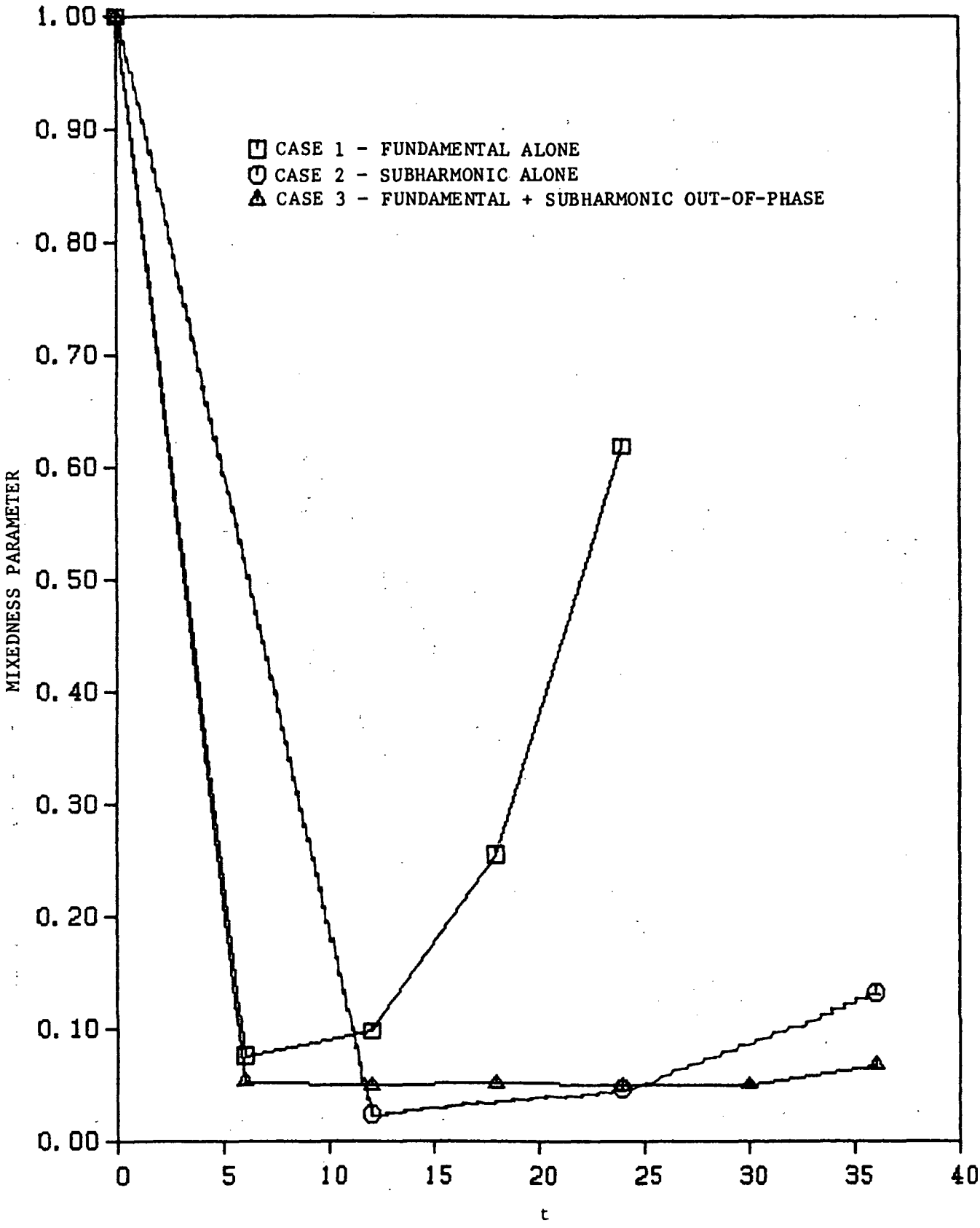

Figure 34. Mixedness Parameter Versus Time - Two-Dimensional Simulations

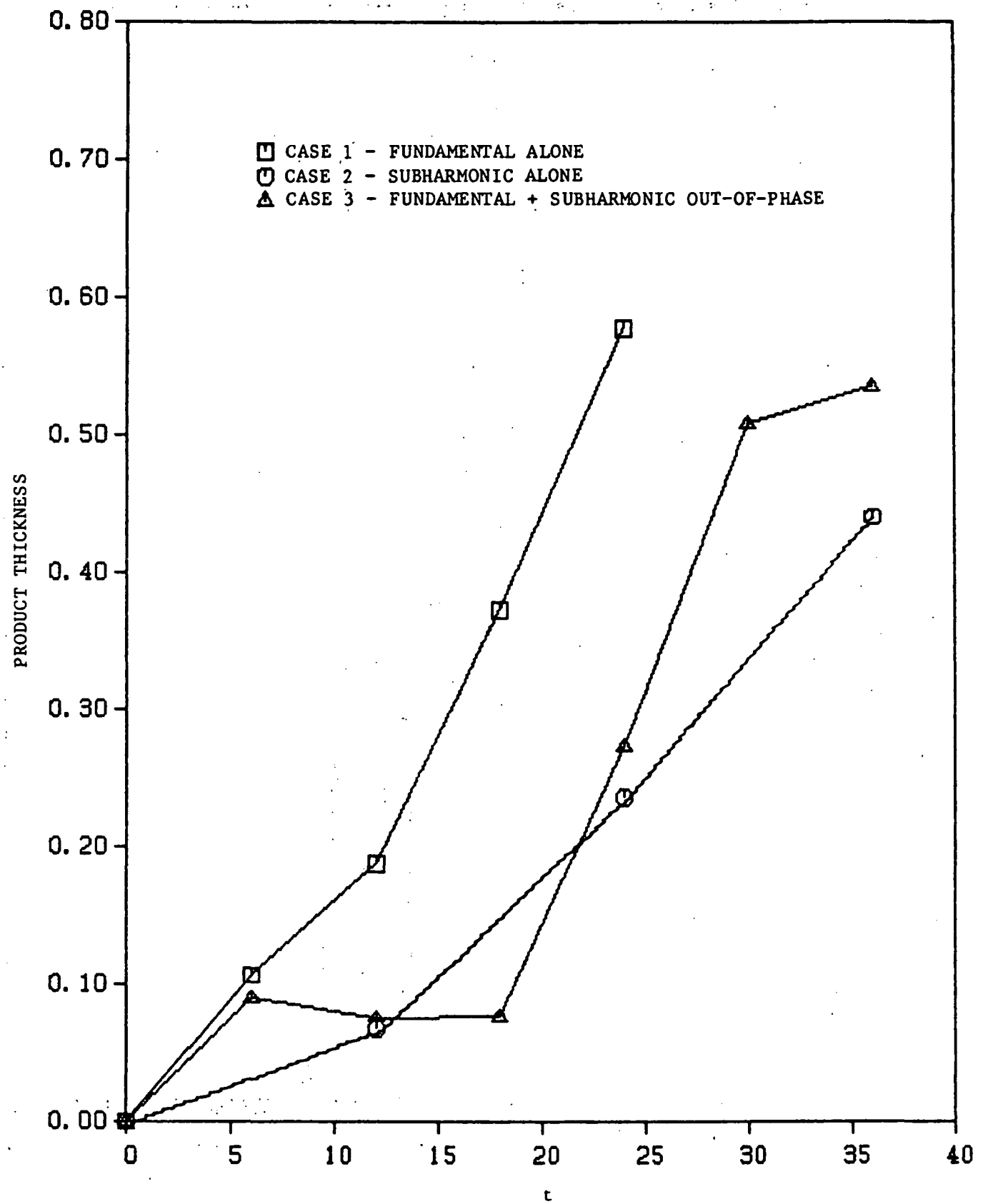

Figure 35. Nondimensional Product Thickness Versus Time - Two-Dimensional Simulations

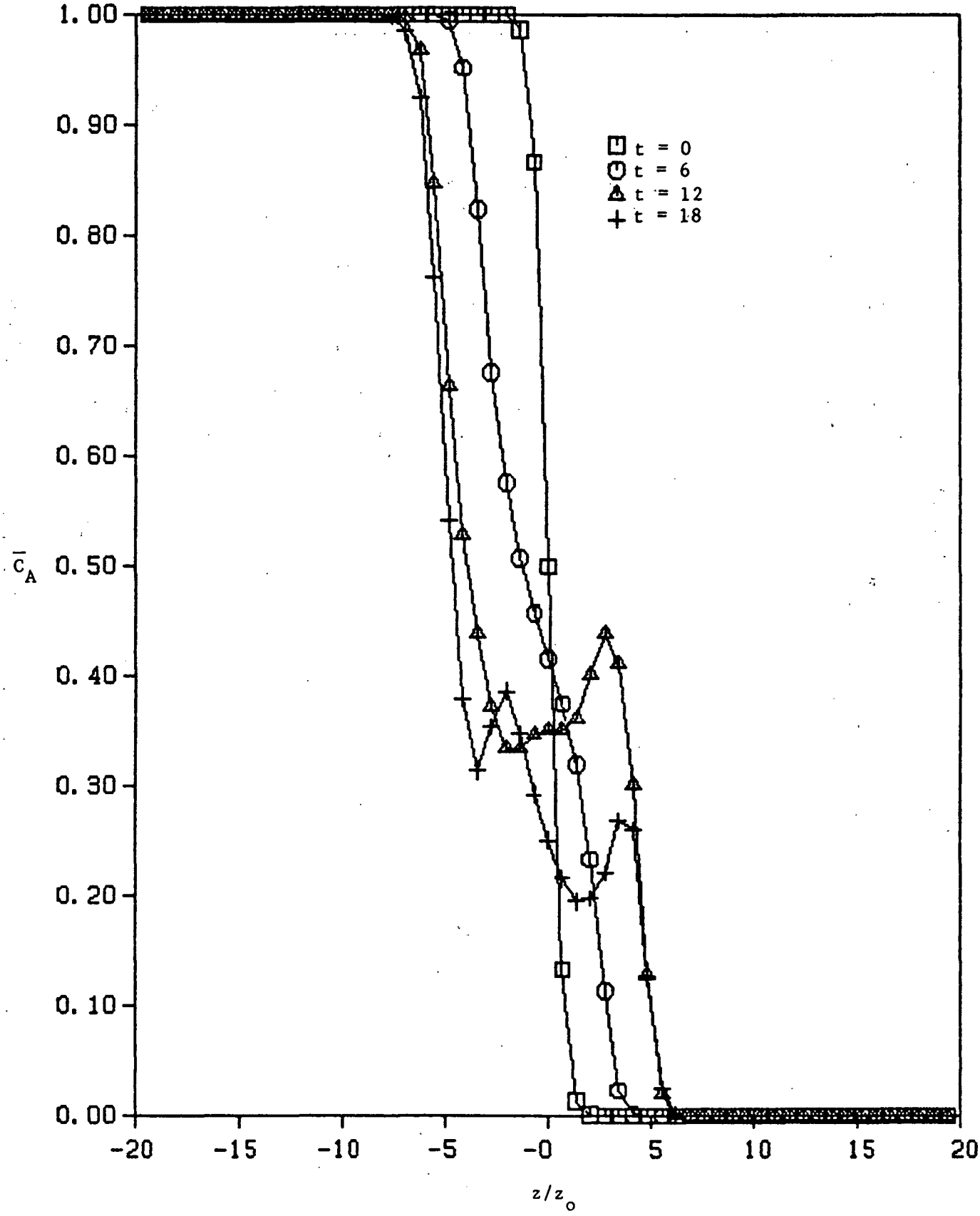

Figure 36. Average Concentration of Species A Versus z for Several Different Times for Case 1 (Fundamental Mode Alone) - Two-Dimensional Simulations

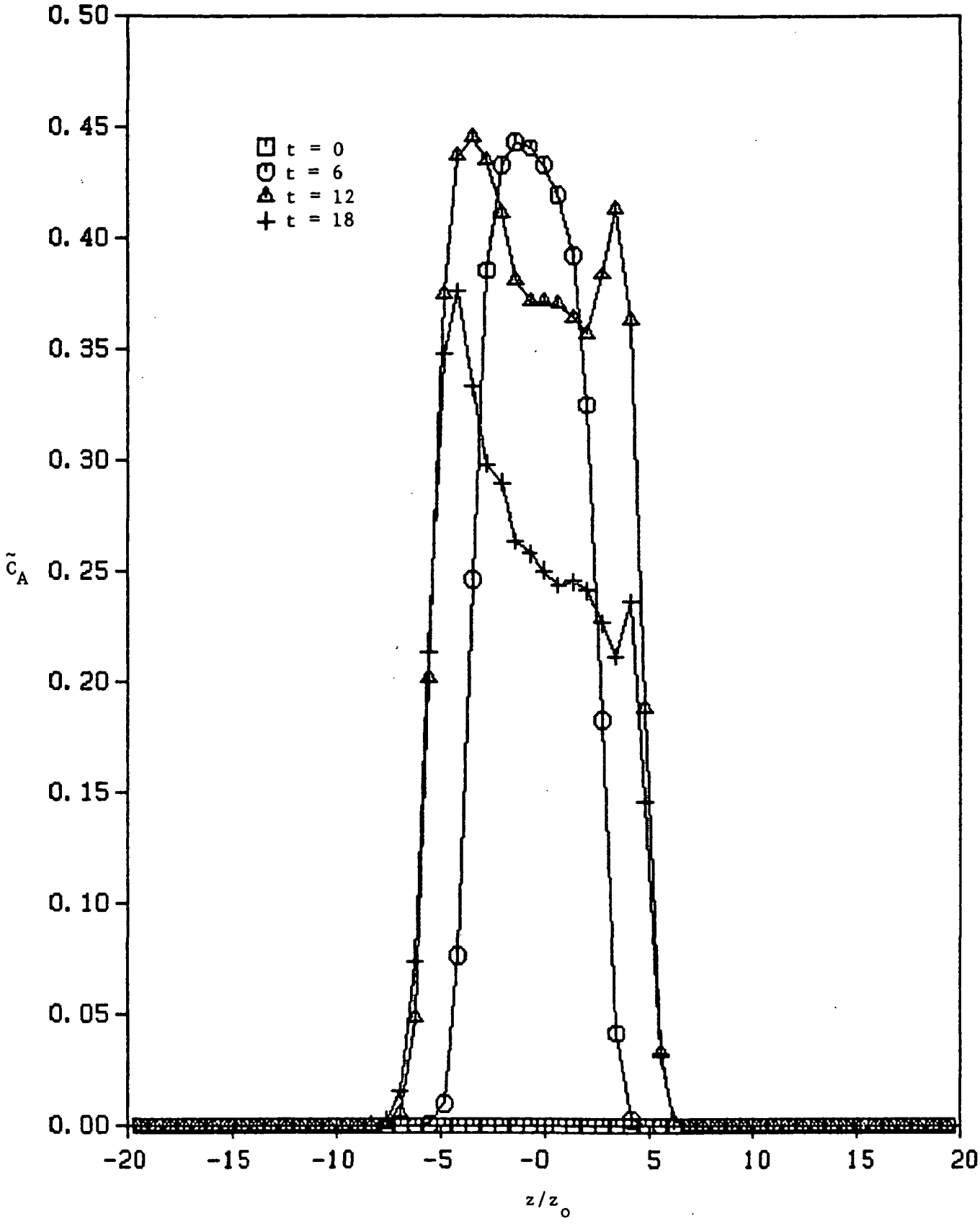

Figure 37. RMS of the Concentration Fluctuation of Species A Versus z for Several Different Times for Case 1 (Fundamental Mode Alone) - Two-Dimensional Simulations

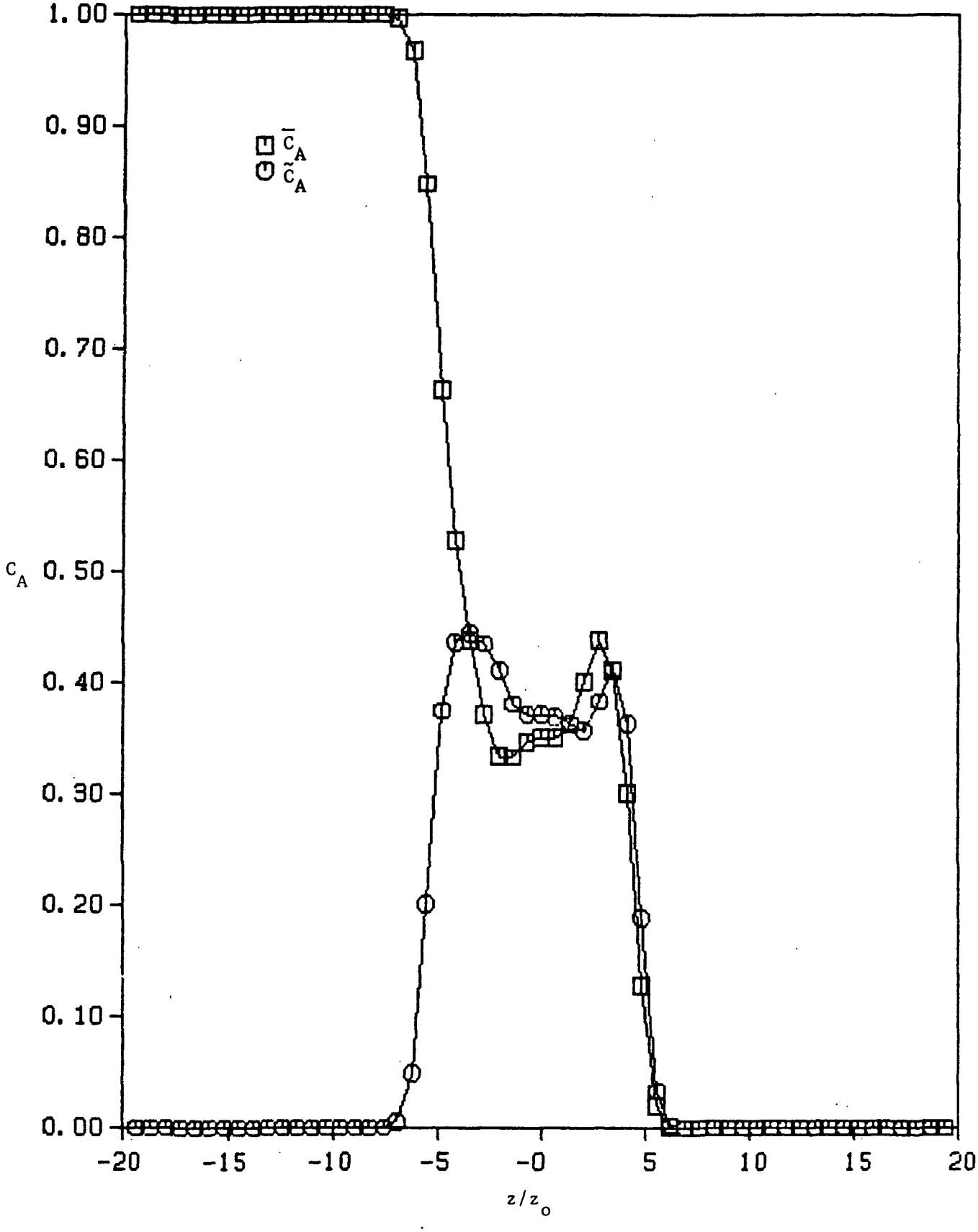

Figure 38. RMS of the Concentration Fluctuation and Average Concentration of Species A at t = 12 for Case 1 (Fundamental Mode Alone) - Two-Dimensional Simulations

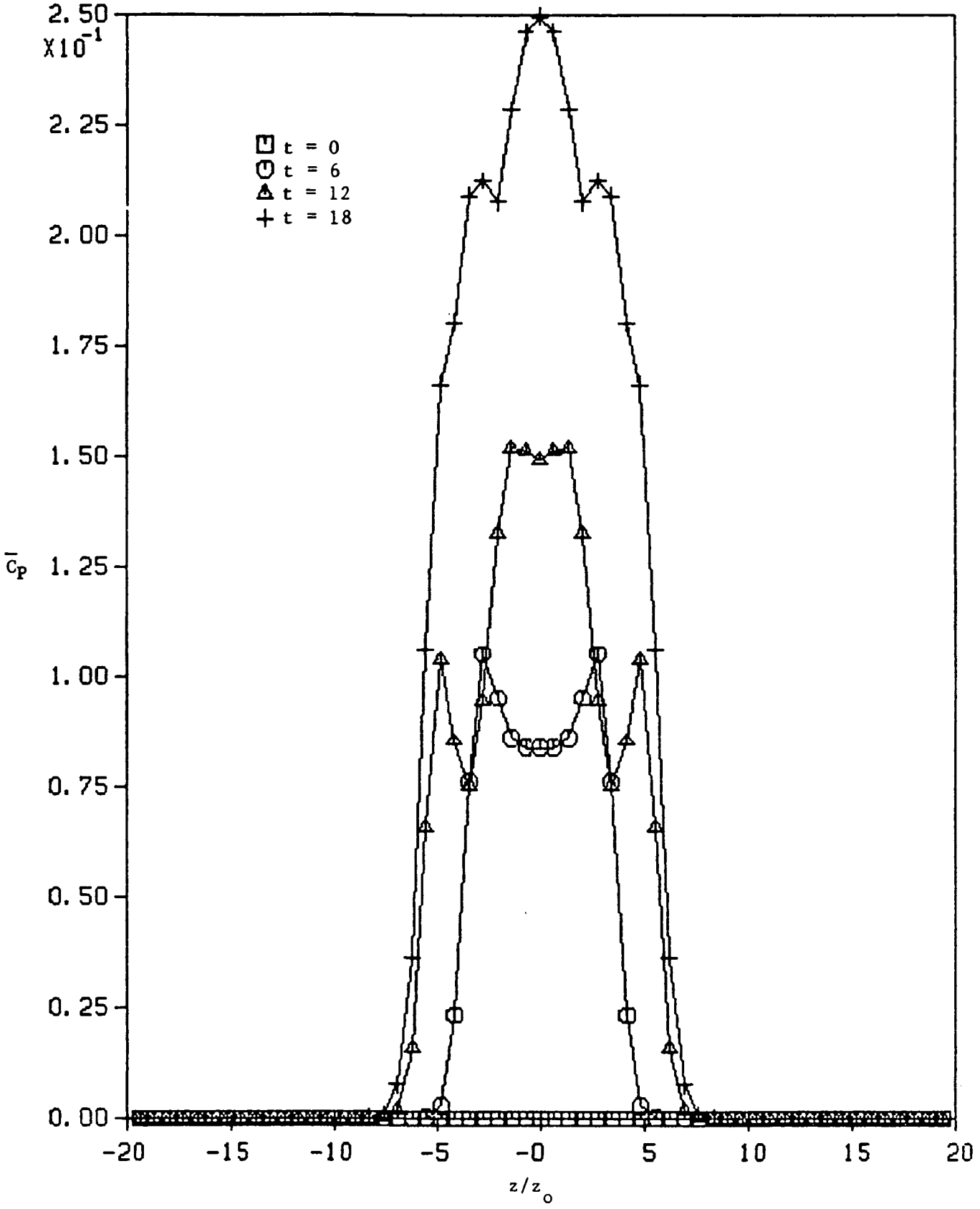

Figure 39. Average Product Concentration Versus z for Several Different Times for Case 1 (Fundamental Mode Alone) - Two-Dimensional Simulations

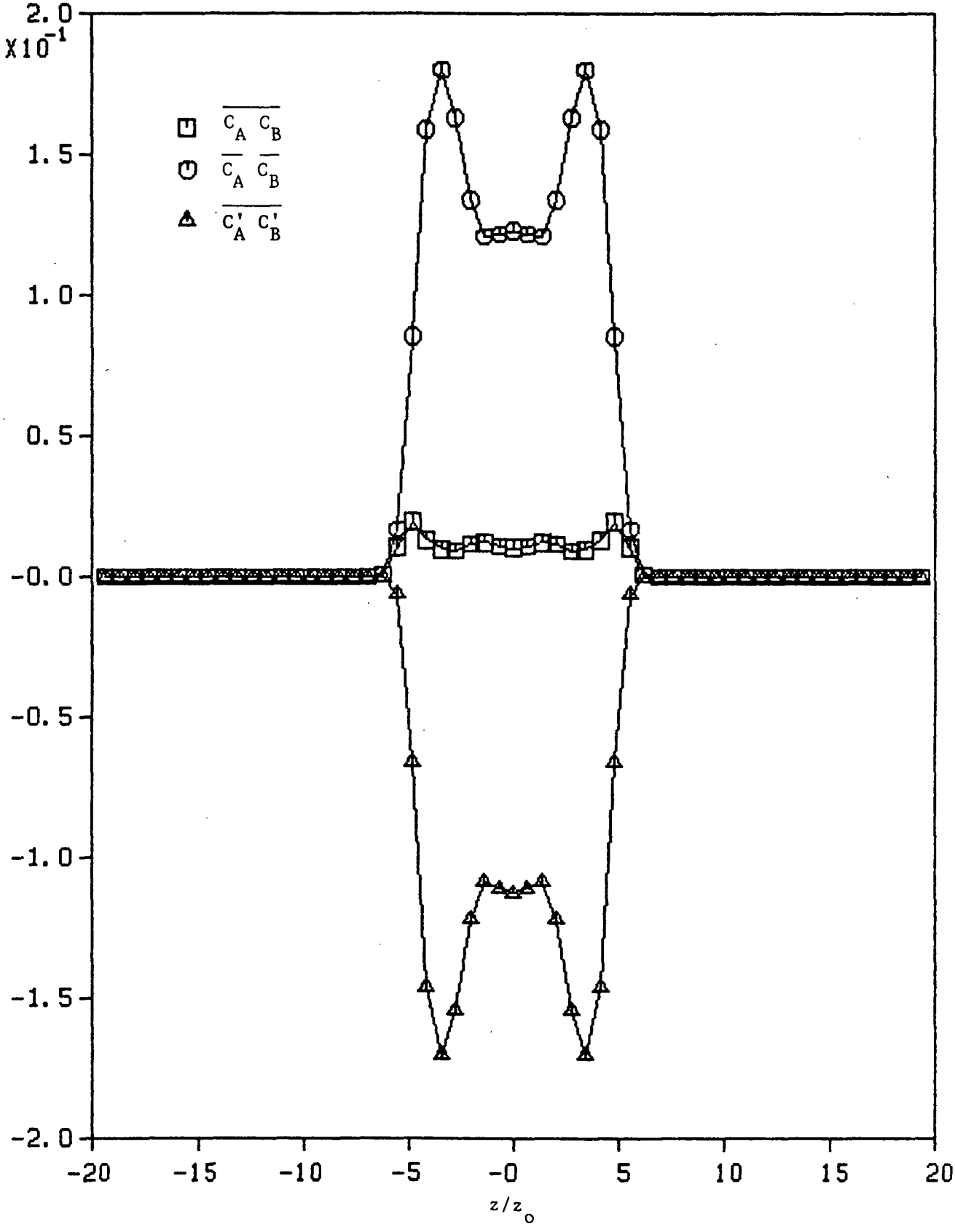

Figure 40. The Average of the Product of the Concentrations, the Product of the Averages, and the Concentration Correlation Versus z for Case 1 (Fundamental Mode Alone) at t = 12 - Two-Dimensional Simulations

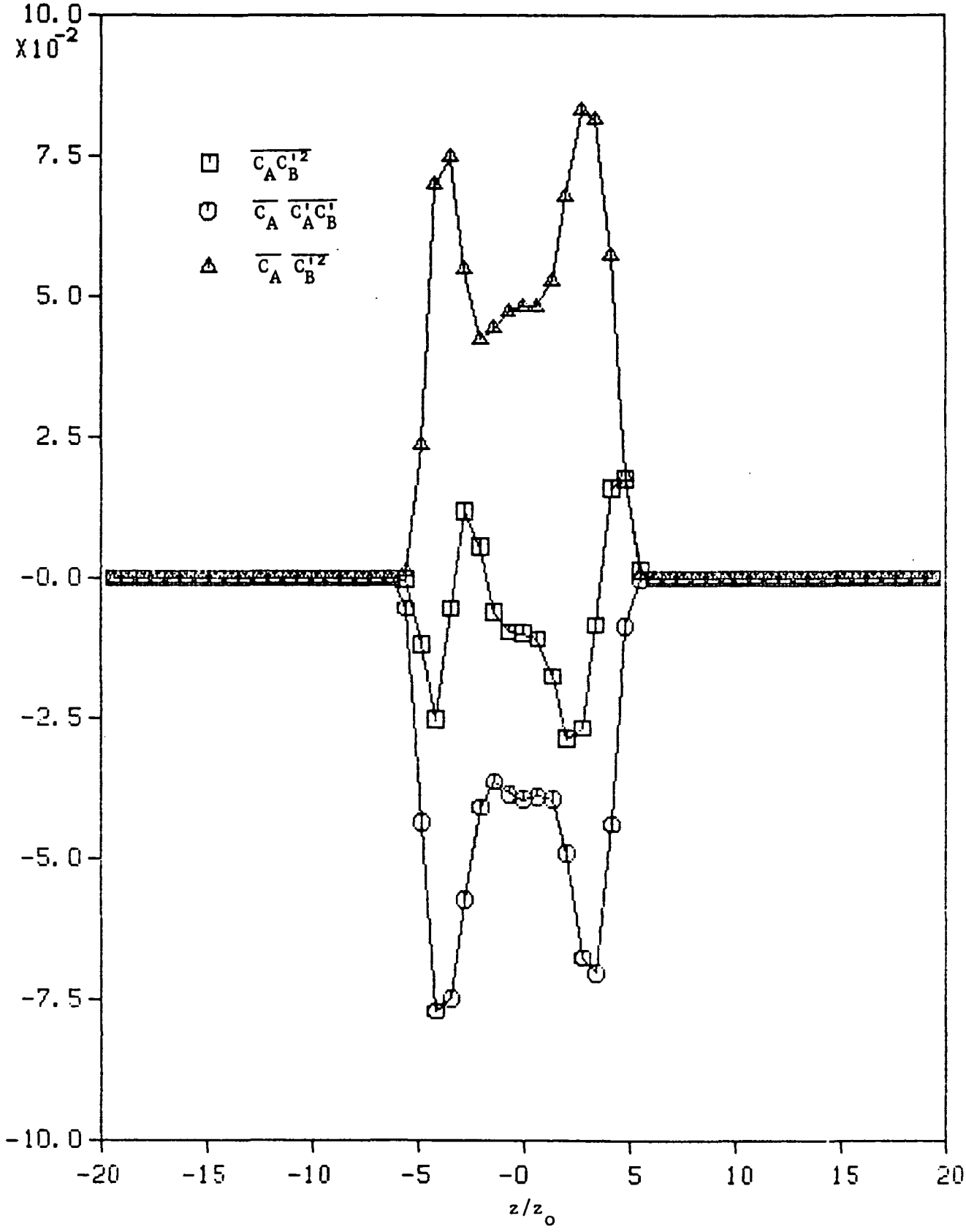

Figure 41. Various Concentration Moments Versus z for Case 1 (Fundamental Mode Alone) at t = 12 - Two-Dimensional Simulations

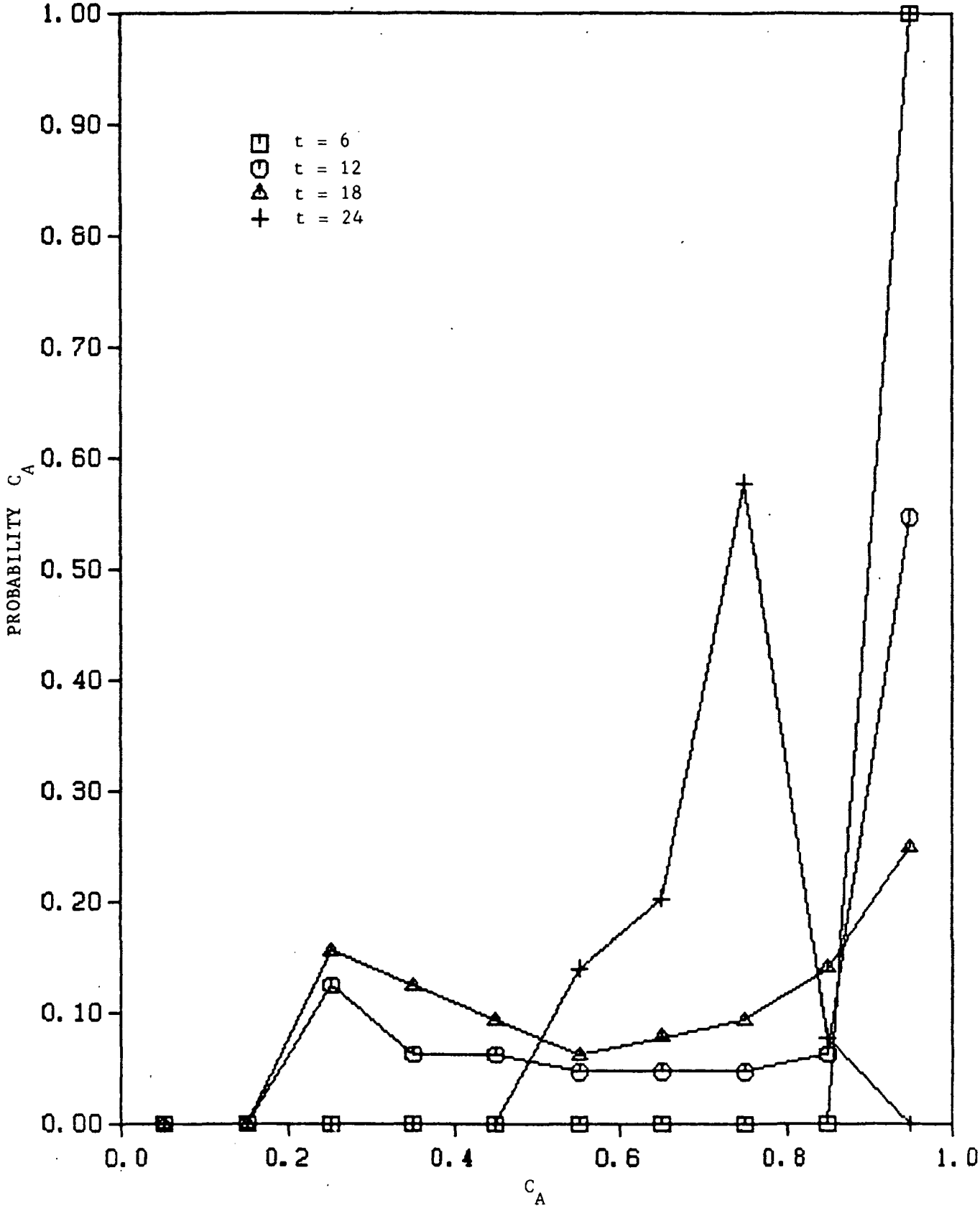

Figure 42. The Probability Density Function for the Concentration of Species A at the Transverse Distance $-\pi/2$ for a Sequence of Times for Case 1 (Fundamental Mode Alone) - Two-Dimensional Simulations

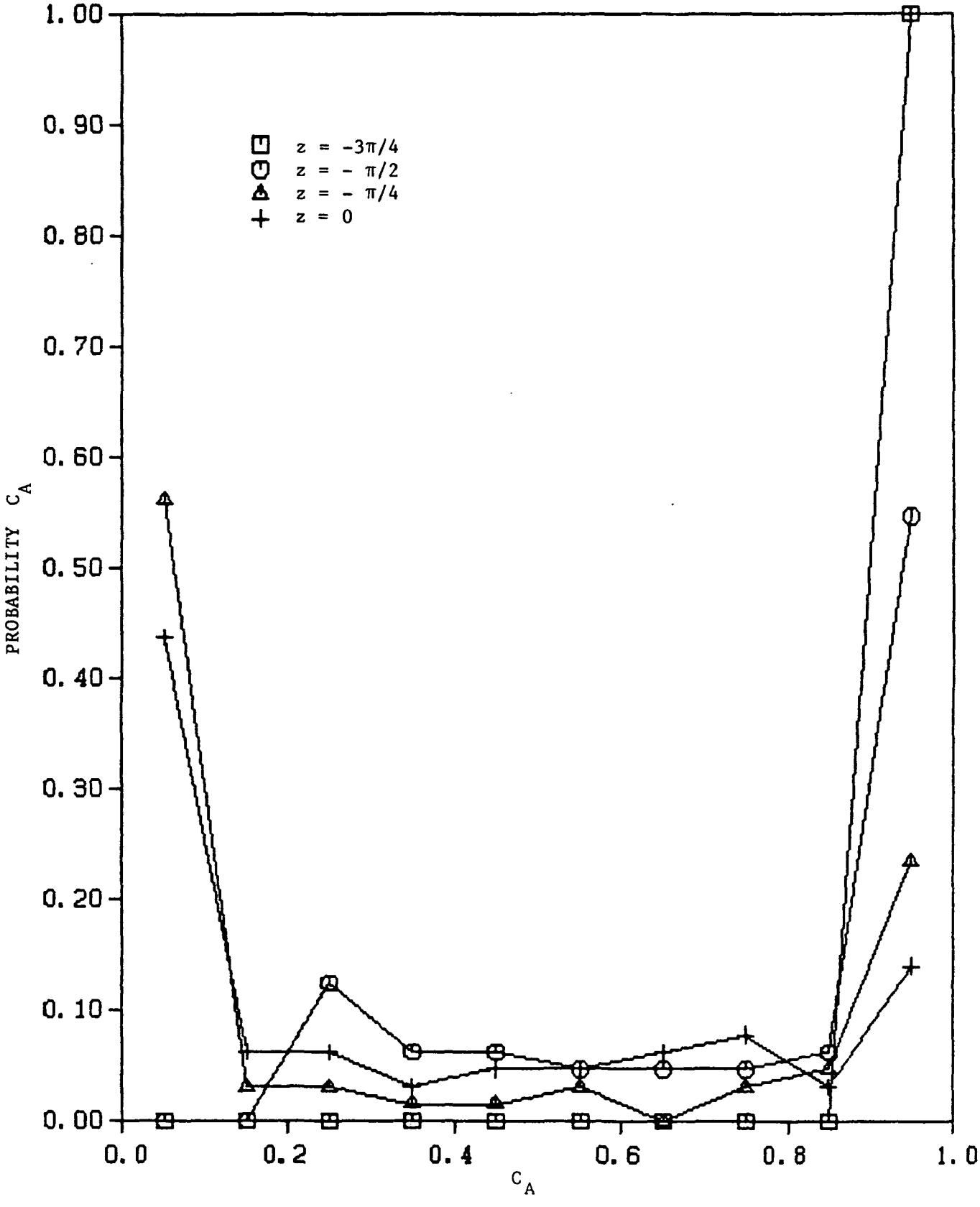

Figure 43. The Probability Density Function for the Concentration of Species A at t = 12 for Various Transverse Distances for Case 1 (Fundamental Mode Alone) - Two-Dimensional Simulations

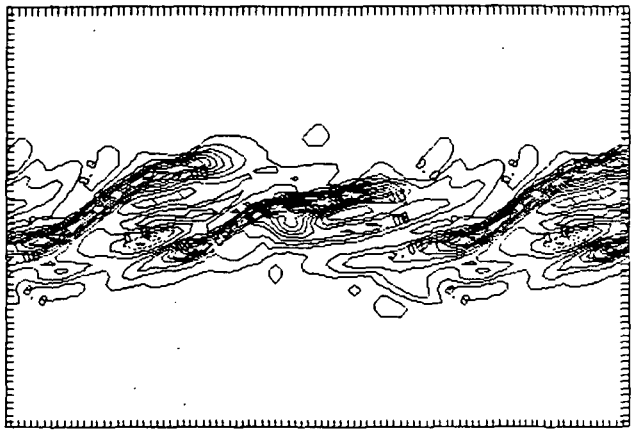

Figure 44a t = 6

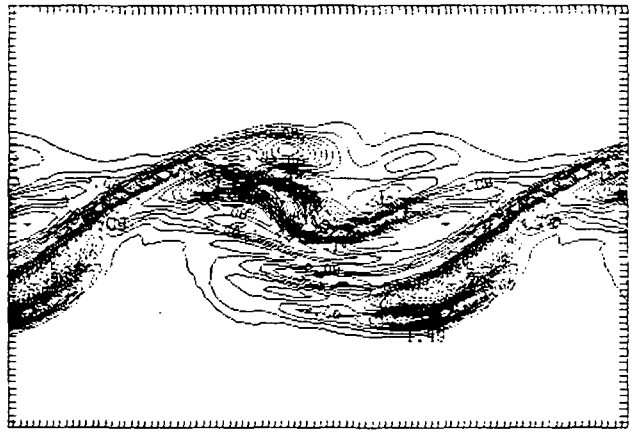

Figure 44b t = 12

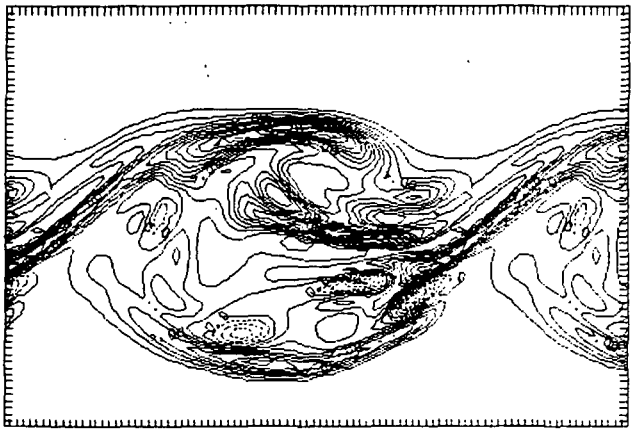

Figure 44c t = 18

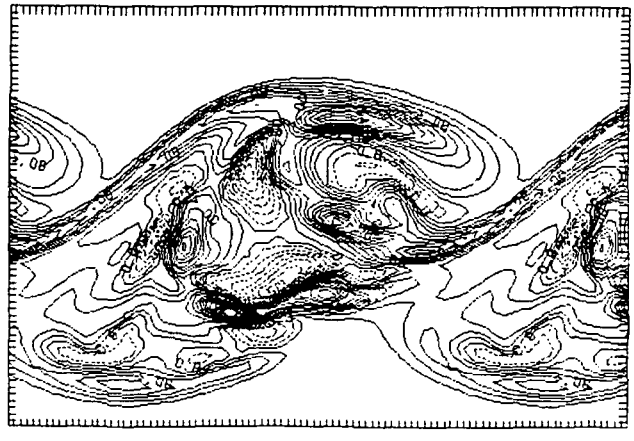

Figure 44d t = 24

Figure 44. Plots of Lateral (y) Vorticity Contours for a Sequence of Times in an x-z Plane - Single Rollup Case, Three-Dimensional Simulations, Run JN20B

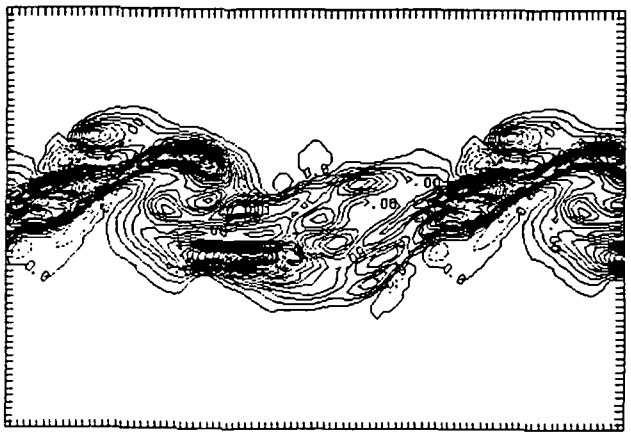

Figure 45a t = 6

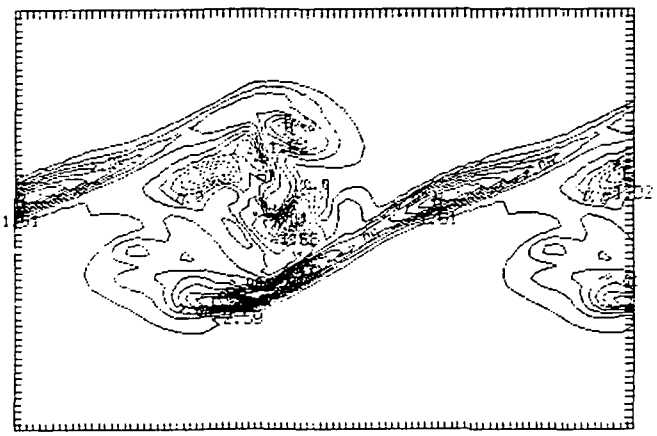

Figure 45b t = 12

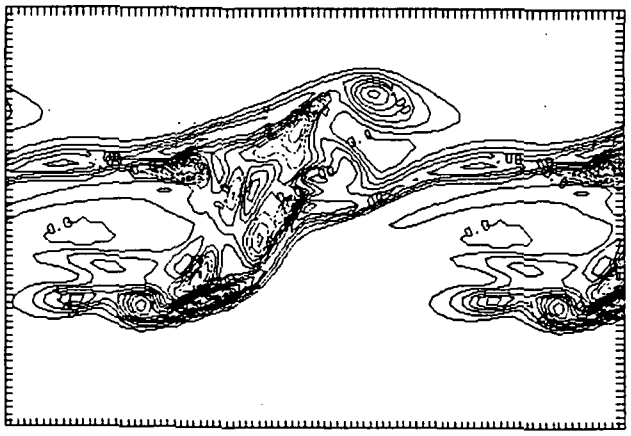

Figure 45c t = 18

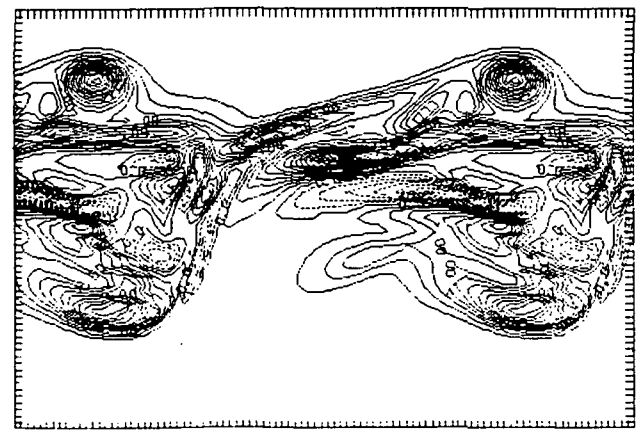

Figure 45d t = 24

Figure 45. Plots of Lateral (y) Vorticity Contours for a Sequence of Times in an x-z Plane Located a Lateral Distance $L_y/2$ from that Depicted in Figure 44 - Single Rollup Case, Three-Dimensional Simulations, Run JN20B

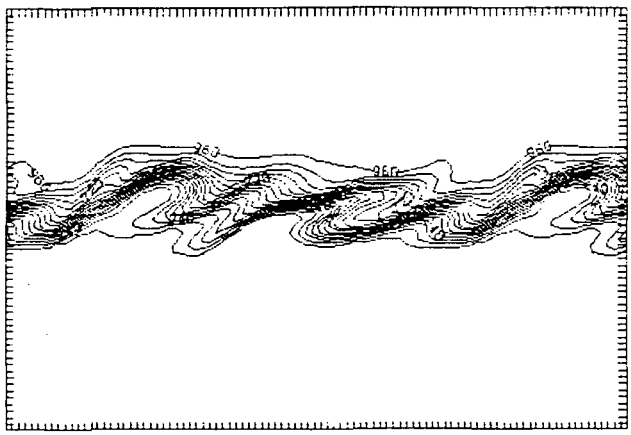

Figure 46a t = 6

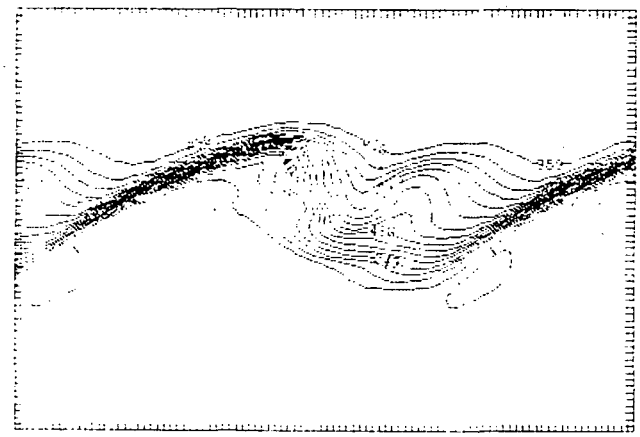

Figure 46b t = 12

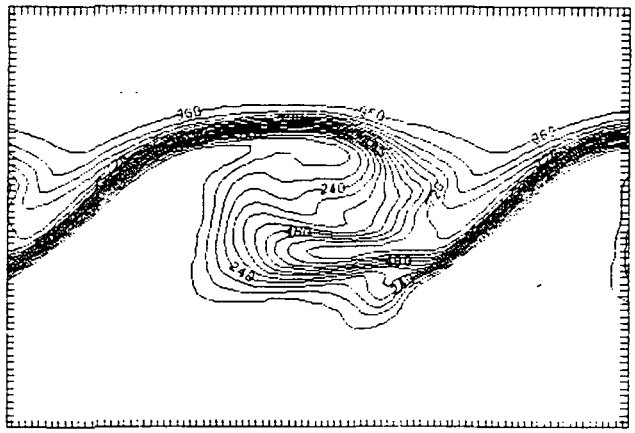

Figure 46c t = 18

Figure 46d t = 24

Figure 46. Plots of Concentration Contours for Species B for a Sequence of Times in the Same x-z Plane as for Figure 44 - Single Rollup Case, Three-Dimensional Simulations

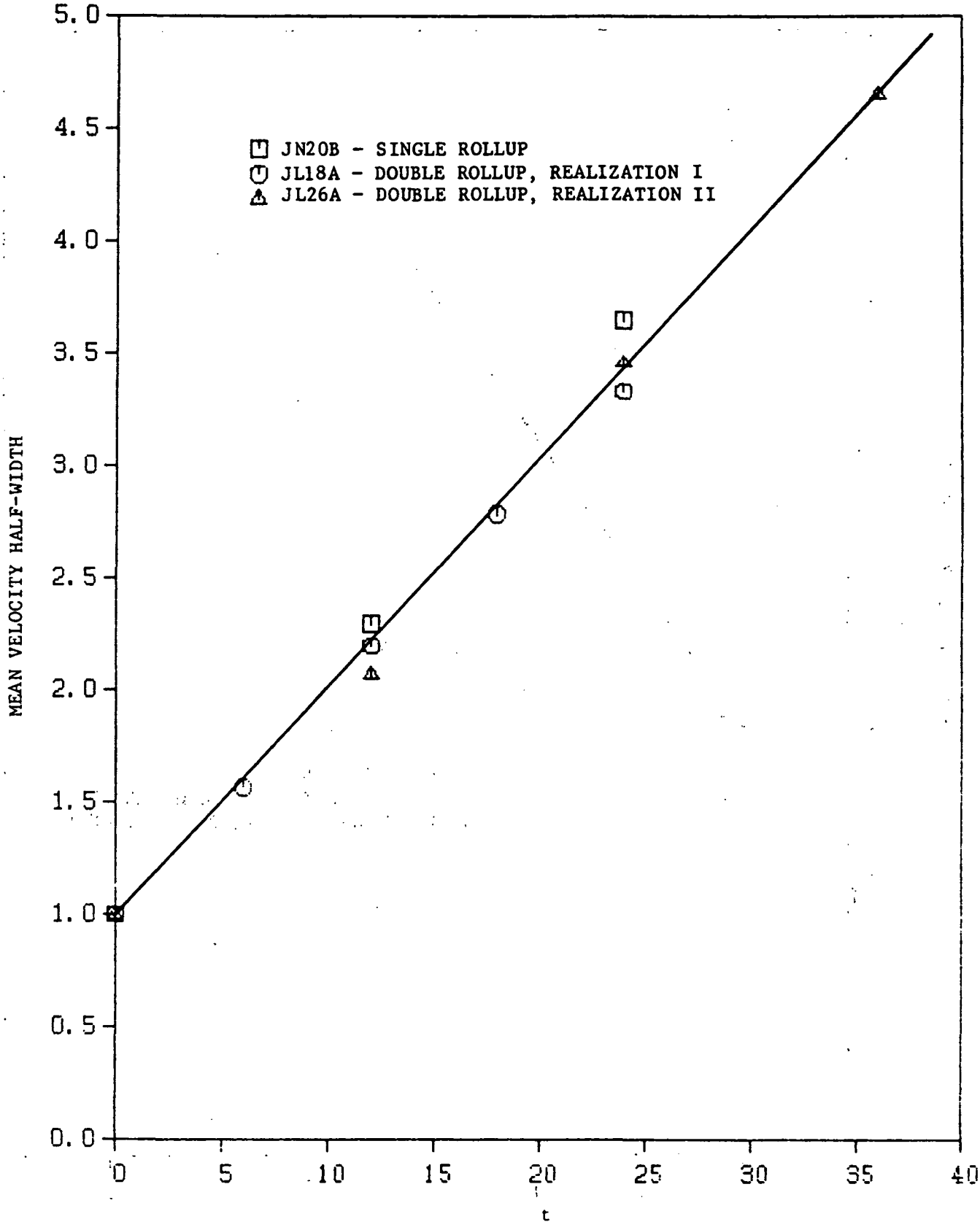

Figure 47. Mean Velocity Half-Width, z_M (= $z_{1/2}$), Versus Time - Three-Dimensional Simulations

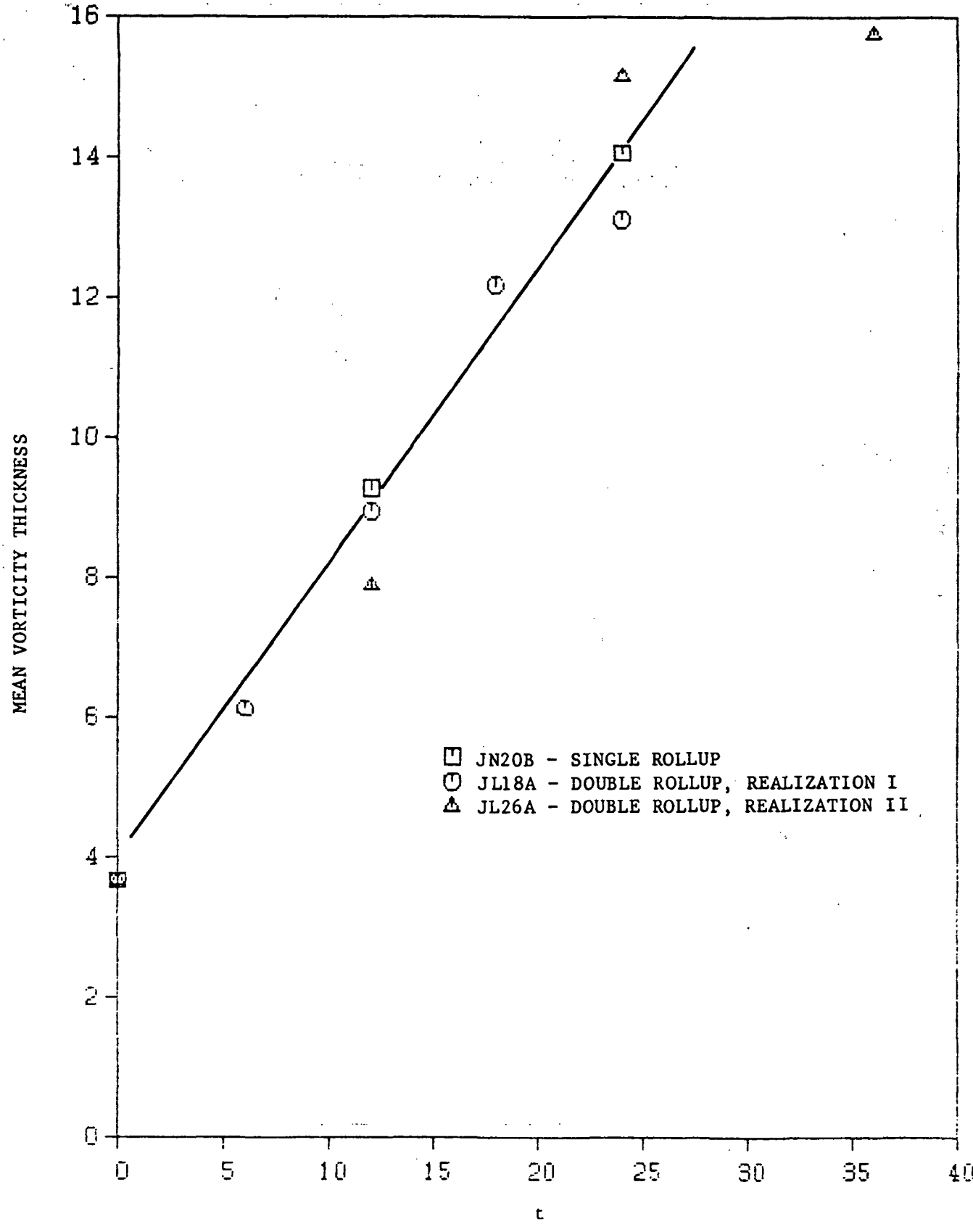

Figure 48. Mean Vorticity Thickness, δ_v, Versus Time - Three-Dimensional Simulations

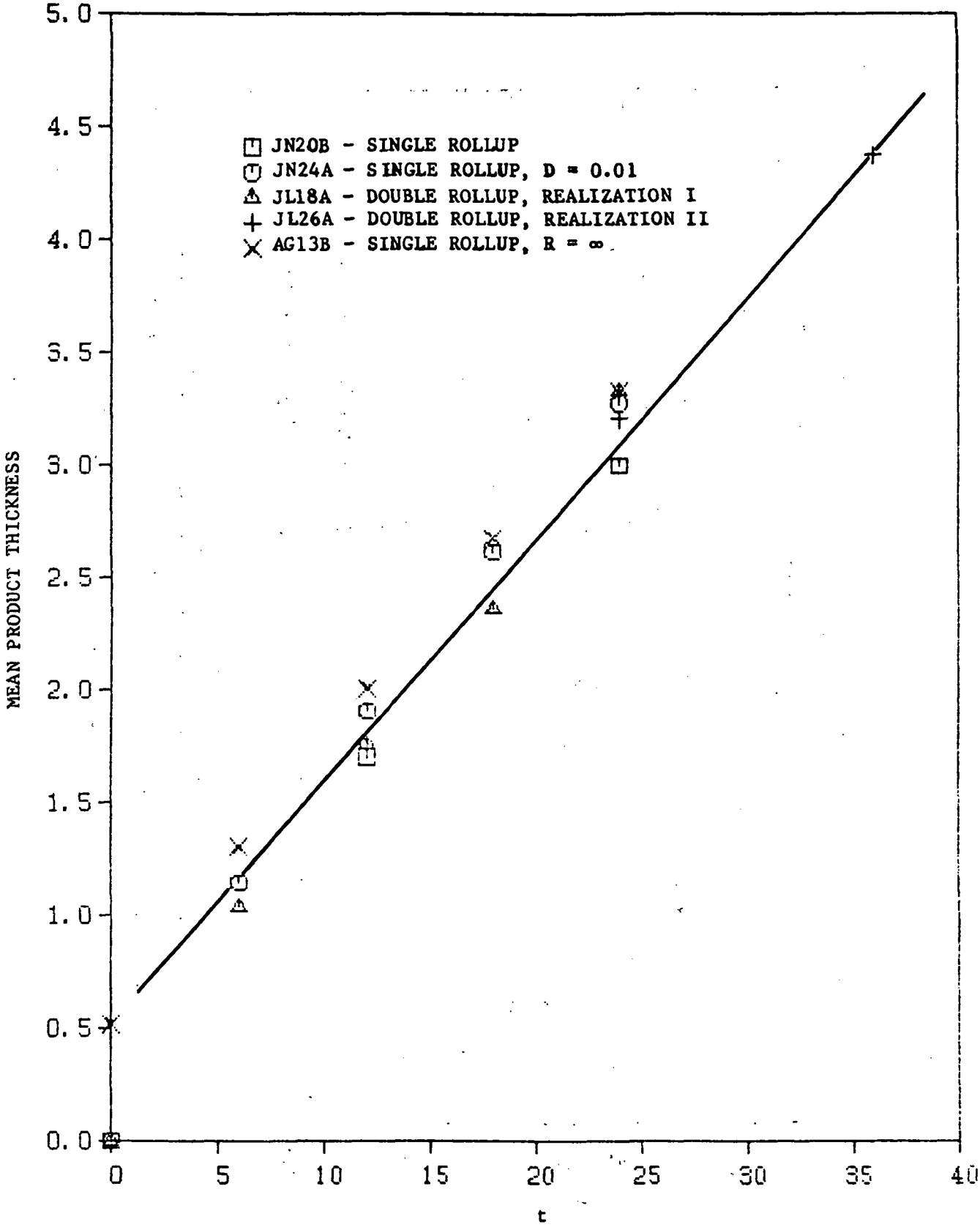

Figure 49. Mean Product Thickness, z_p, Versus Time - Three-Dimensional Simulations

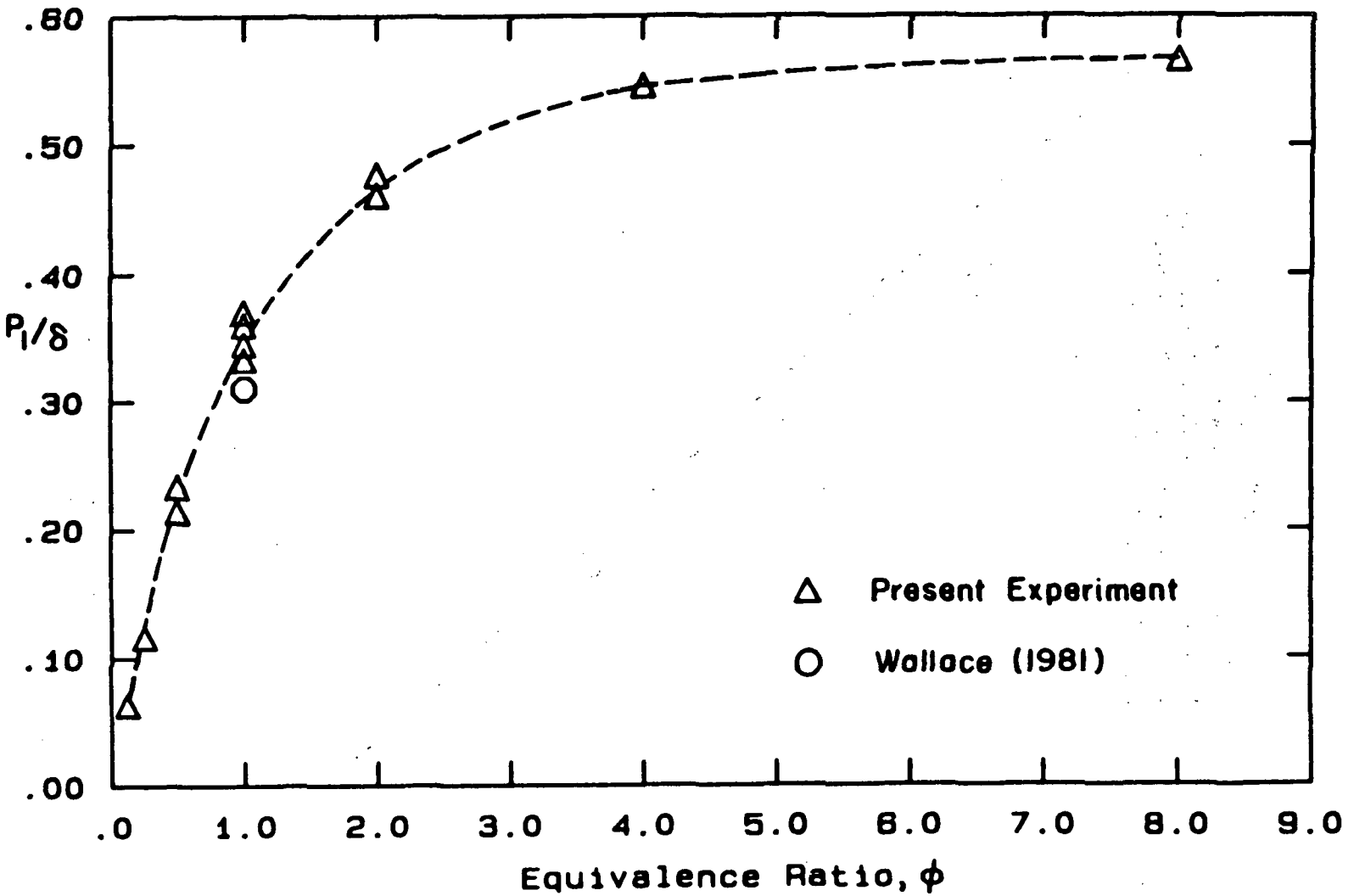

Figure 50. Nondimensional Product Thickness Versus Equivalence Ratio (Taken from Mungal, 1983)

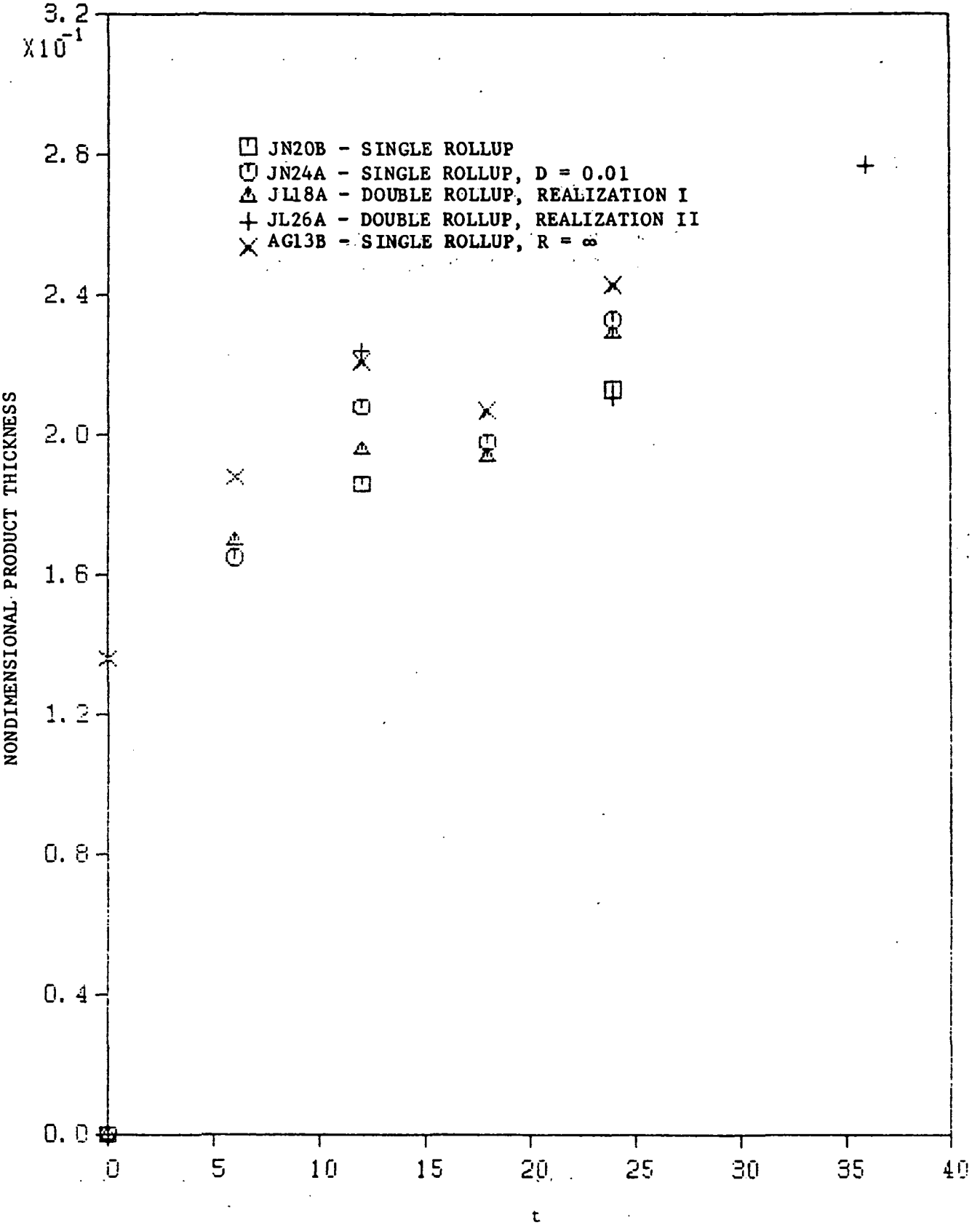

Figure 51. Nondimensional Product Thickness Versus Time - Three-Dimensional Simulations

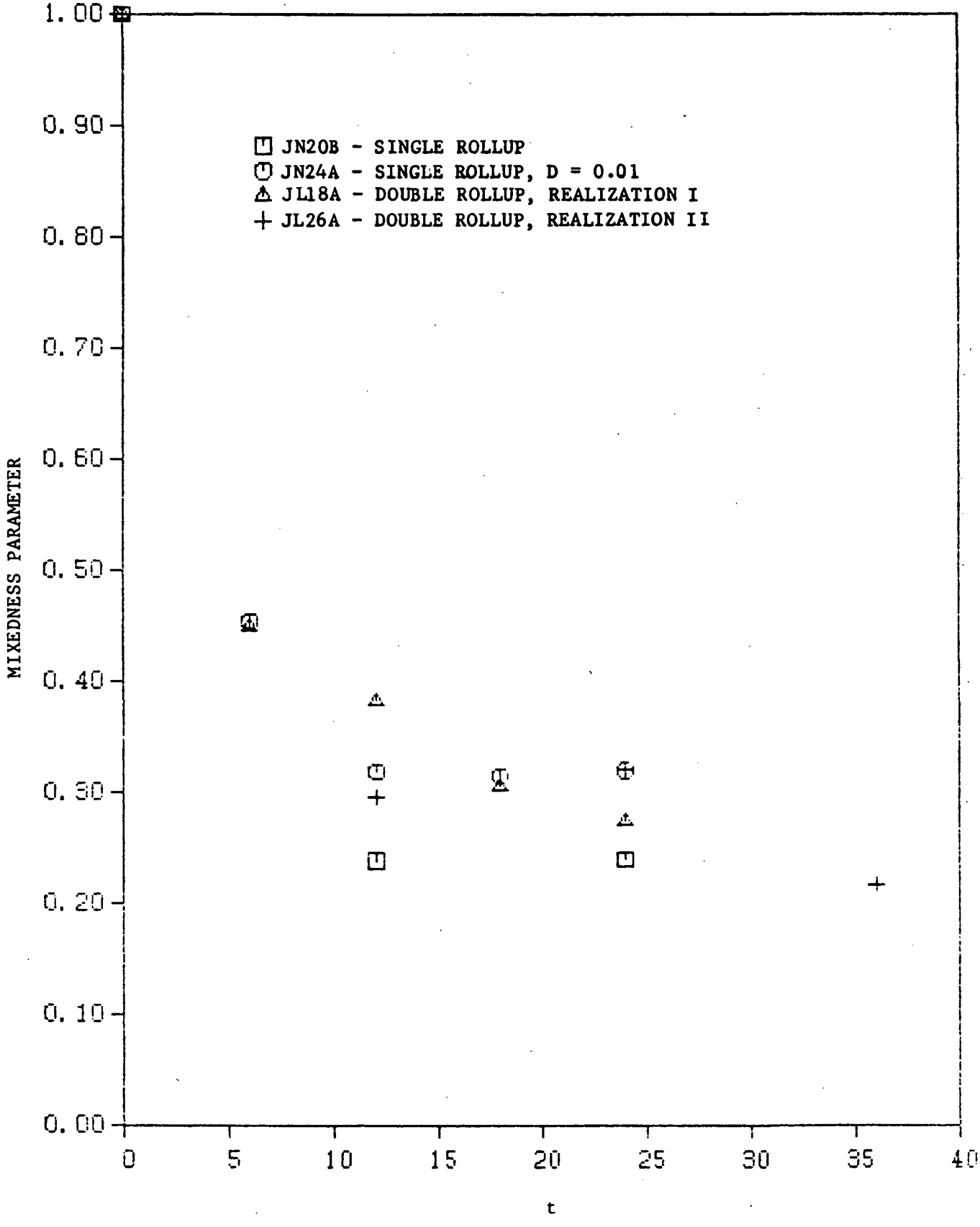

Figure 52. Mixedness Parameter Versus Time - Three-Dimensional Simulations

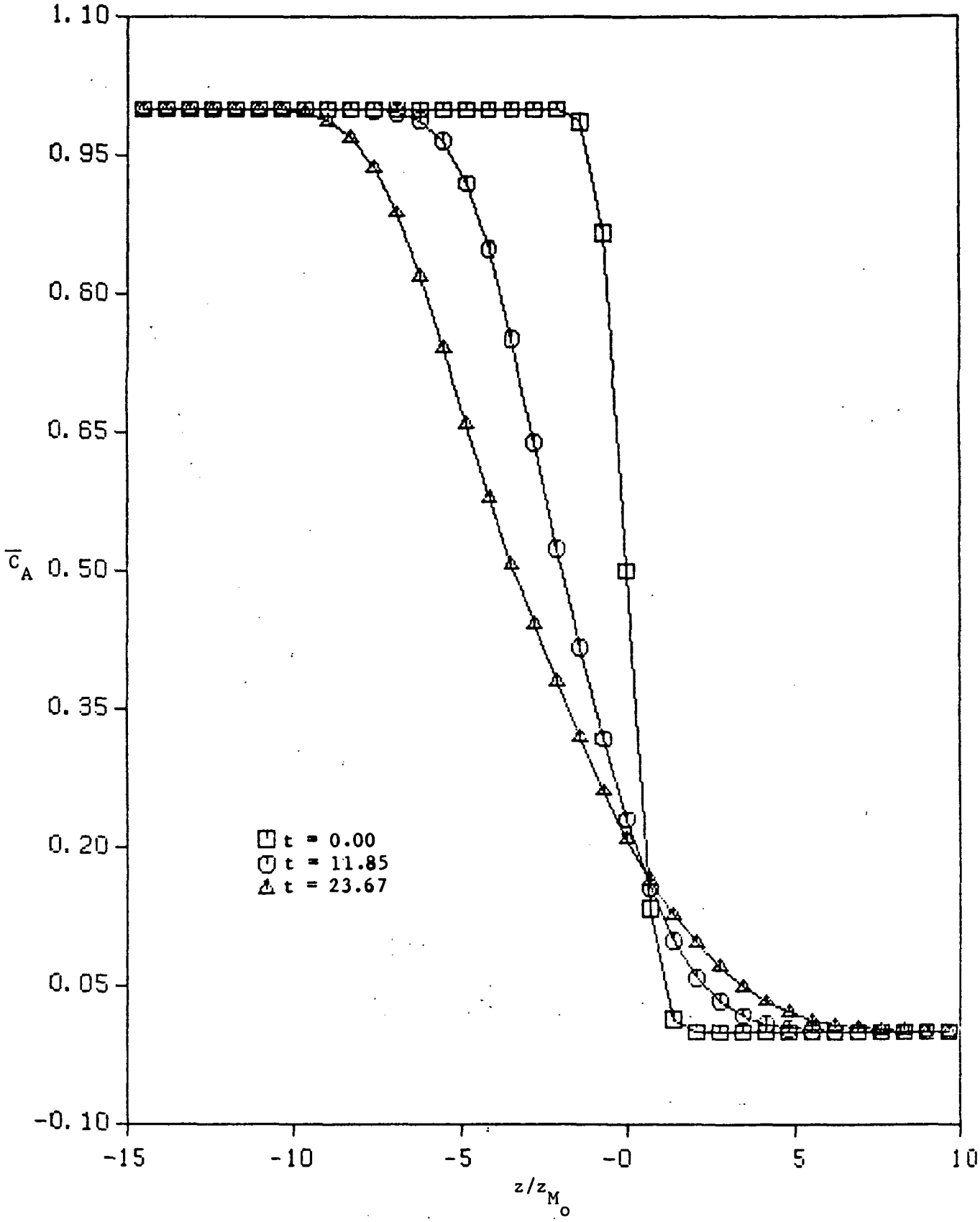

Figure 53. Average Concentration of Species A Versus z for a Sequence of Times - Realization I, Double Rollup Case, Three-Dimensional Simulations

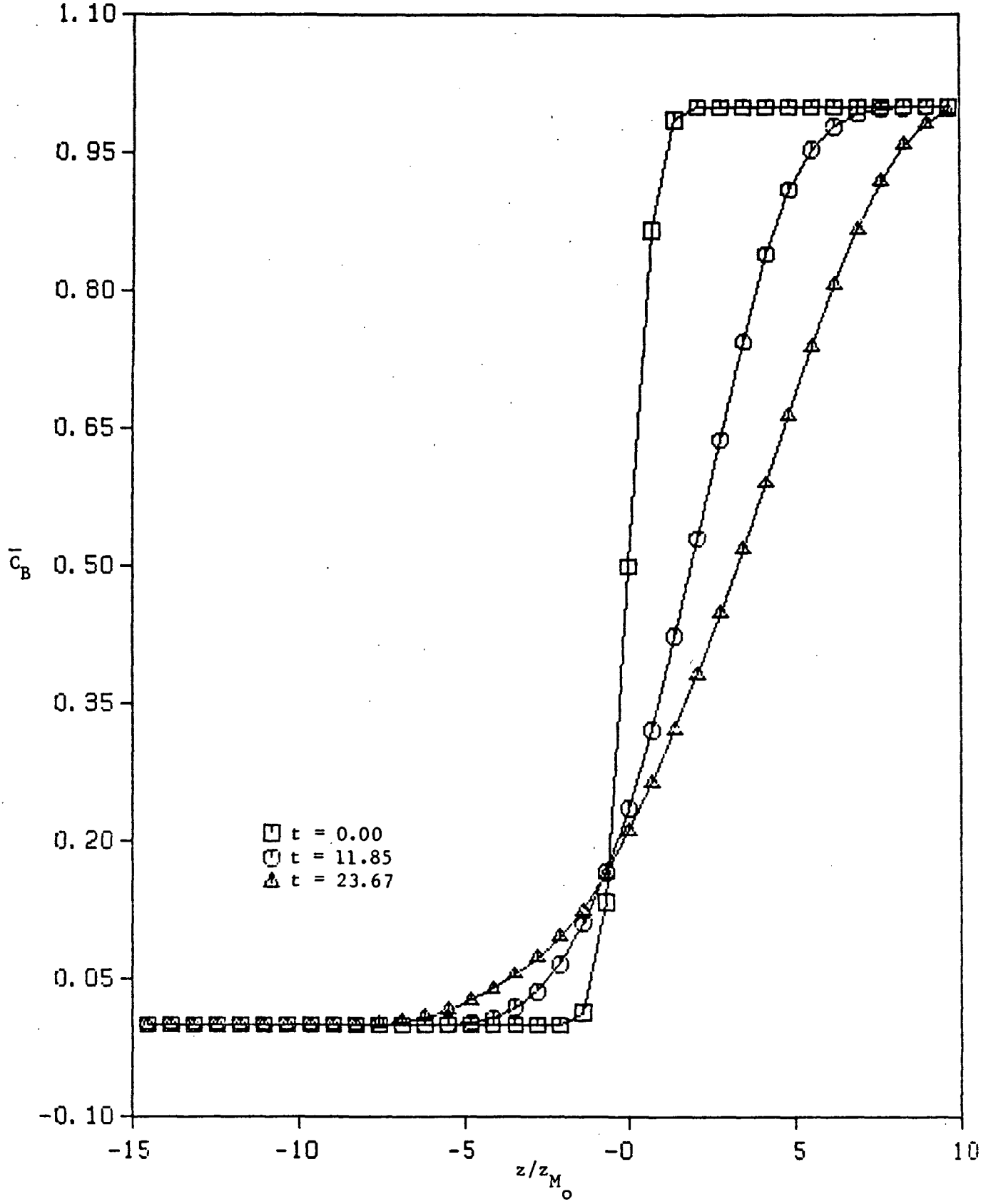

Figure 54. Average Concentration of Species B Versus z for a Sequence of Times - Realization I, Double Rollup Case, Three-Dimensional Simulations

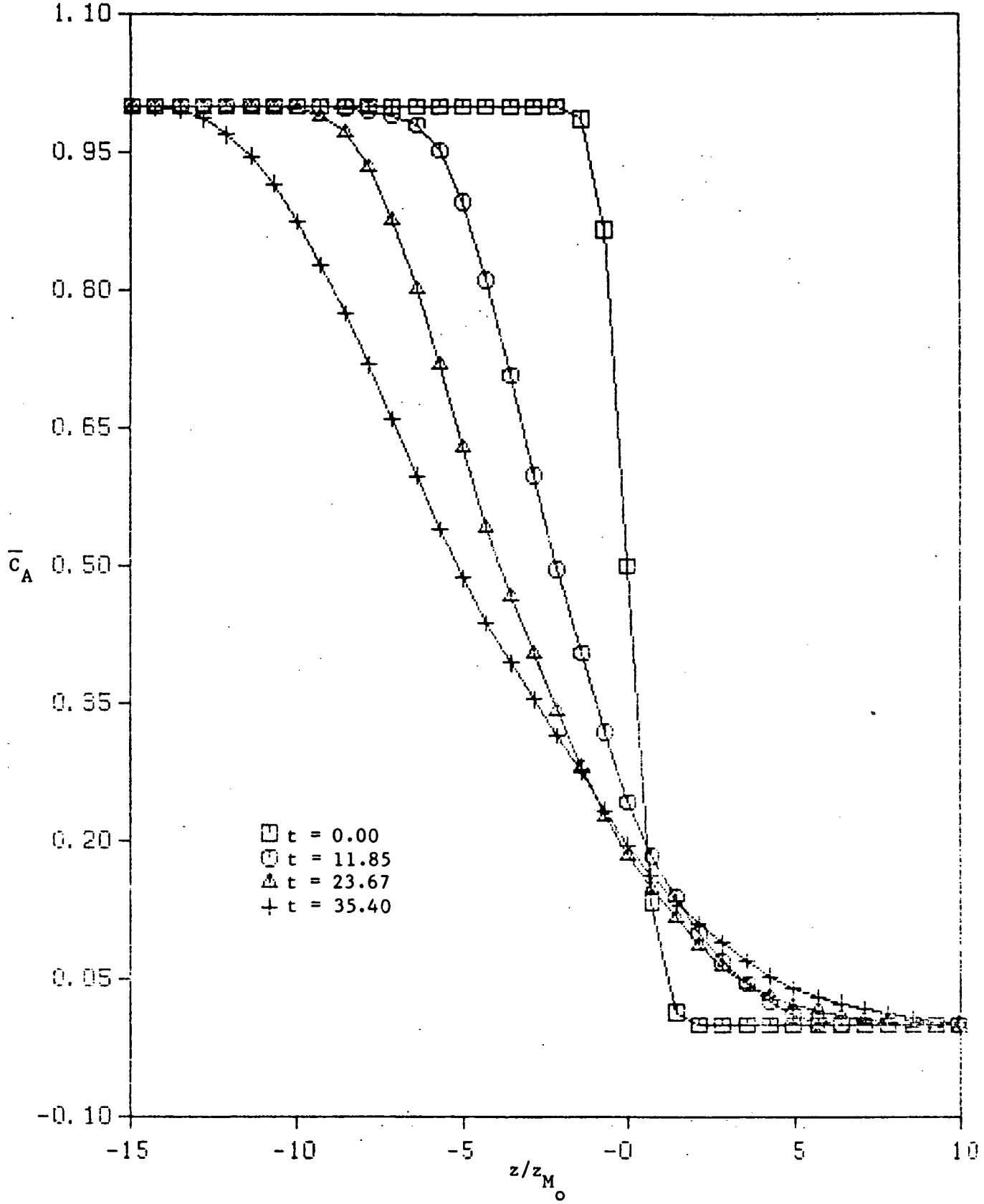

Figure 55. Average Concentration of Species A Versus z for a Sequence of Times - Realization II, Double Rollup Case, Three-Dimensional Simulations

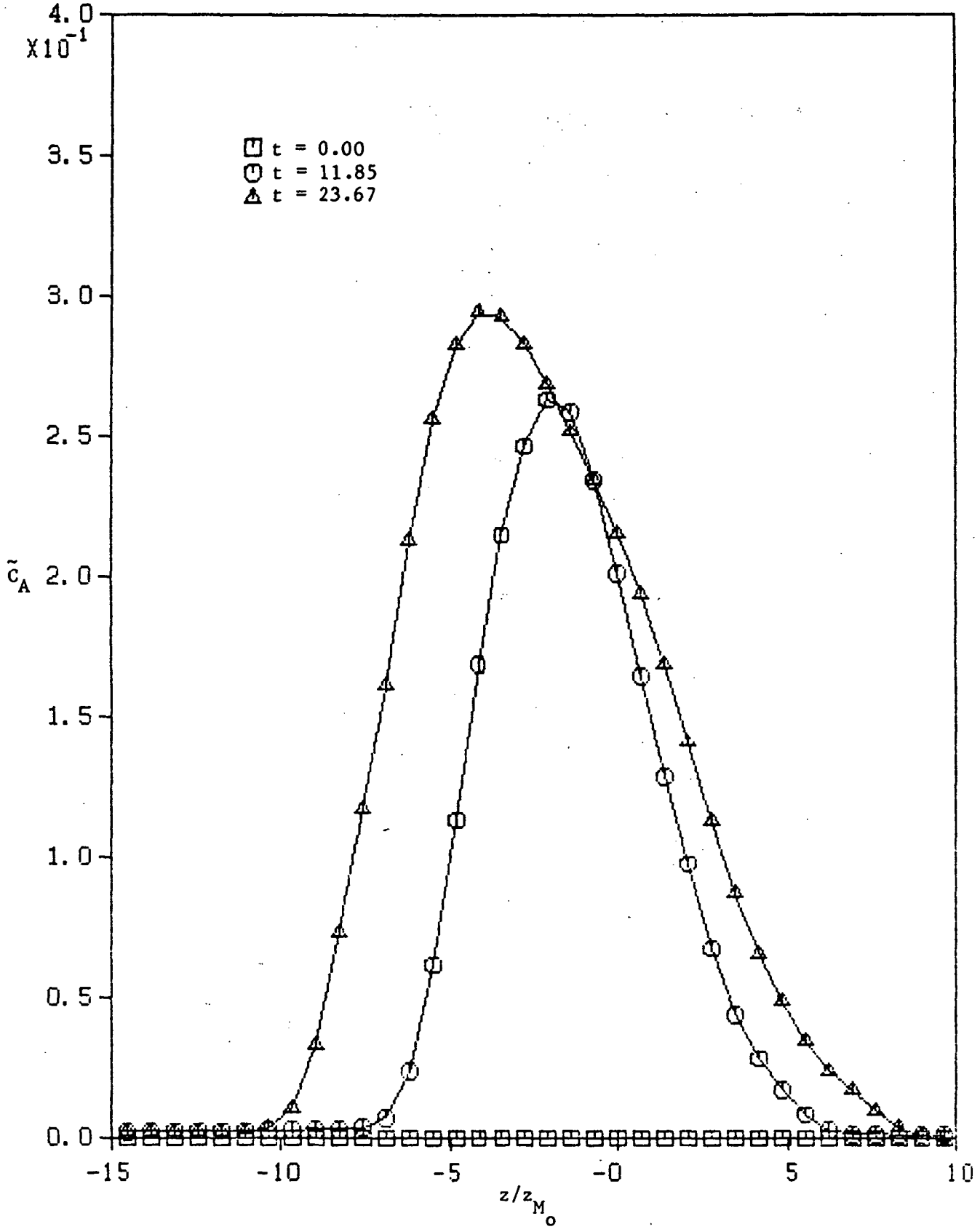

Figure 56. RMS of the Fluctuating Concentration of Species A Versus z for a Sequence of Times - Realization I, Double Rollup Case, Three-Dimensional Simulations

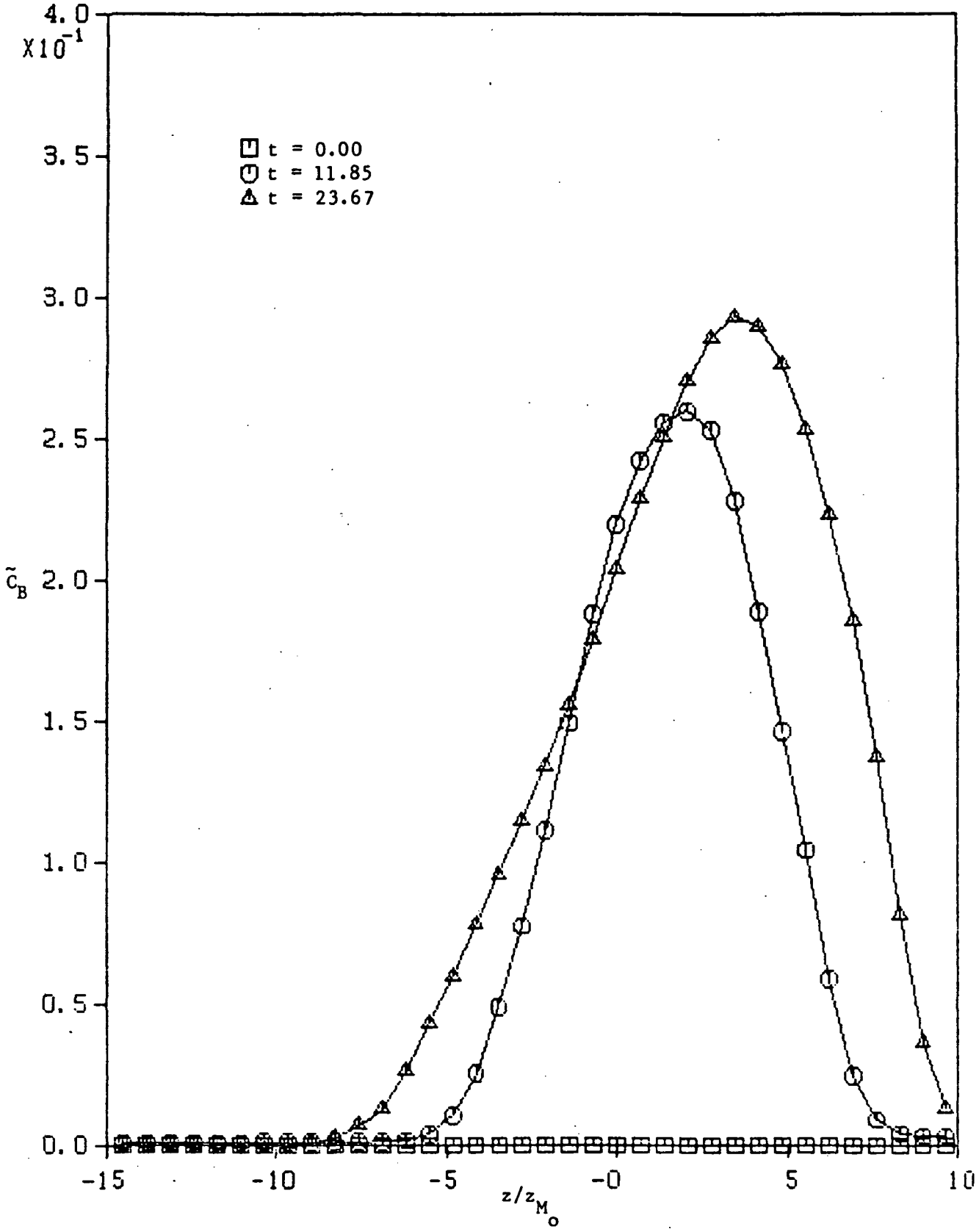

Figure 57. RMS of the Fluctuating Concentration of Species B Versus z for a Sequence of Times - Realization I, Double Rollup Case, Three-Dimensional Simulations

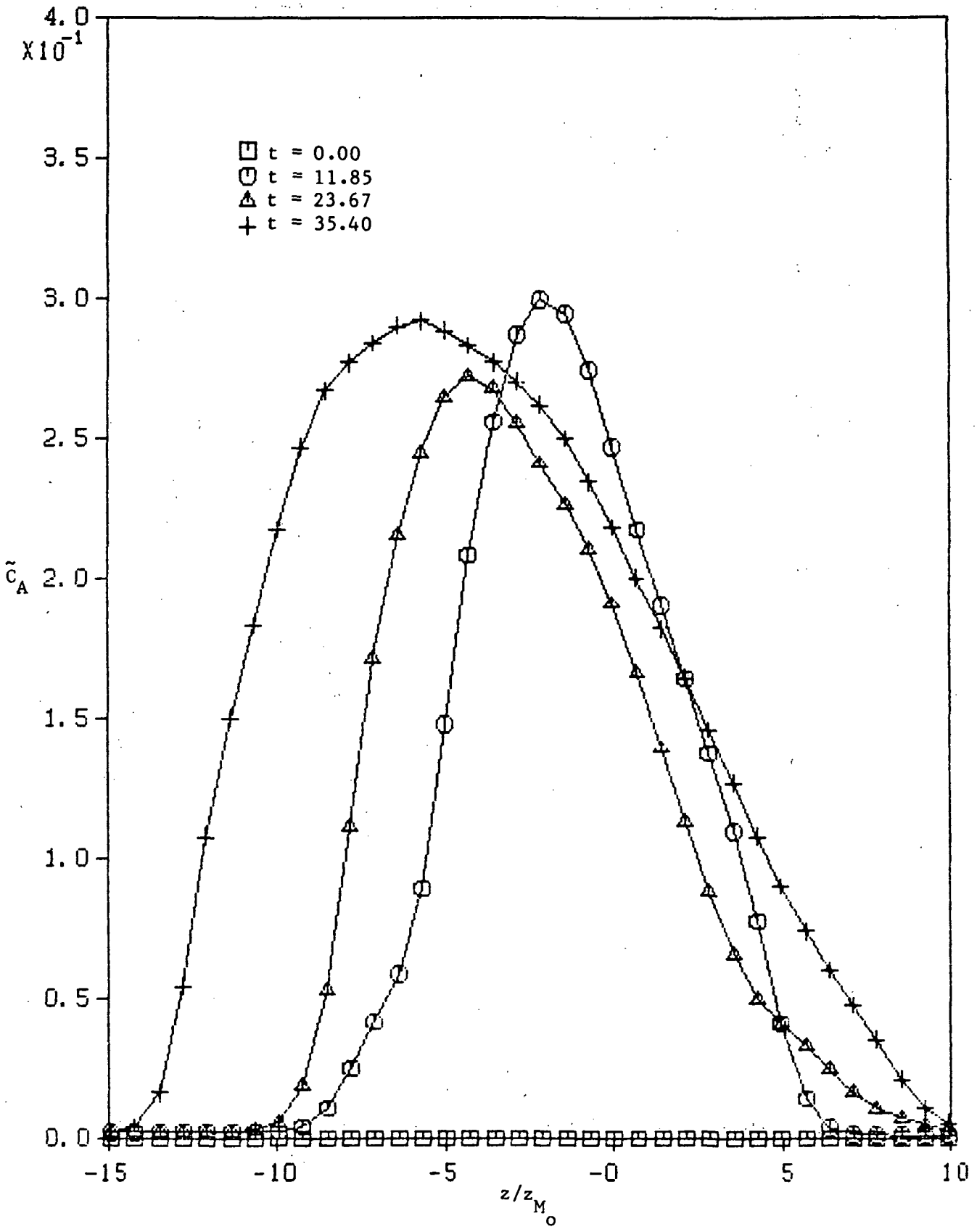

Figure 58. RMS of the Fluctuating Concentration of Species A Versus z for a Sequence of Times - Realization II, Double Rollup Case, Three-Dimensional Simulations

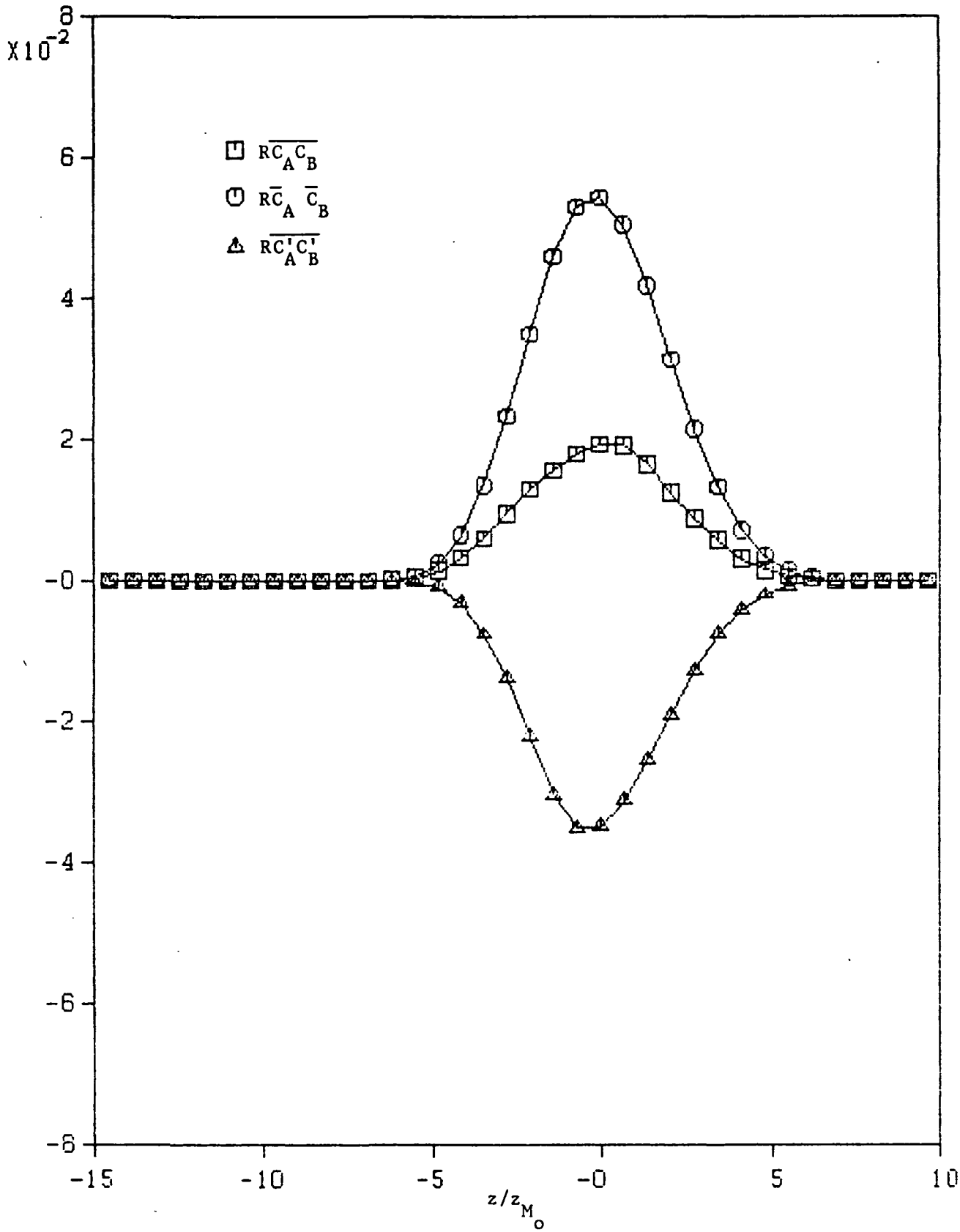

Figure 59. Average of the Product of the Concentrations, the Product of the Averages, and the Concentration Correlation Versus z at t = 12 - Realization I, Double Rollup Case, Three-Dimensional Simulations

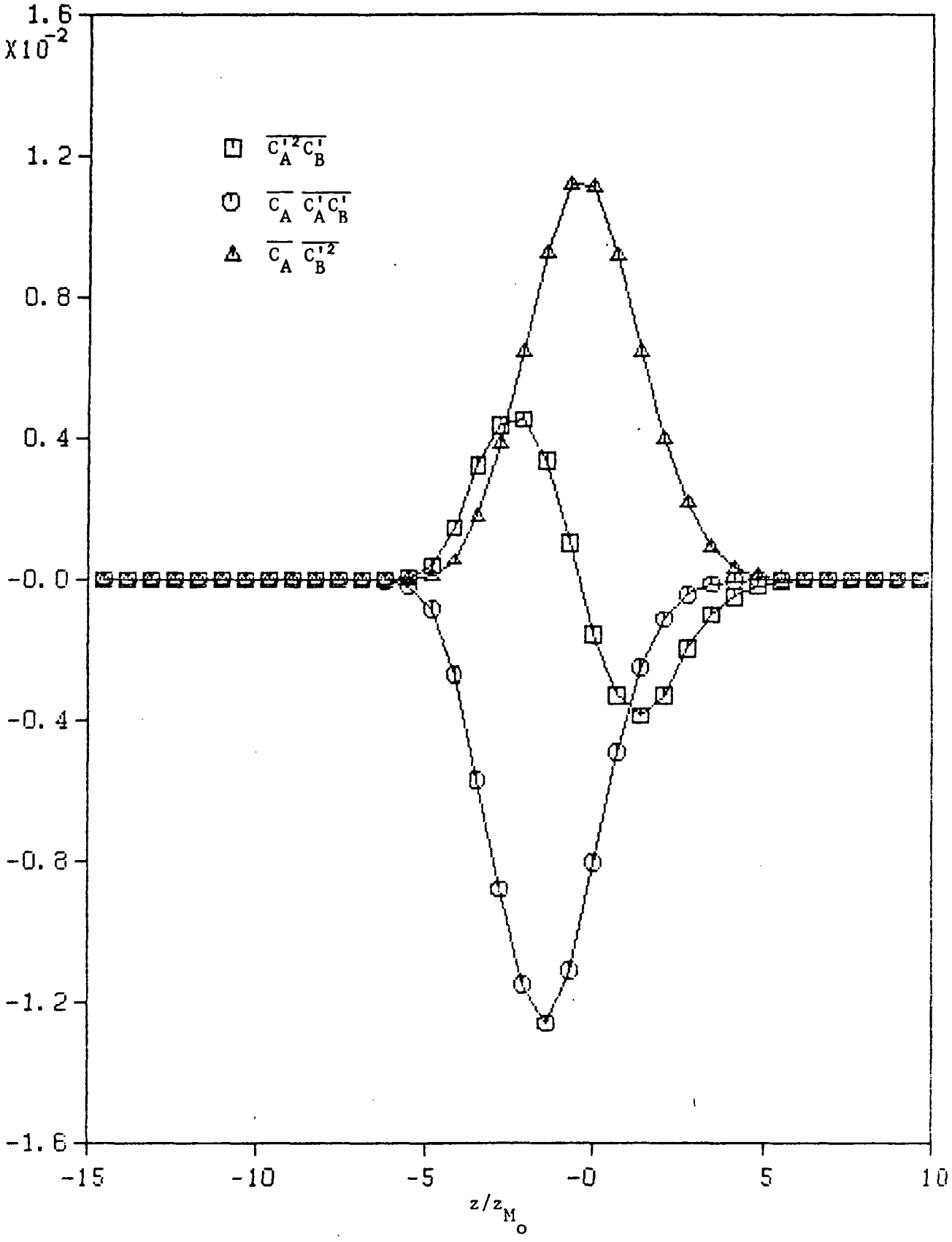

Figure 60. Various Concentration Moments Versus z at t = 12 - Realization I, Double Rollup Case, Three-Dimensional Simulations

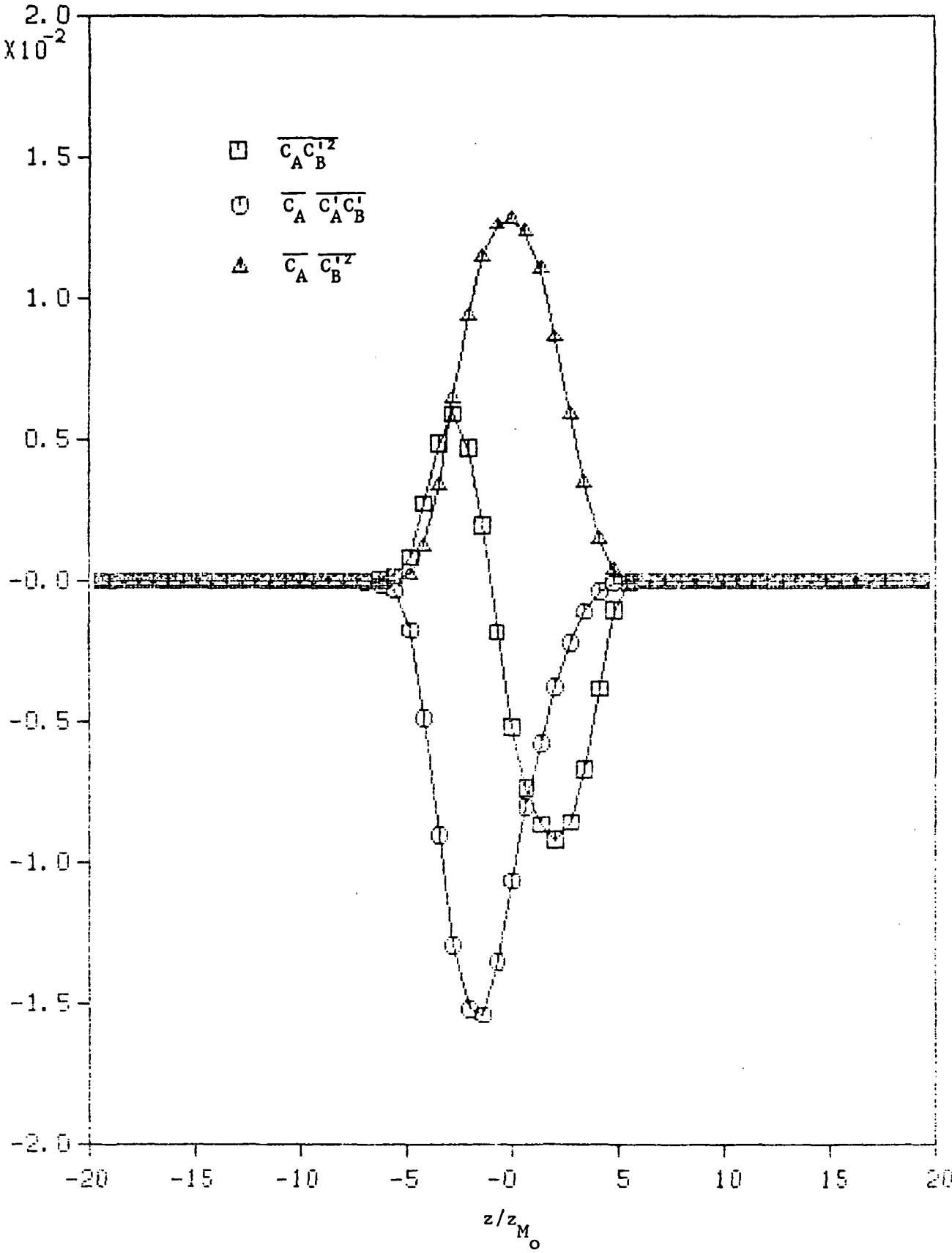

Figure 61. Various Concentration Moments Versus z at t = 12 - Realization II, Double Rollup Case, Three-Dimensional Simulations

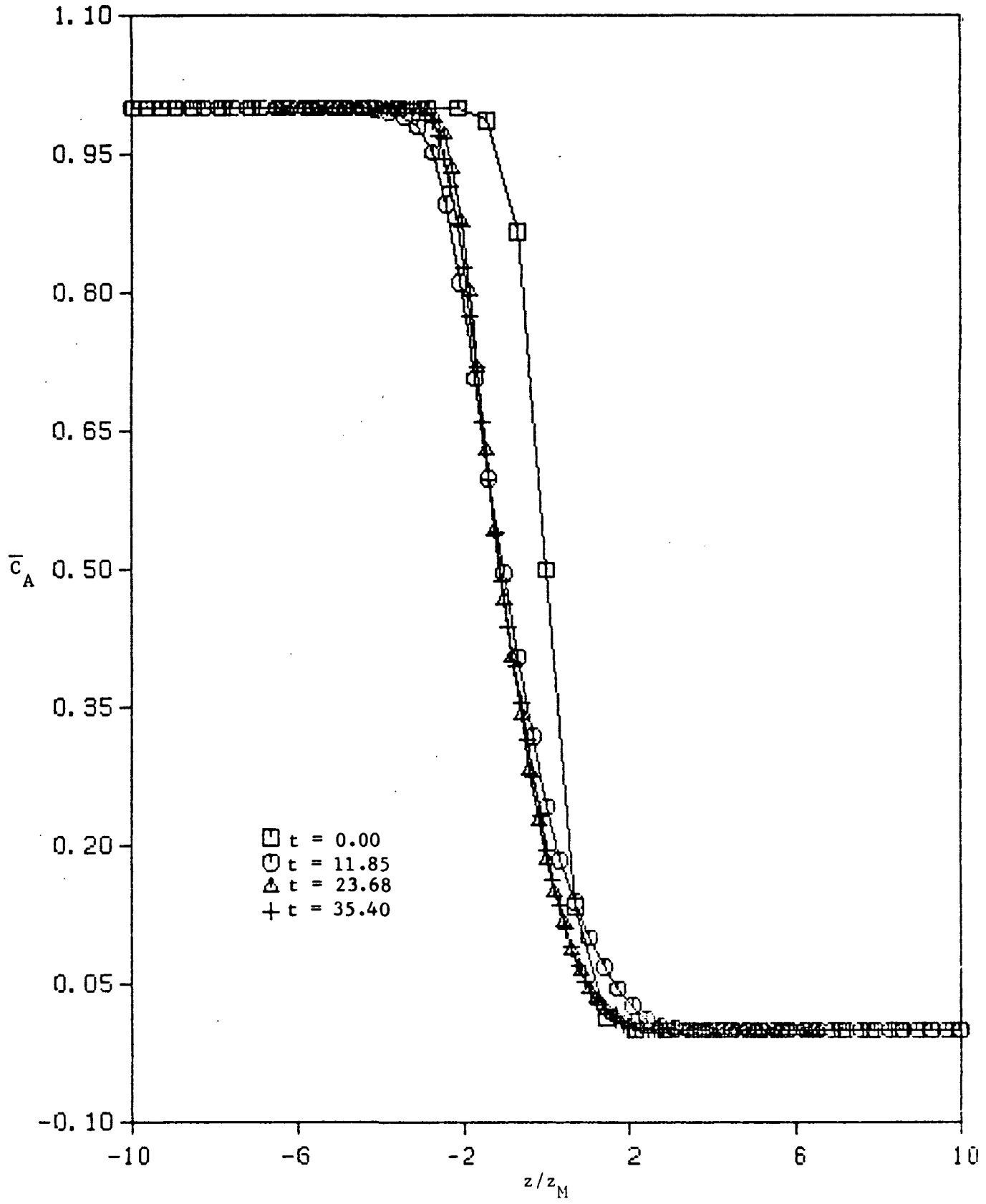

Figure 62. Similarity Plots of $\bar{C}_A/C_{A\infty}$ Versus z/z_M ($= z/z_{1/2}$) for Various Times - Double Rollup Case, Finite Reaction Rate, Three-Dimensional Simulations

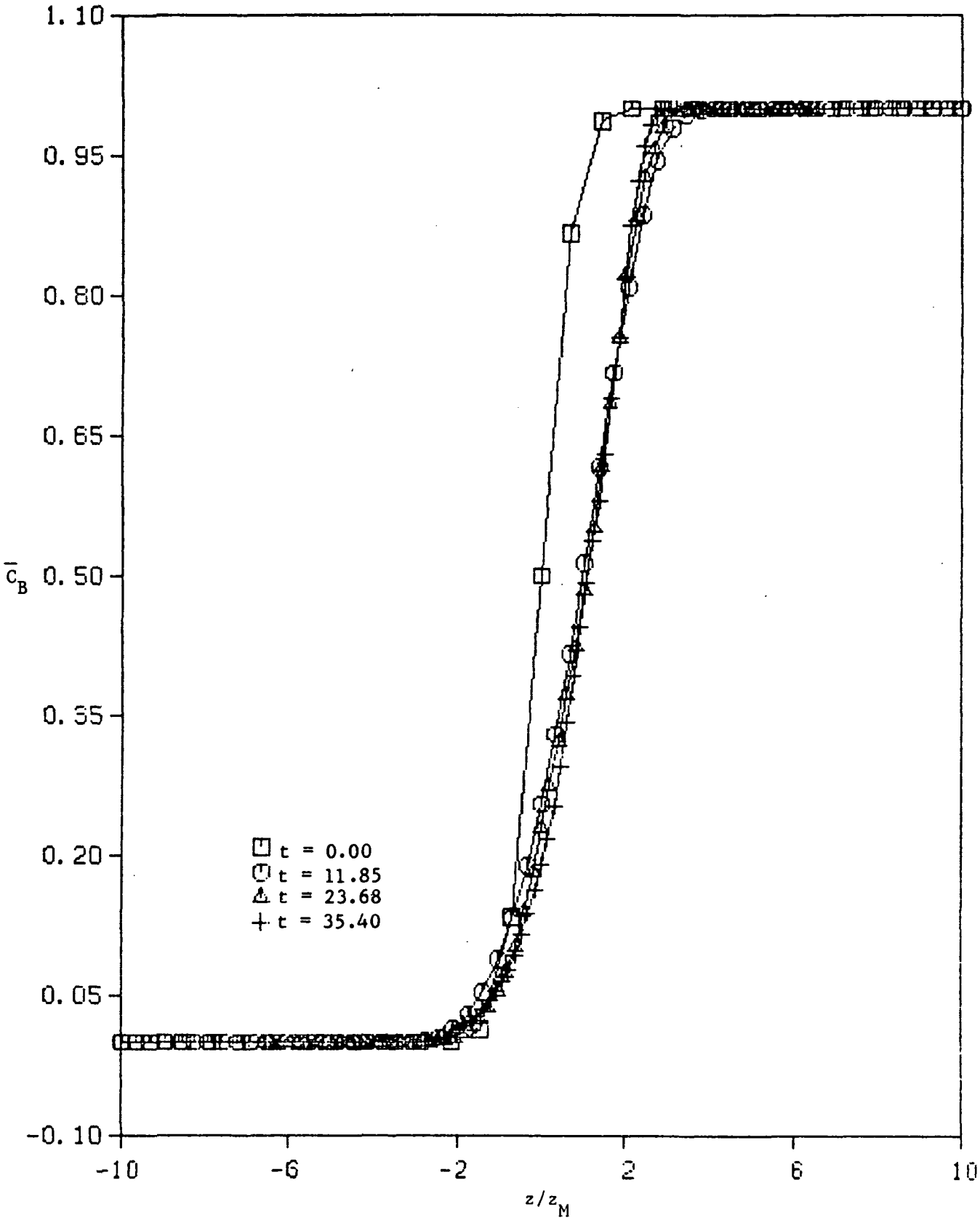

Figure 63. Similarity Plots of $\bar{C}_B/C_{A\infty}$ Versus z/z_M (= $z/z_{1/2}$) for Various Times - Double Rollup Case, Finite Reaction Rate, Three-Dimensional Simulations

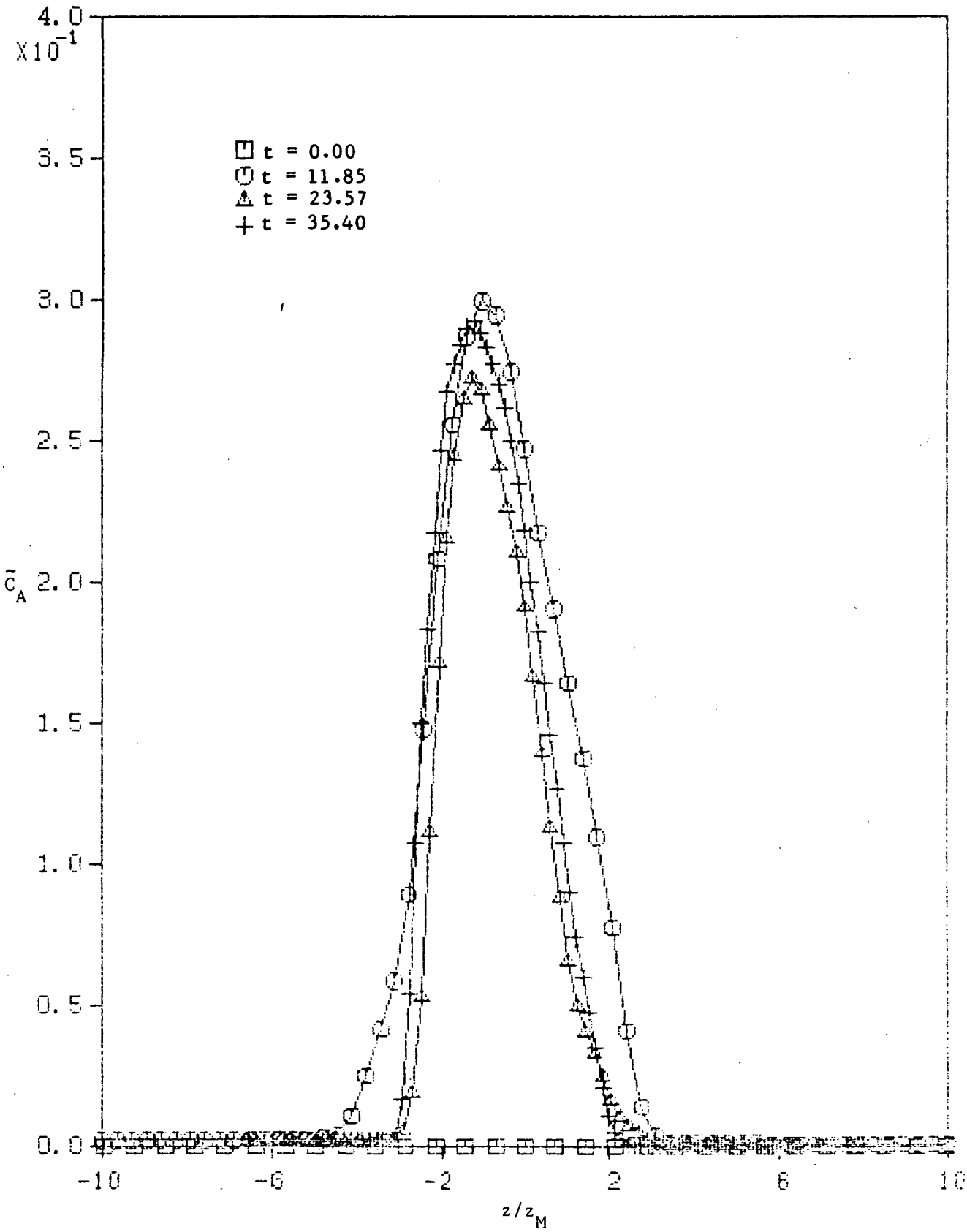

Figure 64. Similarity Plots of $\tilde{C}_A/C_{A\infty}$ Versus z/z_M (= $z/z_{1/2}$) for Various Times - Double Rollup Case, Finite Reaction Rate, Three-Dimensional Simulations

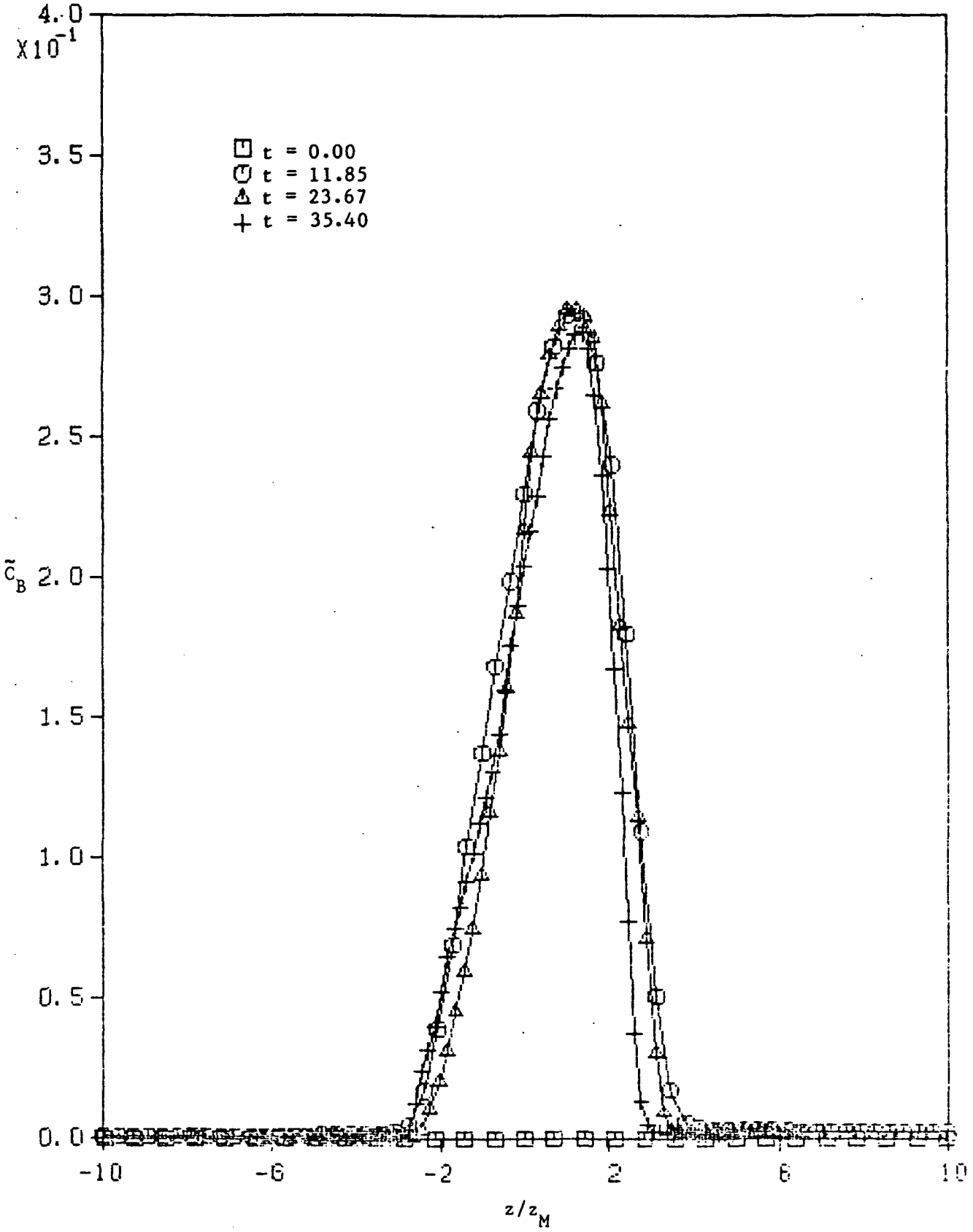

Figure 65. Similarity Plots of $\tilde{C}_B/C_{A\infty}$ Versus z/z_M ($= z/z_{1/2}$) for Various Times - Double Rollup Case, Finite Reaction Rate, Three-Dimensional Simulations

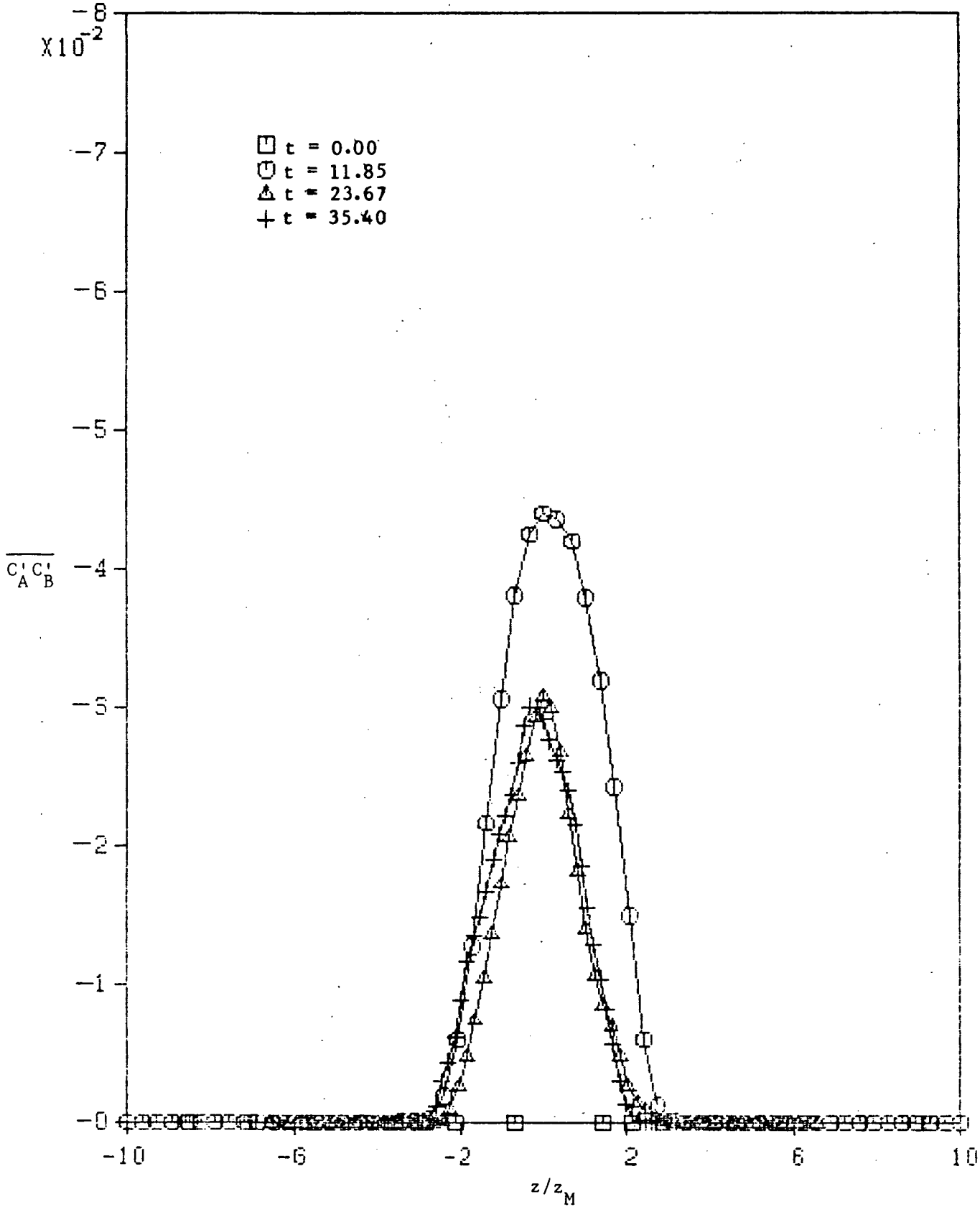

Figure 66. Similarity Plots of $\overline{C'_A C'_B}/C^2_{A\infty}$ Versus z/z_M (= $z/z_{1/2}$) for Various Times - Double Rollup Case, Finite Reaction Rate, Three-Dimensional Simulations

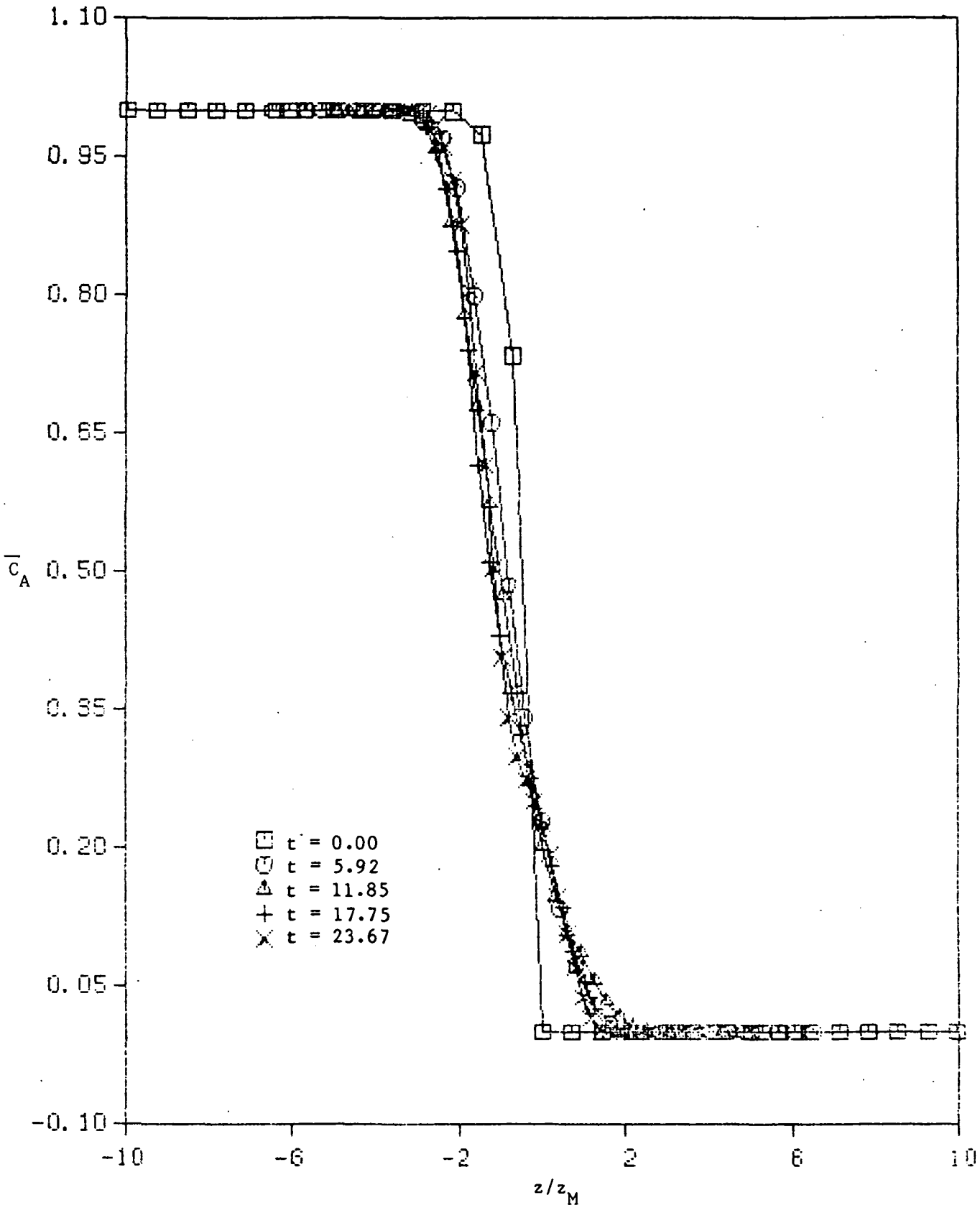

Figure 67. Similarity Plots of $\overline{C}_A/C_{A\infty}$ Versus z/z_M (= $z/z_{1/2}$) for Various Times - Single Rollup Case, Infinite Reaction Rate, Three-Dimensional Simulations

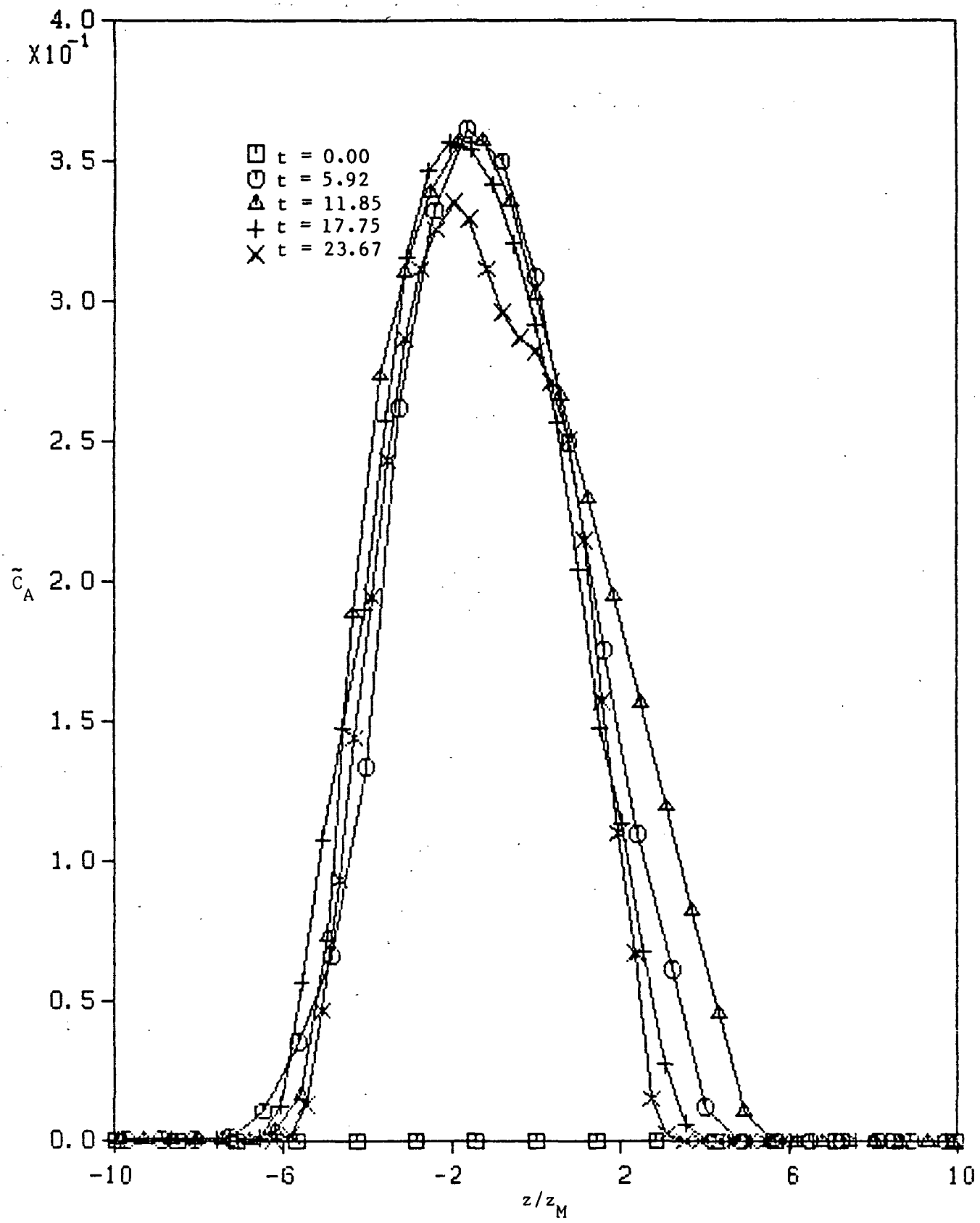

Figure 68. Similarity Plots of $\tilde{C}_A/C_{A\infty}$ Versus z/z_M (= $z/z_{1/2}$) for Various Times - Single Rollup Case, Infinite Reaction Rate, Three-Dimensional Simulations

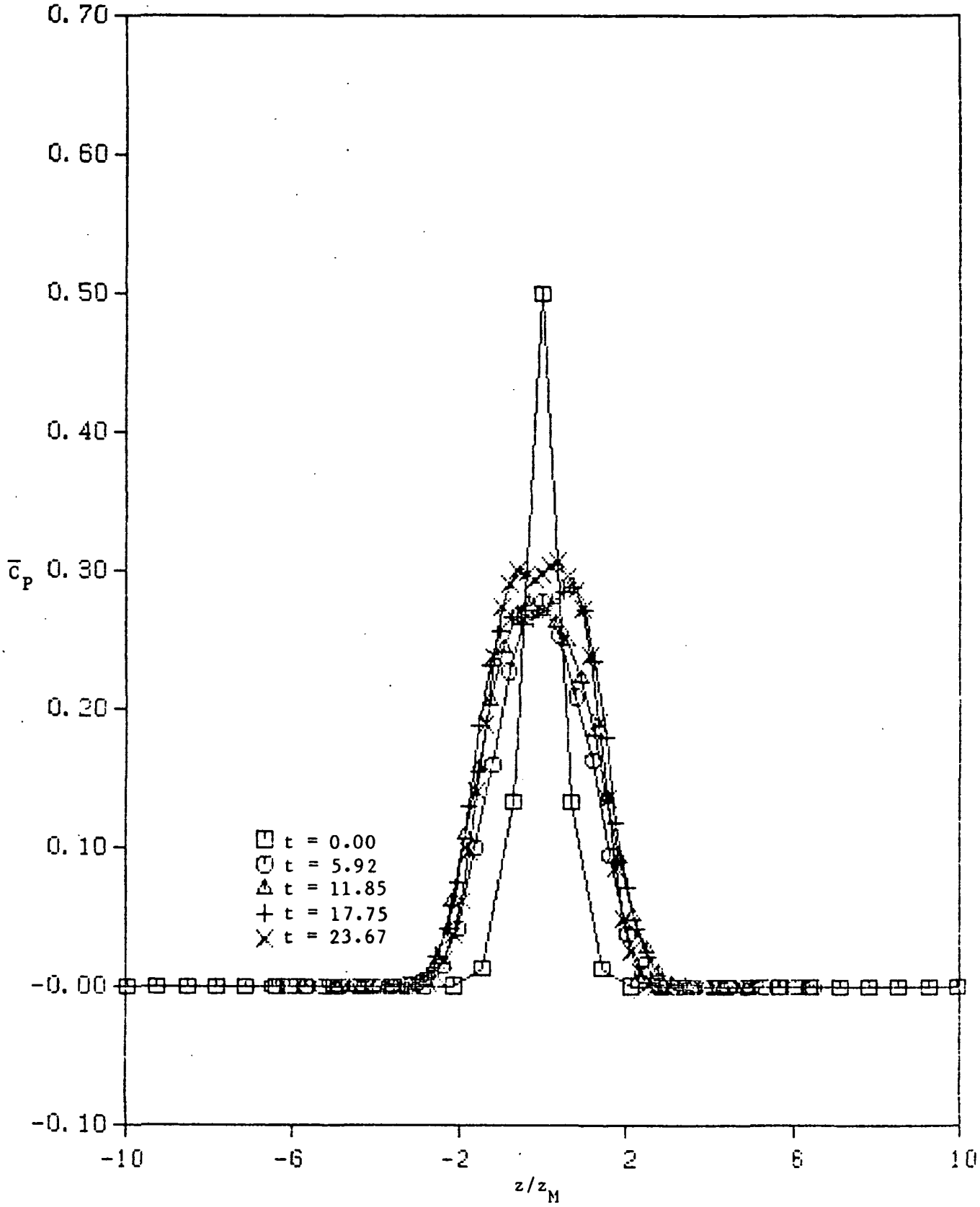

Figure 69. Similarity Plots of $\bar{C}_P/C_{A\infty}$ Versus z/z_M (= $z/z_{1/2}$) for Various Times - Single Rollup Case, Infinite Reaction Rate, Three-Dimensional Simulations

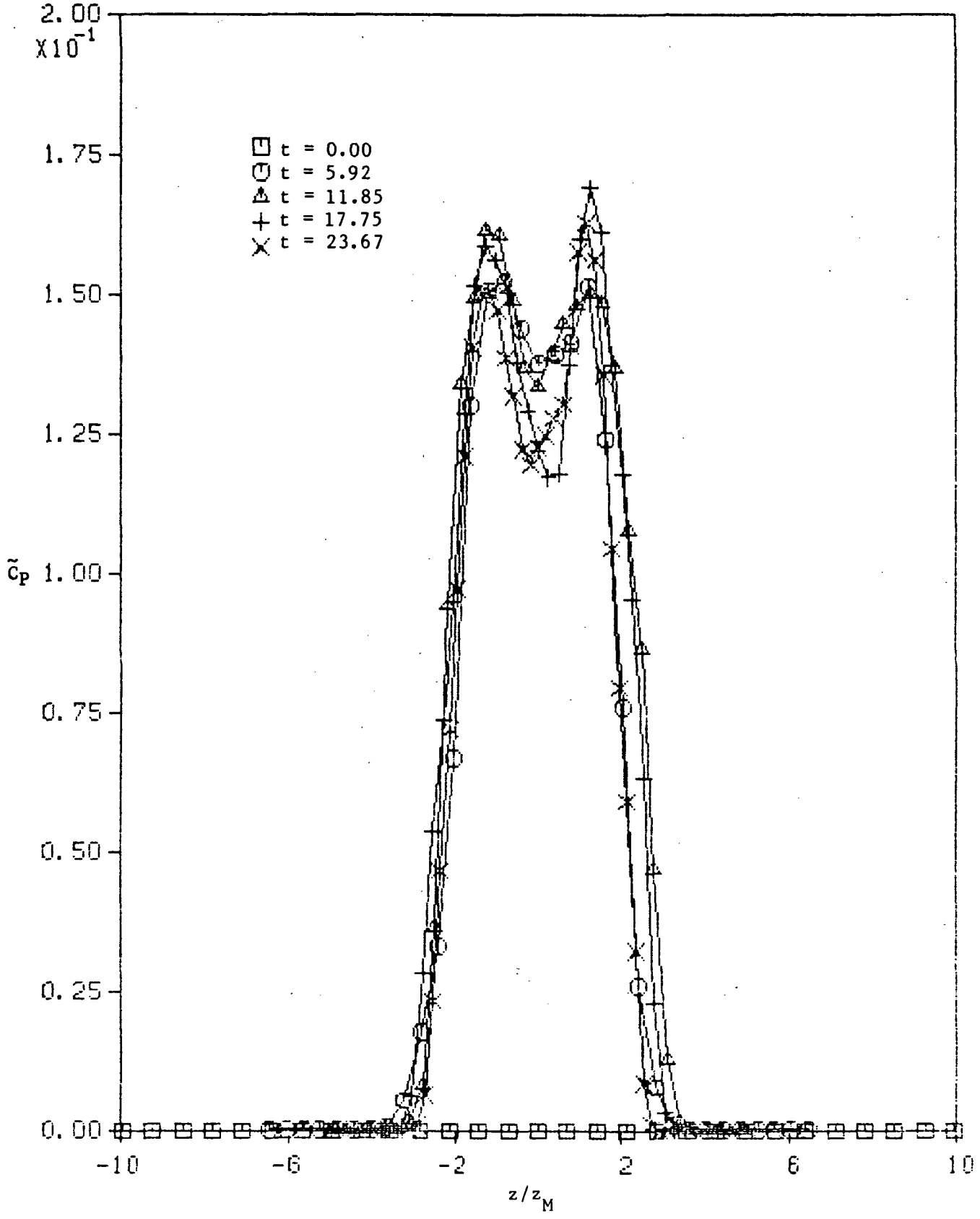

Figure 70. Similarity Plots of $\tilde{C}_P/C_{A\infty}$ Versus z/z_M (= $z/z_{1/2}$) for Various Times - Single Rollup Case, Infinite Reaction Rate, Three-Dimensional Simulations

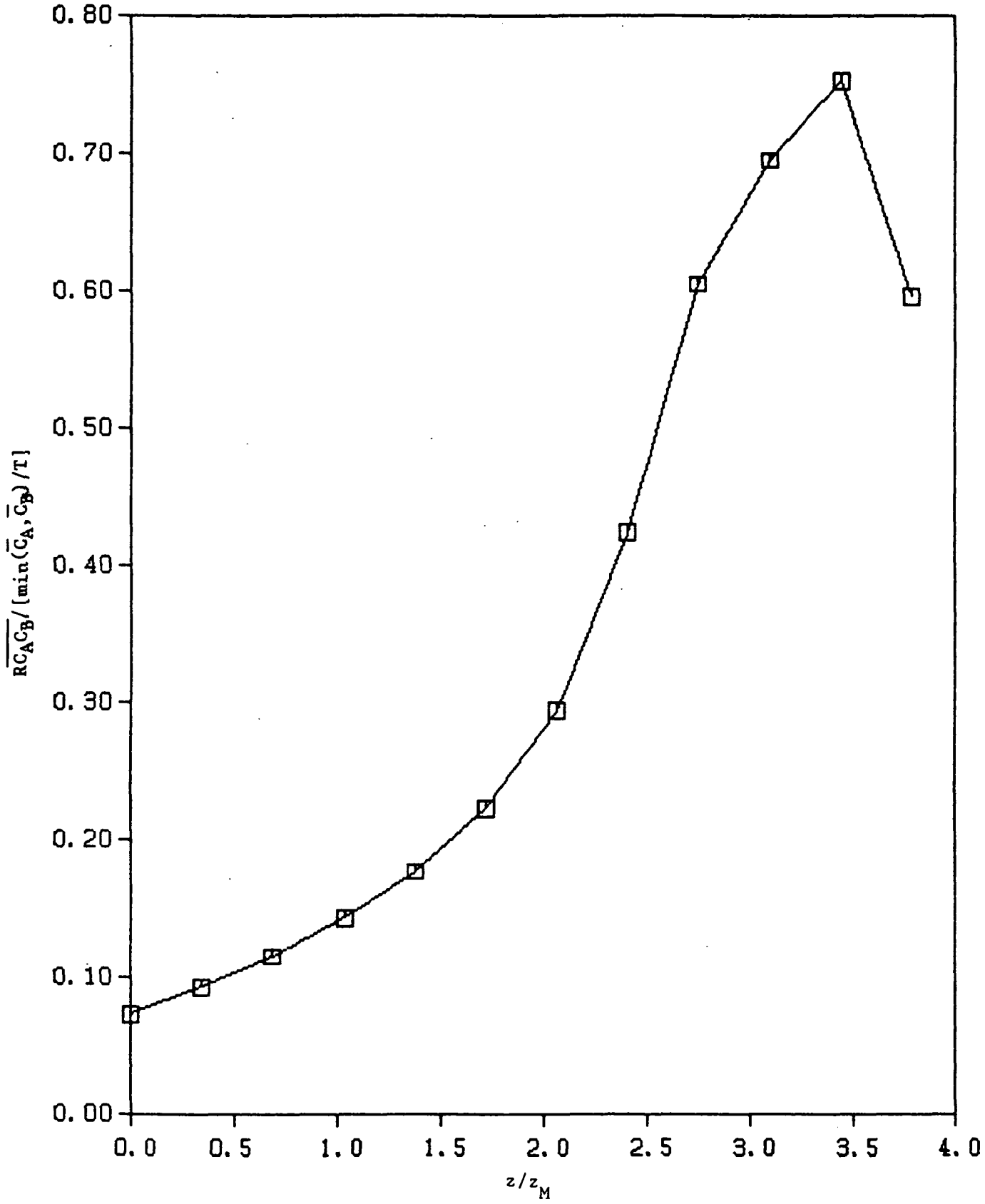

Figure 71. $\overline{RC_AC_B}/[\min(\bar{C}_A,\bar{C}_B)/T]$ Versus z at t = 12 - Double Rollup Case, Finite Reaction Rate, Three-Dimensional Simulations

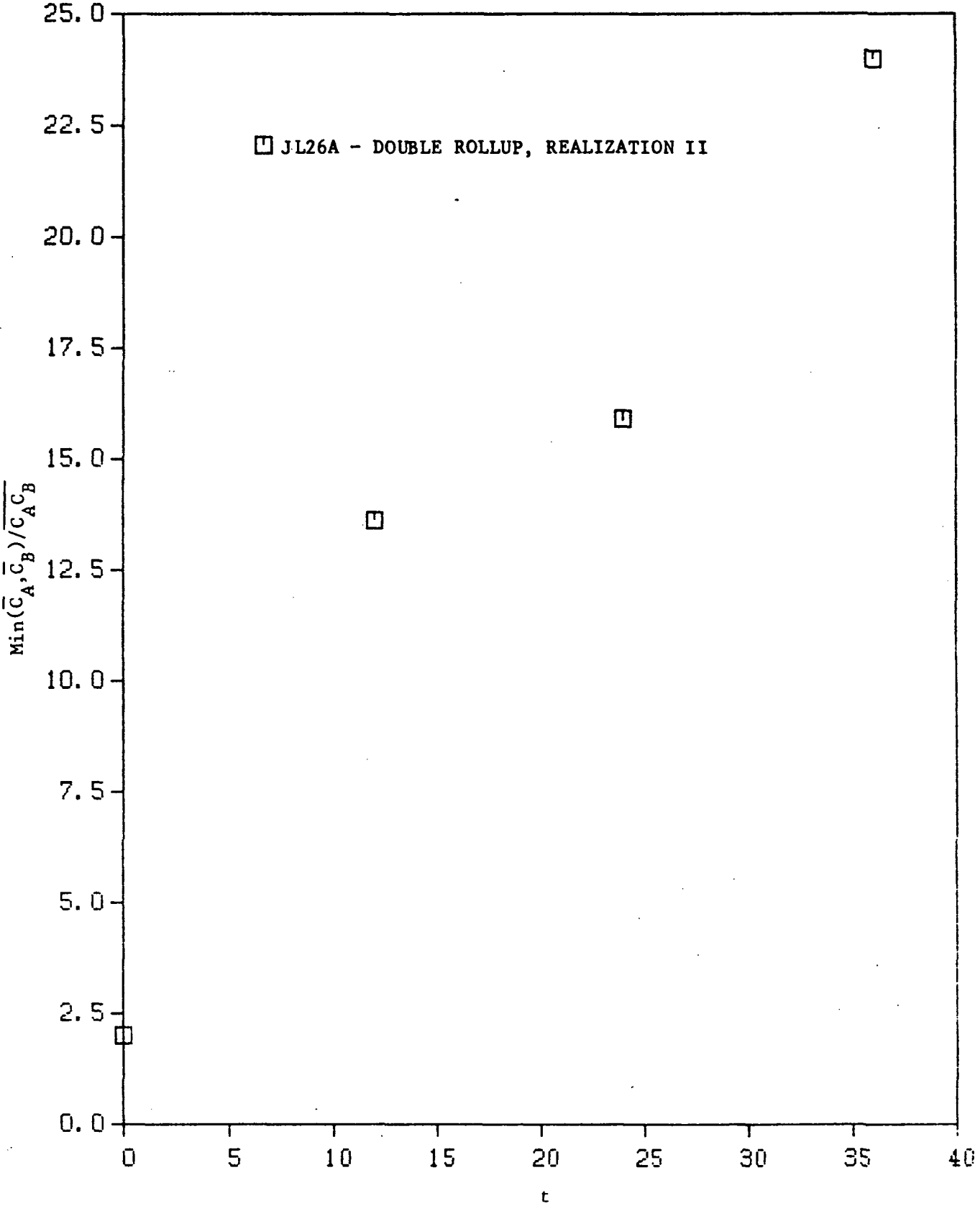

Figure 72. Min($\bar{C}_A$,$\bar{C}_B$)/$\overline{C_A C_B}$ Versus Time Measured at z = 0 - Double Rollup Case, Finite Reaction Rate, Three-Dimensional Simulations

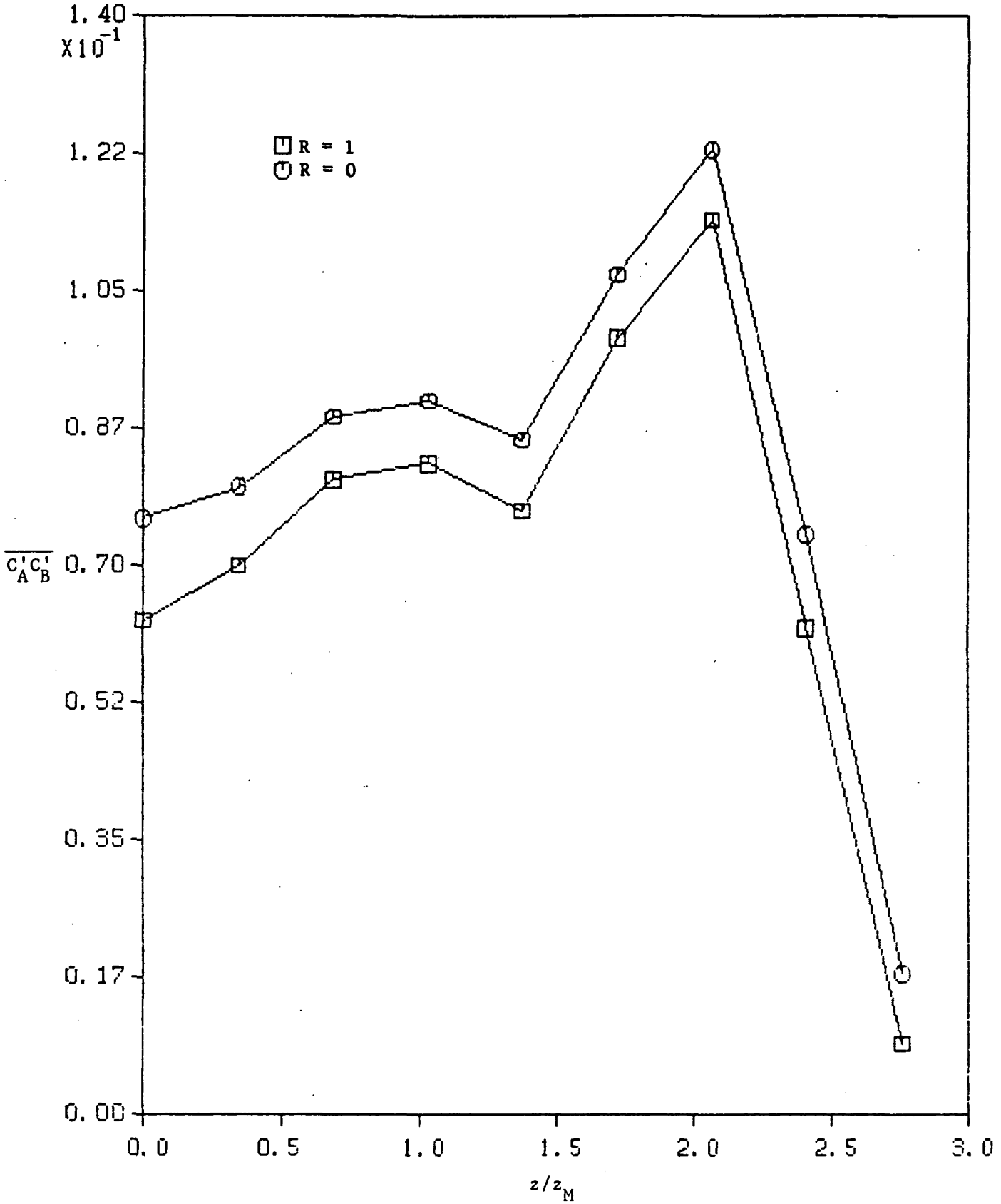

Figure 73. $\overline{C_A'C_B'}/C_{A\infty}^2$ Versus z at t = 16 - Case 1 (Fundamental Mode Alone), Both Zero and Finite Reaction Rates, Two-Dimensional Simulations

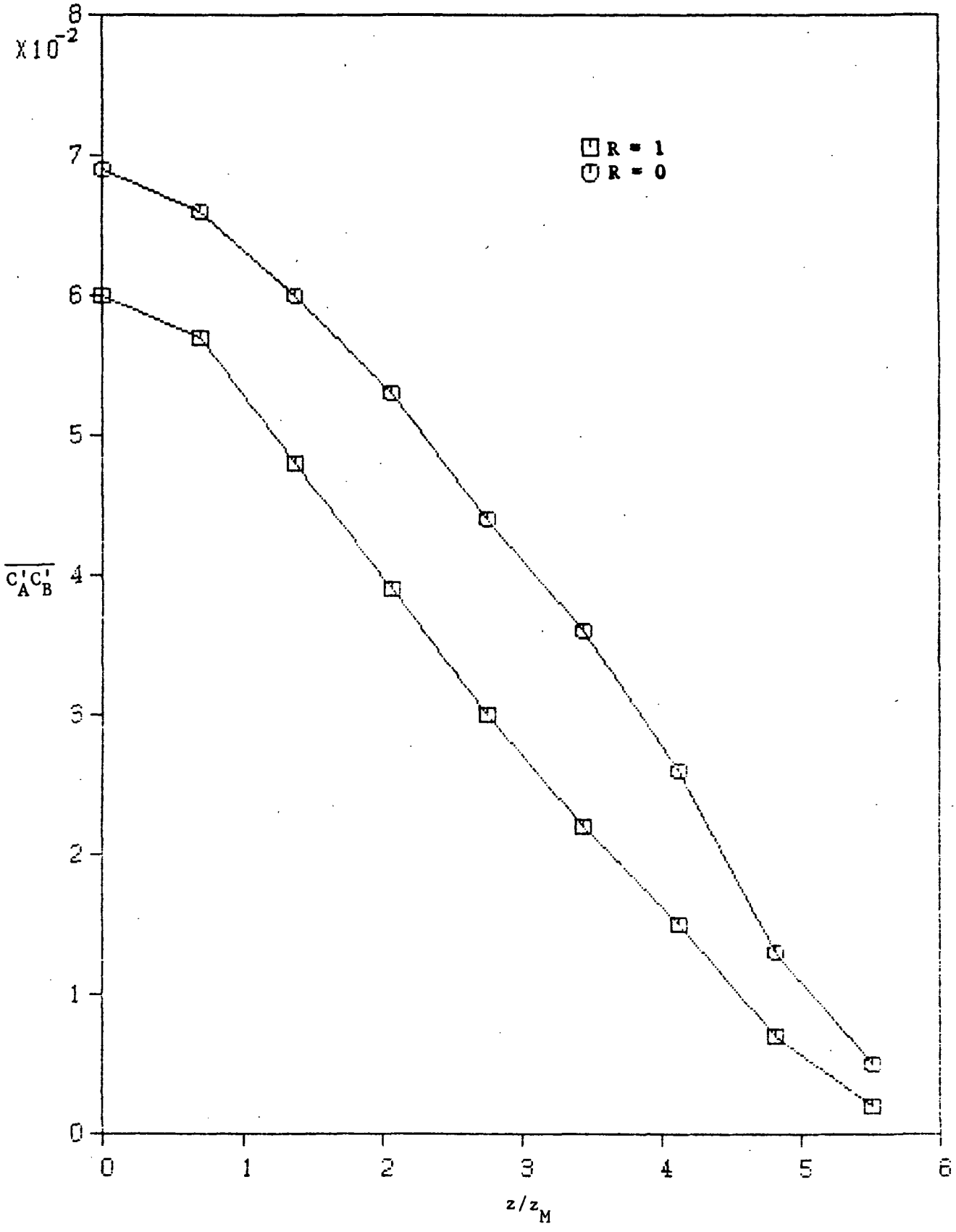

Figure 74. $\overline{C'_A C'_B}/C^2_{A\infty}$ Versus z at t = 12 - Single Rollup Case, Both Zero and Finite Reaction Rates, Three-Dimensional Simulations

1. Report No.	2. Government Accession No.	3. Recipient's Catalog No.
NASA CR-174640		

4. Title and Subtitle	5. Report Date
Direct Simulations of Chemically Reacting Turbulent Mixing Layers	March 1984
	6. Performing Organization Code
7. Author(s)	8. Performing Organization Report No.
James J. Riley and Ralph W. Metcalfe	Report No. 274
	10. Work Unit No.
9. Performing Organization Name and Address	11. Contract or Grant No.
Flow Research Company 21414-68th Avenue South Kent, Washington 98032	NAS 3-23531
	13. Type of Report and Period Covered
12. Sponsoring Agency Name and Address	Contractor Report
National Aeronautics and Space Administration Washington, D.C. 20546	14. Sponsoring Agency Code
	505-32-32

15. Supplementary Notes

Final report. Project Manager, Russell W. Claus, Aerothermodynamics and Fuels Division. NASA Lewis Research Center, Cleveland, Ohio 44135.

16. Abstract

The report presents the results of direct numerical simulations of chemically reacting turbulent mixing layers. The work consists of two parts: (i) the development and testing of a spectral numerical computer code that treats the diffusion-reaction equations and (ii) the simulation of a series of cases of chemical reactions occurring on mixing layers. The reaction considered is a binary, irreversible reaction with no heat release. The reacting species are nonpremixed. The results of the numerical tests indicate that the high accuracy of the spectral methods observed for rigid-body rotation are also obtained when diffusion, reaction, and more complex flows are considered. In the simulations, the effects of vortex rollup and smaller-scale turbulence on the overall reaction rates are investigated. The simulation results are found to be in approximate agreement with similarity theory. Comparisons of simulation results with certain modeling hypotheses indicate limitations in these hypotheses. The nondimensional product thickness computed from the simulations is compared with laboratory values and is found to be in reasonable agreement, especially since there are no adjustable constants in the method.

17. Key Words (Suggested by Author(s))	18. Distribution Statement
Turbulent flow Chemical reaction Direct simulation	Unclassified - unlimited STAR Category 07

19. Security Classif. (of this report)	20. Security Classif. (of this page)	21. No. of pages	22. Price*
Unclassified	Unclassified	148	A07

*For sale by the National Technical Information Service, Springfield, Virginia 22161

National Aeronautics and
Space Administration

Washington, D.C.
20546

Official Business
Penalty for Private Use, $300

SPECIAL FOURTH CLASS MAIL
BOOK

Postage and Fees Paid
National Aeronautics and
Space Administration
NASA-451

NASA

POSTMASTER: If Undeliverable (Section 158
Postal Manual) Do Not Return